FACULTY OF SCIENCE
PALACKÝ UNIVERSITY IN OLOMOUC

Department of Experimental **Physics**

Dissertation thesis

Design and optimization of proportional gas flow counters for Mössbauer spectroscopy

Author	Lukáš Kouřil
Supervisor	Assoc. Prof. Dr. Jiří Pechoušek
Discipline	Applied physics
Study form	full-time
Year	2018

Bibliographical identification

Author's first name and surname	Lukáš Kouřil
Title	Design and optimization of proportional gas flow counters for Mössbauer spectroscopy
Type of thesis	dissertation
Department	Department of Experimental Physics
Supervisor	Assoc. Prof. Dr. Jiří Pechoušek
Year of presentation	2018
Number of pages	55
Number of appendices	3
Language	English
Abstract	This dissertation thesis presents a new prototype of a toroidal proportional gas flow counter. This detector has been developed to be used in the Mössbauer spectroscopy for characterizing the surfaces of the iron bearing samples. The presented proportional counter allows to register both conversion X-rays (6.4 keV) and the backscattered gamma rays (14.4 keV) in the almost 2π geometry with the sufficient efficiency. This thesis demonstrates the structure description of the detector, its basic features for different counting gases (pure argon, its mixtures with different methane concentrations, and pure krypton) and also the optimization process of its use in the backscattering Mössbauer spectroscopy. Despite that the detector could be used in the transmission Mössbauer spectroscopy as well, this thesis also describes more optimized choice for the transmission geometry - cylindrical proportional gas flow counter.
Keywords	proportional gas counter, gas filled detector, soft X-rays detector, low energy gamma rays detector, Mössbauer spectroscopy

Jméno a příjmení autora	Lukáš Kouřil
Název práce	Návrh a optimalizace proporcionálních plynových detektorů pro Mössbauerovu spektroskopii
Typ práce	dizertační
Pracoviště	Katedra experimentální fyziky
Vedoucí práce	doc. RNDr. Jiří Pechoušek, Ph.D.
Rok obhajoby práce	2018
Počet stran	55
Počet příloh	3
Jazyk	anglický

Abstrakt

Tato dizertační práce představuje nový prototyp průtokového toroidního proporcionálního plynového detektoru. Tento detektor byl vyvinut pro účely charakterizace povrchů železo obsahujících vzorků pomocí Mössbauerovy spektroskopie. Představovaný proporcionální detektor umožňuje registraci jak konverzního RTG záření (6,4 keV) tak i zpětně odraženého gama záření (14,4 keV) v téměř 2π geometrii s dostatečnou účinností. Tato práce demonstruje popis konstrukce detektoru, jeho základní parametry pro různé čítací plyny (čistý argon, jeho směsi s metanem v různých koncentracích a čistý krypton) a proces optimalizace pro použití v Mössbauerově spektroskopii zpětného rozptylu. Přestože tento detektor by mohl být stejně tak použit v transmisní Mössbauerově spektroskopii, tato práce také popisuje průtokový válcový proporcionální plynový detektor, který je výhodnější volbou pro tento typ transmisní geometrie.

Klíčová slova	proporcionální plynový čítač, plynový detektor, detektor měkkého RTG záření, detektor nízkoenergetického gama záření, Mössbauerova spektroskopie

I declare that I have written this thesis by myself using the cited references. Neither the thesis nor any of its part was previously used for obtaining any other academic degree.

In Olomouc . . . .
                                                                                                  signature

Contents

Introduction

Gas filled ionization detectors belong to the oldest types of instruments used in the area of nuclear physics. Their low price, adjustment to different experimental conditions (including low and high temperatures, non-sensitivity to external magnetic field, dimension versatility, etc.), ability to register almost all types of charged particles (even X and γ-rays) makes them very common in nuclear physics community.

Proportional gas counters appeared in late 1940s and became very popular in wide area of nuclear techniques requiring spectrometric detector regime (distinguishing particle energy). About twenty years later (after discovery of Mössbauer effect in 1958) proportional gas counters found their utilization in Mössbauer spectroscopy covering large group of Mössbauer effect observations. Nowadays they are commonly used especially in the backscattering ^{57}Fe Mössbauer spectroscopy techniques.

The main aim of this dissertation thesis is to introduce a new toroidal proportional gas flow counter prototype enabling the 6.4 keV X-rays and the 14.4 keV gamma rays registration in almost 2π geometry. It took three years to develop structure and design of the toroidal proportional gas flow counter for meeting all specified conditions. All the prototype versions were printed by 3D printers (the first one even from plastic material and painted by carbon conductive glue). Despite that many versions (including different materials, anode configuration, safety high voltage connector housing, window shapes, etc.) have been tested, the best one is presented in this dissertation thesis. The toroidal proportional gas counter was tested with different counting gases (pure argon, pure krypton and argon-methane mixtures with different concentration) for optimization counter parameters (such as energy resolution and detection efficiency). Consequently, this counter was tested for the conversion X-rays, backscattering gamma and transmission ^{57}Fe Mössbauer spectroscopy.

For the purpose of the transmission ^{57}Fe Mössbauer spectroscopy, the toroidal proportional gas counter was replaced by the cylindrical one. This counter was filled by pure krypton, whose escape peak is usually described as its disadvantage. However, this thesis demonstrates that this ''disadvantage'' could be also beneficial.

1. Mössbauer spectroscopy

Mössbauer spectroscopy is a non-destructive resonance spectroscopic technique, which is based on the physical phenomena of recoilless nuclear emission and resonant absorption of gamma rays. In 1958, the Mössbauer effect was discovered by German physicist Rudolf Ludwig Mössbauer. For this discovery he was awarded a Nobel Prize in Physics (1961).

Since the time of its discovery, Mössbauer spectroscopy has become very important experimental method. It finds applications in physics, chemistry, biology, geology, archeology, material research, metallurgy etc. This experimental technique provides quantitative analysis of materials (structural, phase and magnetic information), which contains specific elements (most often iron or tin). Being selective to certain nuclei type, Mössbauer spectroscopy allows identification even of those ones with a very low concentration. This thesis focuses on Mössbauer spectroscopy of Fe-bearing materials, thus the method based on measuring the ^{57}Fe isotope is described in details.

1.1. Mössbauer effect

The theory of Mössbauer effect has been presented in many publications, i.e. [1–4]. Therefore this chapter provides only a brief overview of this phenomena. R. L. Mössbauer studied the resonant absorption of gamma rays on ^{191}Ir with the energy $E_\gamma = 129$ keV and the low recoil energy E_r = 0.046 eV [5]. The resonant emission and absorption of gamma rays means that the absorbed and emitted gamma rays have approximately the same energy [6]. He experimentally proved that the value of resonance absorption increases with a decrease in temperature. However, more detailed study revealed a critical role of solid lattice in these types of experiments. The recoil energy E_r is given by the expression

$$E_r = \frac{E_\gamma^2}{2mc^2},\tag{1}$$

where m is the nuclear mass and c is the speed of light [2]. As the nucleus is actually a part of the crystal (it is not free), the recoil energy inversely depends on the mass of the solid lattice (with a value many times higher than only for one nucleus). It means that the momentum is transmitted to the whole crystal and the recoil energy is virtually zero. However, the absorption or the emission of gamma rays can be involved into energy transfer to lattice vibrations (phonons). In this case no Mössbauer effect is observed. The probability (without inducing any energy transfers to lattice vibrations) is called Debye-Waller factor f (for ^{57}Fe in α-iron metal at room temperature, f is equal to 0.76 [6]). Normally, ^{57}Co (with half-life of $\tau = 271.8$ days) is used as an emission source for the ^{57}Fe Mössbauer spectroscopy, which utilizes the emission of the Mössbauer gamma rays (14.41 keV, 9 %) [7]. ^{57}Co decays to ^{57}Fe by an electron capture and its decay scheme is demonstrated in Figure 1.
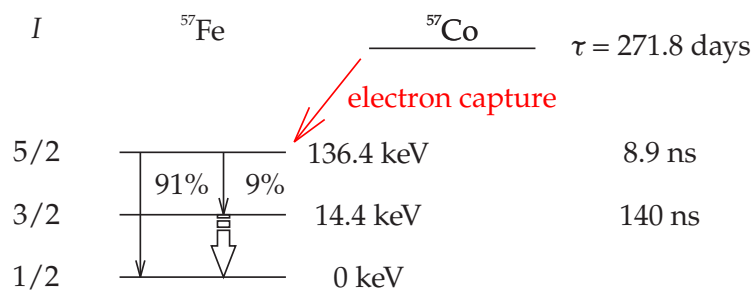
Figure 1 | *The decay scheme of ^{57}Co (I is the nuclear spin); modified from [2].*

The energy distribution from recoilless emitted gamma rays has ideally a Lorentzian line shape with a natural width of approximately 4.7 neV [6]. As this width is lower than the difference in energy between nuclear levels, Mössbauer spectroscopy provides a recordable energetic resolution in registering electromagnetic radiation.

The modulation of the emitted gamma rays is required for experimental observation of the Mössbauer effect. This process is usually provided by the motion of the radiation source (moving with absorber is not so common, but it could be also used) while using the Doppler effect. Due to this, the emission line shift ΔE is given by the equation 2

$$\Delta E = E_\mathrm{p} \frac{v}{c} \cos \alpha, \tag{2}$$

where v is the velocity of the radiation source, c is the speed of light, E_p is the energy of transition, and α is the angle between the orientation of the velocity motion and the emission of the gamma photon [2]. Then the Mössbauer spectrum is the number of counts passing through the absorber (eventually emitted by it) as a function of the relative velocity of the radiation source and the sample. The typical velocity range for the ^{57}Fe Mössbauer spectroscopy is from -10 mm/s to $+10$ mm/s.

1.2. Methods of observing Mössbauer effect

From the geometrical point of view, the observation methods of the Mössbauer effect could be generally divided into two groups. The difference is in the arrangement of the sample and the detector (see Figure 2).
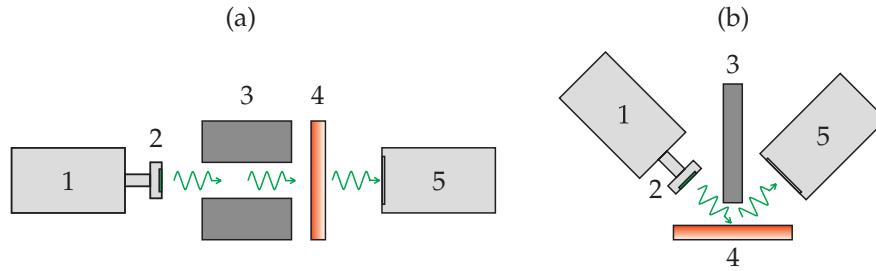

Figure 2   *(a) The transmission geometry and (b) the backscattering geometry used to observe Mössbauer effect, where 1 is the velocity driver, 2 is the radiation source (^{57}Co), 3 is the collimator, 4 is the absorber (sample) and 5 is the detector.*

1.2.1. Transmission geometry

The transmission Mössbauer spectroscopy (TMS) is the most common method from all Mössbauer techniques. In this type of geometry, the absorber is located between the radiation source and the detector (see Figure 2 (a)). It provides information about the intensity of transmitted gamma rays through the sample, so the recorded Mössbauer spectra provides information about the whole sample (i.e., from the whole volume of the sample). On the other hand, this geometry is able to analyze only thin layers or powder materials. In the case, when the TMS could not be used, the scattering techniques are applied (this geometry is shown in Figure 2 (b)).

1.2.2. Backscattering geometry

Backscattering geometry allows to analyze surfaces of bulk materials. As different processes take place by gamma rays interaction with sample atoms after an individual Mössbauer absorption (see Figure 3), various types of scattering methods could be used.

In general, there are three most common scattering methods used to observe the Mössbauer effect. The conversion electron Mössbauer spectroscopy (CEMS) usually focuses on registering the K conversion electrons and the KLL Auger electrons due to their high emission probability [9]. The CEMS techniques can be used to study the surface depths up to 400 nm. Other scattering method is based on the registering the 6.4 keV conversion X-rays. The conversion X-rays Mössbauer spectroscopy (CXMS) analyzes the material surface up to the depths of 1-20 μm. The last of them is the backscattering gamma rays Mössbauer spectroscopy (BGMS), which allows to describe the sample surface up to the depths of 20-100 μm. However, the CEMS and CXMS are mostly used, as the probability of backscattered gamma photon emission is quite low.

1.3. Construction of Mössbauer spectrometers

There are two basic types of Mössbauer spectrometers. The first of them is the Mössbauer spectrometer using constant velocity. In this case the measurement is divided into sequences, and
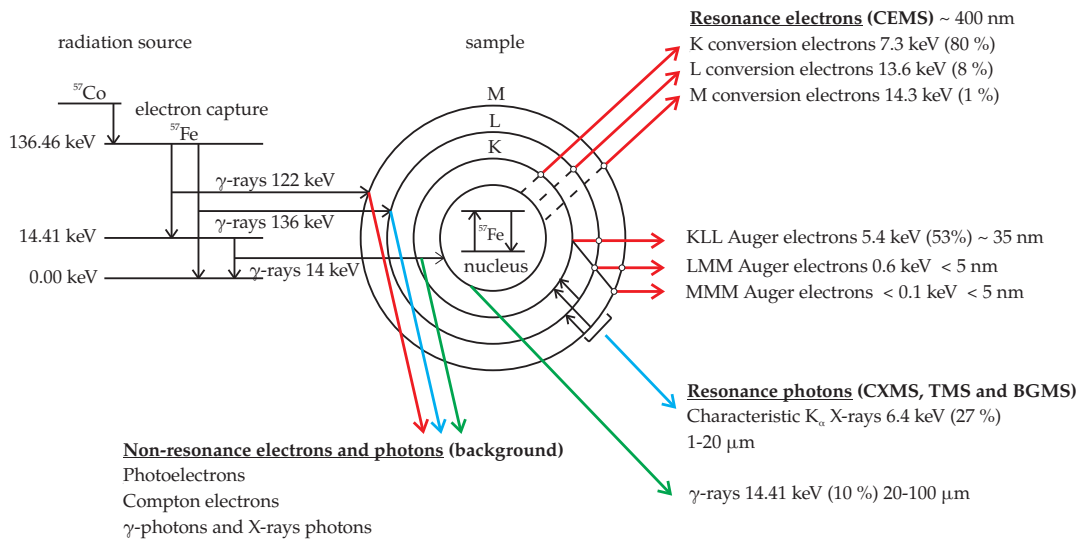
Figure 3 | *Processes taking place after an individual Mössbauer absorption;* modified from [8].

every single experimental point of the spectrum is measured independently. The velocity generator controls the velocity driver and switches the channels of the registration unit simultaneously. The detector registers the intensity of gamma rays transmitting through the sample. The energy component is selected by differential discriminator. The second type of the Mössbauer spectrometer uses the relative variable velocity of the radiation source and the sample. The pulses from the detector correspond to actual velocity values. They are distributed to different channels of the multichannel analyzer [2].

Nowadays, there is a large amount of systems, which are able to record the Mössbauer spectra. The solution by using a microcomputer or a microprocessor is very common [10–12]. Some Mössbauer spectrometers are based on the plug-in computer boards [13,14] or on the commercial card [15]. In the laboratories of the Department of Experimental Physics of Palacký University in Olomouc, the Mössbauer spectrometers based on the virtual instrumentation [16,17] are widely used to record the spectra. In this technique the data acquisition is provided by the NI-PCI (NI - National Instruments), NI-PXI or NI-USB digitizers [18]. The user application processing data was developed in the graphical programming environment LabVIEW^{TM}. The critical parameter of this type of system is the dead time of the Mössbauer spectrometer (zero percent ideally). These values are reached when the PCI bus or PXI modular system is used for data acquisition and processing. However, the USB 2.0 (Universal Serial Bus) provides lower transfer rates and minimal 50 % dead time has been reached via this type of communication. Usage of another low-cost configuration based on stand-alone instruments [19] is also possible, which has 66 % dead time.

1.3.1. Velocity driver and PID regulation

The most important part of every Mössbauer spectrometer is the velocity driver and the PID (proportional-integral-derivative) controller, as they provide precise movement of the radiation source (eventually the sample). This movement determines the quality of the entire spectrometer.

Different methods to realize the motion with a radiation source or a sample (mechanical, hydraulic, electrodynamical or piezoelectric) can be used. The choice of the method to be used is usually determined by the required velocity range. Nowadays, the electromechanical method (transducer) is commonly used in the ^{57}Fe Mössbauer spectroscopy. This transducer consists of primary and secondary coils located in permanent magnets. Whereas the primary coil ensures the motion of the radiation source, the secondary one monitors the actual velocity of the source. The precise feedback between the reference signal (primary coil) and the drive signal (secondary coil) can be provided by the analog solution [20] or by the digital PID controller [21,22].

1.3.2. Detectors for Mössbauer spectroscopy

There are three main types of detectors used in Mössbauer spectroscopy – scintillation detectors, proportional gas counters, and semiconductor detectors.

i. **Scintillation detectors**

Scintillation detectors use inorganic or organic scintillators. Transition of ionization rays (gamma rays or X-rays) in a scintillator causes light flashes in the material. Consequently, these flashes are registered by the photomultiplier or photodiode. Formerly, the most common scintillation crystal used in ^{57}Fe Mössbauer spectroscopy was NaI:Tl. However, this type of material is not suitable for registering events of the high-activity sources, as the output pulses are too long (i.e. 400 ns). That is why this scintillation crystal was substituted by the YAP:Ce. Pulses from this scintillation crystal are almost eight times shorter than in the case of NaI:Tl crystal [23]. In general, the scintillation crystals are applicable in a wide interval of energies (depending on the choice of suitable scintillator). They are characterized by high detection efficiency, low price, and easy handling. Disadvantage lies in their parameters dependence on the magnetic field and the temperature.

ii. **Proportional gas counters**

The detailed description of this type of detectors and their utilization in Mössbauer spectroscopy is provided in the following chapter 2.

iii. **Semiconductor detectors**

Semiconductor detectors are based on the formation of negative electrons and positive holes in the p-i-n (p-type semiconductor, intrinsic region and n-type semiconductor) region as a result of the incident gamma rays. When electric field is applied, these charge carriers are drained by the relevant electrodes. Then the current pulse from the detector is transformed into a voltage pulse, which is processed by the amplifier. The lithium-drifted germanium (Ge(Li)) or lithium-drifted silicon (Si(Li)) are mostly used in Mössbauer spectroscopy when the high energy resolution is required. However, their energy resolution drops with a decrease of the registered energy and increase of the noise [1]. The decrease of noise could be reached when liquid nitrogen is used in the cooling system. On the other hand, this type of detector provides high energy resolution (1-2 keV), fast operation time (the pulse width is approximately 100 ns), low operational voltage, small size, and ability to work under strong magnetic fields, at low temperatures or in vacuum [2].

2.   Proportional gas counters

Gases are very good insulators under normal conditions. However, if they are exposed to the ionization rays, the neutral gas atoms or molecules are transformed into positively charged ions and electrons. This effect causes the increase in the gas conductivity. This feature is used by gas-filled detectors for detecting ionization rays. These detectors can be divided into three groups according to the region of high voltage:

a) ionization chambers,

b) proportional gas counters,

c) Geiger-Müller counters.

Ionization chambers and proportional counters are able to distinguish energy of the particles, whereas the Geiger-Müller counters are not. Different regions of gas filled detector operation are shown in Figure 4. It shows the dependence of the number of ions collected and the high voltage, which is applied between the anode and the cathode. The first region (i) represents low intensities of the electric field, where the recombination process is faster than the charge collecting. This region is called the recombination area or the region of Ohm law. The ionization chambers work in the second region (ii), where the number of collected ions N_c is given by the expression

$$N_c = N_\alpha \text{ or } N_c = N_\beta, \tag{3}$$

where N_α is the number of ion pairs created by α particles and N_β is the number of ion pairs created by β particles. This region is called the region of saturation. The next region (iii) is the typical area, where the proportional gas counters work. The number of collected ions N_c is higher than the number of created ion pairs N_α or N_β and depends on the multiplication factor M, i.e.,

$$N_c(\alpha) = MN_\alpha;\ N_c(\beta) = MN_\beta;\ N_c(\alpha, \beta) = M(N_\alpha + N_\beta). \tag{4}$$

The region of limited proportionality (iv) is not usually used in the regime of the gas filled detectors. When the high voltage increases, the gas filled detector will start working as the Geiger-Müller counter. In the Geiger-Müller region (v), the detector can work only in the non-spectrometric mode. With the next increase of the high voltage (not marked in the Figure 4) the detector moves into the discharge region.
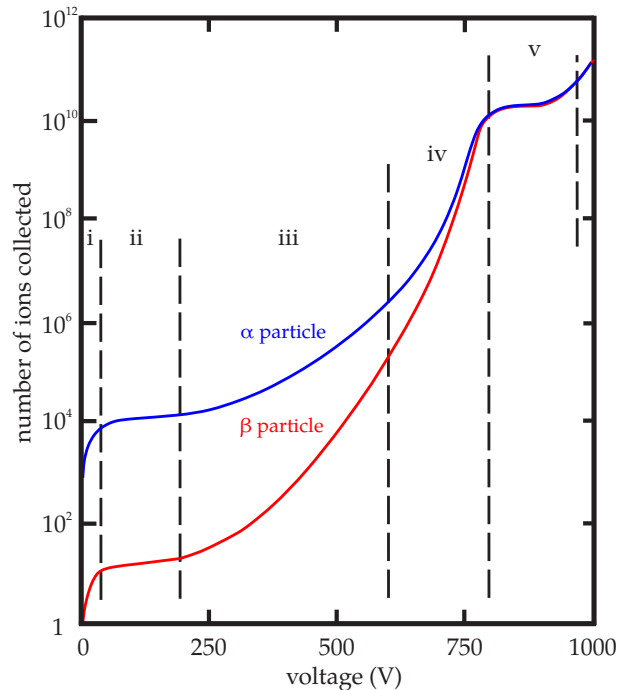

Figure 4 | *The different operation regions of gas filled detectors;* modified from [24].

The simplest design of a proportional gas counter is shown in Figure 5. The typical shape of a proportional gas counter adopts a cylindrical geometry, where the body of the detector is the cathode and the anode in the form of a very thin wire (typically 10 - 100 μm) is placed in the middle of the cylinder. The detector is equipped with a window, which enables transmission of the registered particles or photons into the gas volume.
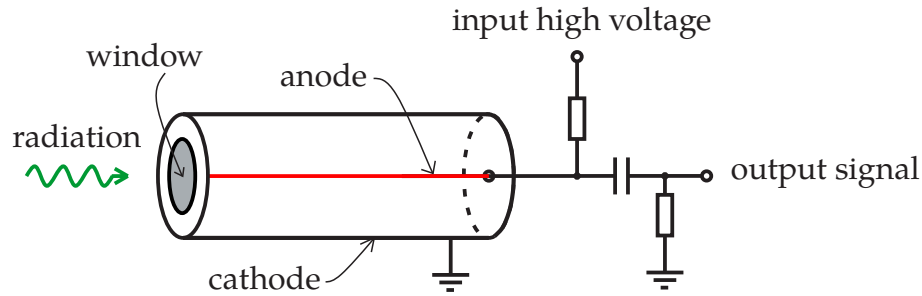

Figure 5 | *The simplest design of a proportional gas counter with a cylindrical geometry.*

2.1. Basic principles of particle energy loss in matter and behavior of ions and electrons in gases

The principle is similar to the one used in ionization chambers. It is based on the charged particle energy loss in the matter. The molecules of the filling gas could be ionized by the light particle energy loss, heavy ion energy loss, and by photon interactions. This issue has been studied in many works (see, e.g., [24,25]). When gamma rays or X-rays are detected, the neutral gas molecules interact with the photons and create a pair of negative electron and positive ion. Depending on the photon energy, it can be induced by different mechanisms – photoelectric absorption, Compton scattering and pair production [25]. However, the photon energies detected in the iron based Mössbauer spectroscopy are quite low (the 6.4 keV soft X-rays and the 14.4 keV low gamma rays), so the photoelectric absorption is the dominant process. The next two processes occur, only when higher energies of photons are detected.

This process is commonly known as a primary ionization. Its effects, in terms of number of formed electron-ion pairs N_i depend on the particle energy E_i according to equation

$$N_i = E_i w^{-1}, \tag{5}$$

where w is the mean energy for creating one electron-ion pair. The charge depends on the particle energy which causes the ionization. It is described by the expression

$$Q = e N_i M, \tag{6}$$

where Q is the collected charge, e is an electron charge and M is the multiplication factor. In the case of the ionization chamber, the multiplication factor M is equal to 1 [26]. This multiplication factor is a key feature of every proportional gas detector, so the next chapter 2.2 is devoted to this issue.

Positive ions and free electrons (originated during the primary ionization) have a tendency to diffuse in the direction of decreasing concentration of the particles with the same charges. This leads to the collision between these particles. If there is a collision of a positive ion with the neutral molecule of the gas, the transmission of the charge could occur. The electron from the neutral molecule moves to the positive ion and the ion becomes a neutral molecule, while the neutral molecule becomes a positive ion. This transmission of charge is especially significant when the gas mixture contains various types of molecules. The tendency is to transmit the whole positive charge in the gas with the lower ionization energy.

Occasionally, free electron could be captured by neutral molecule and create a negative ion. This feature is typical for oxygen, water vapor, halogens, HCl, NH_3 and SiF_4. Noble gases, nitrogen, hydrogen and methane have low coefficient of the electron capture. This is why the moving electron remains a free one.

The collisions of positive ions and free electrons lead to the recombination. The free electron is captured by positive ion and then the ion becomes electricaly neutral. Next recombination process

supervenes when there is a collision of positive and negative ions. In both cases the original charge is lost and could not contribute to the generation of the signal in the detector [26].

In gas detectors (including proportional gas counters), electric field is applied across the gas volume. This electric field induces a motion of created ions and electrons in the relevant direction. Positive ions move to the cathode (negative electrode) with the drift velocity v_i defined by the formula

$$v_i = \mu \frac{E}{p}, \tag{7}$$

where E is the intensity of electric field, p is gas pressure, and μ is mobility of the ions. Because of their small size, the electrons move much faster than ions in the gas (approximately 1000 times), which decreases the probability of the collision with neutral molecules [24]. According to Townsend [27], the drift velocity of electrons v_e can be expressed by equation

$$v_e = \frac{e}{2m} E\tau, \tag{8}$$

where e is the elementary charge, m is weight of the electron, E is intensity of the electric field, and τ is the mean time between collisions. The drift velocity of electrons strongly depends on the intensity of the electric field. Many authors dealt with this issue and published the real values of the drift velocity of the electrons in different gases [28–30].

2.2. Gas multiplication factor

The proportional gas counters are based on the secondary ionization process which occurs only when the high voltage is applied between the anode and the cathode. When strong electric field is applied between the electrodes, the electrons are attracted to the anode and the collision between the accelerated electrons and neutral gas molecules supervenes. These collisions generate the Townsend avalanche. The time development of the Townsend avalanche is shown in Figure 6. Firstly an ion-electron pair is created by the primary ionization (a). The created electron is accelerated by the electric field toward the anode, while next electrons are created (b) due to the collisions with neutral gas molecules. The electrons surround the anode, grouping in a drop-shaped avalanche (c, d). This process is terminated when all the free electrons are collected on the anode (very fast process lasting approximately 1 ns). However, the positive ions have lower drift velocity than the electrons, so there is still a cloud of them moving slowly toward the cathode (d).
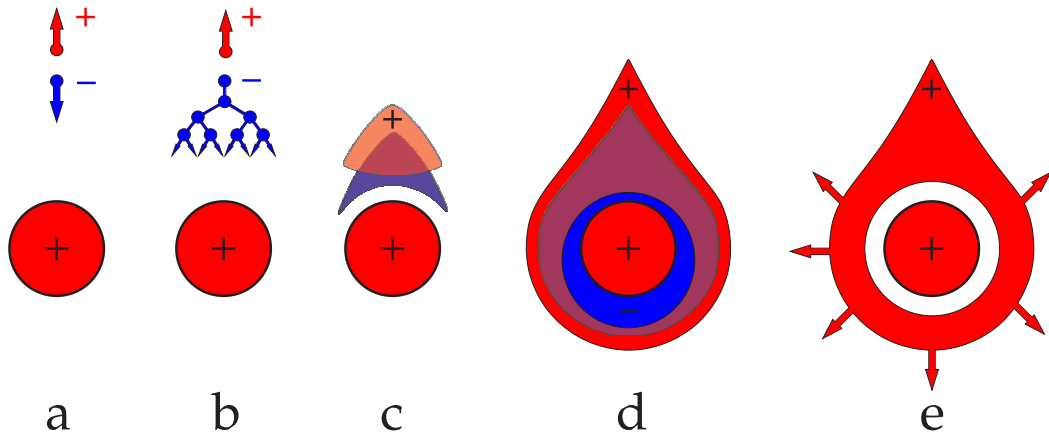

Figure 6 | *The time development of the Townsend avalanche;* modified from [25].

The requirements of the values of electric field are very high ($E(r) \geq 10^5$ V/cm at normal pressure), thus the anode is usually a fine wire. The electric field $E(r)$ is given in the cylindrical proportional gas counter by the equation

$$E(r) = \frac{V}{r\ln\left(\frac{b}{a}\right)}, \tag{9}$$

where V is the voltage applied between anode and cathode, a is anode radius, b is the inner radius of the cathode and r is the distance of the electric field from the center of the wire [26]. Because the required values of E are reached in very short distances of r, generation of the avalanches takes places only in the proximity of the anode. Diethorn [31] gave the following expression 10 for the multiplication factor M, which characterizes well the proportional gas counters filled with the methane, i.e.,

$$M = \exp\left[\frac{V}{\ln\left(\frac{a}{b}\right)} \frac{\ln 2}{\Delta V} \ln\left(\frac{V}{Kpa\ln\left(\frac{b}{a}\right)}\right)\right],$$ (10)

where V is voltage, a is anode radius, b is cathode inner radius, ΔV and K are constants for a given gas (the potential variation between two successive ionizations) and p is gas pressure. Kiser [32] proved that the expression 10 adequately describes gas amplification for methane, methane-argon and ethanol-argon mixtures. On the other hand, Zastawny [33] proposed the expression 11 based on his observations for proportional gas counter filled with carbon dioxide, where Diethorn equation was inadequate to use.

$$M = \exp\left[\frac{V}{\ln\left(\frac{b}{a}\right)}\left(A + B\left\{\ln\left[\frac{V}{Cpa\ln\left(\frac{b}{a}\right)} + \frac{Cpa\ln\left(\frac{b}{a}\right)}{V} - 1\right]\right\}\right)\right]$$ (11)

A, B and C are constants of the filling gas and all other parameters are the same as in the Diethorn equation 10. However, the comparison of both equations for xenon filled proportional counters [34] shows that both equations fit the data almost equally well. The multiplication factor should be constant to enhance good energy resolution. Because it depends on the high voltage (according to equations 10 and 11), it is necessary to use a very stable high voltage supply. Some of the Diethorn parameters are shown in Table 1 [35], where W is the average energy to create an ion-electron pair.

Table 1 | *Diethorn parameters for different gas mixtures.*

Gas or a gas mixture	W(eV)	K x 10^{-4}(V/cm atm)	ΔV(eV)	Reference
90 % Ar, 10 % CH$_4$	26.0	4.80	23.6	[36]
95 % Ar, 5 % CH$_4$	26.0	4.50	21.8	[36]
CH$_4$(methane)	29.2	6.90	36.5	[36]
C$_3$H$_8$(propane)	23.6	10.00	29.5	[36]
96 % He, 4 % isobutane	40.0	1.48	27.6	[36]
15 % Xe, 75 % Ar, 10 % CO$_2$	25.6	5.10	20.2	[36]
19.9 % Xe, 69.4 % Ar, 10.7 % CH$_4$	25.3	5.45	20.3	[36]
24.7 % Xe, 64.6 % Ar, 10.7 % CO$_2$	25.0	6.00	18.3	[36]
90 % Xe, 10 % CH$_4$	21.7	3.62	33.9	[34,37]
95 % Xe, 5 % CO$_2$	21.6	3.66	31.4	[34,37]

2.3. Choice of the filling gas

There are different choices of the filling gas for every type of ionizing radiation. Because of the unique features, the family of noble gases is very common. The first of them are the values of their mass attenuation coefficients μ, which characterize how easily the gases could be penetrated by the radiation. When the radiation passes through the gas, it loses the energy, and this loss is characterized by the mass-energy absorption coefficients μ_{en}. The values of these coefficients for the most used elements in the proportional gas counters lying in the range of energy from 1 keV to 100 keV are shown in Figure 7 (the data were collected from [38]).

Despite the fact that the noble gases are very common in the area of the proportional counters, they are widely used in gas mixtures with other more complex gases. The reason is that they do not offer large gains without entering into a permanent discharge regime. The quenching gases (like methane, propane, isobutane or carbon dioxide) are mostly added to the pure noble gas to transfer the charge from the noble gas molecule to the complex molecules. The most common ratio is 10 % of the quenching gas and 90 % of the noble gas. The adding of the quenching gas decreases the dead time of the detector, while the recombination of the noble gas molecules is faster. On the
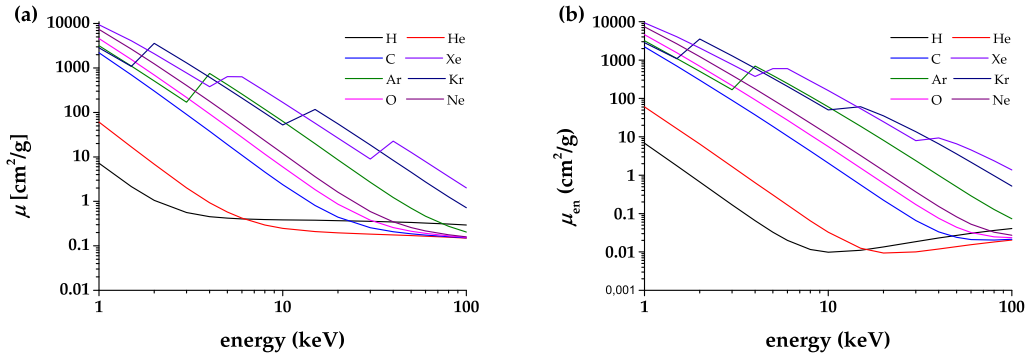
Figure 7 | *(a) The mass attenuation coefficients and (b) the mass-energy absorption coefficients for several noble gases and other elements used in the proportional gas counters.*

other hand, it causes an increase in the high voltage which has to be applied between the electrodes to obtain the avalanche effect in the detector. It has also a negative impact on the ageing effect of the detector [39,40]. Different energy ranges E, proton numbers Z, and their positions of K absorption edges for some noble gases are shown in Table 2 [26].

Table 2 | *Energy ranges of utilization and positions of K absorption edges for some noble gases.*

Gas	Ne	Ar	Kr	Xe
Z	10	18	36	56
E**(keV)**	0.1 - 4	≤ 10	≥ 10	≥ 10
K**(keV)**	0.851	2.96	12.6	29.7

2.4. Basic properties of proportional gas counters

The advantages of the proportional gas counters application include their low price, relatively small size, good energy resolution, resistance to the magnetic field, and ease operation. The main pro- perties of every proportional gas counter are detection efficiency, energy resolution, and resolution time of the proportional counter.

2.4.1. Detection efficiency

The detection efficiency is the registration probability of the ionization rays, which go through the sensitive volume of the counter. The efficiency depends on the type of the gas, its pressure, type of the ionization rays and the size of the detector. The maximum efficiency (close to 100 %) could be reached, when the heavy charged particles are detected. On the other hand, the efficiency for other types of ionization rays (neutrons, X-rays and gamma rays) is distinctly lower (0.001 - 1 %) [26]. The possible reasons are as follows:

a) The particles do not create any ion-electron pairs.

b) There is only a small number of created ion-electron pairs, which do not provide enough signal. This signal does not exceed the discrimination threshold (the reason could be the contamination of the filling gas with the gas, which creates the negative ions).

c) The time interval of the interaction is shorter than the resolution time of the electronics, which is responsible for the registration (the system requires higher sampling frequency). In this case, the efficiency decreases with the increasing number of counts.

The lower primary ionization effect (a) and (b) could be also influenced by the high absorption coefficient of the counter window material. The best solution is to use a material with a low proton number Z. The most common materials are: aluminum ($Z = 13$), metalized plastic foil, and beryllium ($Z = 4$). The beryllium windows are optimal solution from the transparent point of view. However, the disadvantages of the material are its chemical toxicity, small mechanical resistance

(it is very brittle), and high price. The thickness of the windows also influences the number of the ion-electron pairs created by the primary ionization. The typical thicknesses are from one micrometer up to hundreds of micrometers. The optimal thickness and the window material always depend on the energy of the registered ionization rays.

The detection efficiency ϵ_d could be expressed as

$$\epsilon_d(\%) = \frac{N_c}{N_e}100,\tag{12}$$

where N_c is the number of counts (detected events) and the N_e is the number of emitted photons, which fall on to the proportional counter.

2.4.2. Energy resolution

Energy resolution is the detector ability to distinguish two different peaks with nearly the same energy. The shape of the main photopeak of the ionization rays is never characterized by a delta function, but by the Gaussian function. The reasons are primarily the statistical fluctuation of the charge creation and noises from the preamplifier (eventually from the linear amplifier). The Full Width at Half Maximum (*FWHM*) of the Gaussian function is commonly used to obtain the energy resolution of the detectors. The energy resolution could be either expressed absolutely (by the energy unit eV) or relatively by percent of energy corresponding to the maximum position of the peak in the spectrum. The energy resolution R_E can be written as

$$R_E(\%) = \frac{FWHM(E)}{E_p}100.\tag{13}$$

The value of R_E should be as low as possible for achieving a good energy resolution of the detector. For example, typical energy resolutions of the proportional counters are 18 % (^{55}Fe, 5.98 keV), 11.5 % (^{57}Co, 14.4 keV) and 8.5 % (^{109}Cd, 22.1 keV) [26].

2.4.3. Resolution time of the proportional counter

Resolution time of the proportional counter is a very important parameter, as the preamplifier is proposed for the specific detector. If the proportional counter operates in the spectrometric mode, a short resolution time (10 - 100 μs) is required. In this case, it is recommended to choose the time constant in the optimal interval $t_{ce} \ll RC \ll t_{c+}$. Then, t_{ce} represents the collecting time of electrons on the anode and t_{c+} is the collecting time of positive ions on the cathode. Because the collection time of electrons is very short ($t_{ce} \approx 1$ ns), the first part of the condition is easy to reach. The electron contribution to the signal is very small, whereas the ions create nearly the whole signal. The collecting time of the positive ions t_{s+} is defined by the equation

$$t_{s+} = \frac{pb^2\ln\left(\frac{b}{a}\right)}{2\mu + V},\tag{14}$$

where p is gas pressure, b is the inner radius of the cathode, a is the anode radius, μ is the mobility of positive ions, and V is the applied voltage [26].

2.5. Utilization of the proportional gas counters in the Mössbauer spectroscopy

Because the proportional gas counters provide a good energy resolution, they are commonly used in the area of Mössbauer spectroscopy. They are widely used for detection of the conversion electrons emitted from different shells of the atoms (K, L and M) on the surface of the sample. As the electrons have a short mean free path in the air, the location of the samples is usually inside the detector [41–43]. The presented proportional detector [44] allows to measure the Mössbauer spectra by collecting the conversion electrons or the conversion X-rays (6.4 keV) in a temperature range from 100 to 700 K. Other studies describe the operation of proportional gas counters recording CEMS spectra at low temperatures down to 15 K using different filling gases (pure helium, He - CH$_4$, He - H$_2$, He - N$_2$, He - CO, pure neon or hydrogen) [45–47]. The next solution demonstrates CEMS analysis at 4.2 K under magnetic field 3 T [48], which is possible only when a pure helium is used as a filling medium. In addition, a combination of two proportional gas counters allows the detection of the conversion electrons and the conversion X-rays at the same time [49].

It is also possible to use three-chambers (respectively two-chambers) system for recording three different Mössbauer spectra simultaneously. The three-chambers system consists of the chamber detecting conversion X-rays, the chamber detecting conversion electrons and the chamber detecting transmitted gamma rays (14.4 keV) [50]. The two-chambers system is based on the chamber detecting both conversion X-rays and backscattered gamma rays (14.4 keV), while the second chamber serves to detect the conversion electrons [51]. All of these systems are based on a multiwire gas flow detector using 2π geometry. Furthermore, the sample should be always located directly in the detector. So it is not possible to measure bulk samples, as this method could be destructible for these types of samples. To keep the non-destructive feature of Mössbauer spectroscopy for bulk materials, conversion X-rays or backscattered gamma rays could be detected by a commercial cylindrical proportional gas counter. The detector is located in front of the sample at the proper angle. The beam from the radiation source has to be well-collimated and should not incident on the window of the proportional counter. The same type of the detector could be also used to detect the transmitted gamma rays. This method is suitable for analysis of thin films or powder materials. If one wants enshrine the high efficiency by keeping the 2π geometry, the toroidal proportional counters can be used. These types of detectors are described in details in the next chapter 3.

3. Toroidal proportional gas counter

The first construction of "toroidal" proportional gas counter for ionization rays detection was published in 1972 by Keisch [52]. This detector was developed for the purpose of examining works of art containing iron-bearing pigments. In fact, the detector shape was not a true toroid. While the ideal toroid is a ring in the cross section, the presented detector [52] is a hexagon. The body of the detector (cathode) was made from aluminum and the anode (a wire with 25 μm in diameter) was centered via quartz support rods in the middle of the hexagon. The detector windows were made from nylon and sealed by two O-rings. The window interior was aluminized by using the vacuum deposition. The shielding of the detector was provided only by lead. As the detector was primarily designed for the purpose of backscattered gamma rays Mössbauer spectroscopy, the gaseous fill was a mixture of 90 % krypton and 10 % methane. However, the author recommended using flow of a mixture of 90 % argon and 10 % methane to register 6.4 keV conversion X-rays while using an aluminum filter (approximately 250 μm thick) located between the radiation source and the sample for absorbing the non-resonant X-rays.

Next study [53] introduced the first so called toroidal proportional gas counter, which has a ring shape (inside a block of aluminum). The anode (20 μm diameter gold plated tungsten wire or 80 μm Megapyr wire) was located in the middle of the detector. The detector windows were fabricated from the organic material – the acetal resin Delrin (Delrin is a registered trademark of Du Pont) [53]. This material (approximately 500 μm thick) allows to transmit over 92 % of 14.4 keV gamma rays. The shielding part of the detector was made by using the tungsten and lead discs. The authors achieved an energy resolution of 25 % (using Megapyr wire) and 20 % (using gold plated tungsten wire) for 14.4 keV gamma rays, while the Kr-CH$_4$ mixture (0.1 MPa) was used. The extension of this study [54] provided values of absorption for energy in the ^{57}Fe Mössbauer spectroscopy for three different counting gases (see Table 3).

Table 3 | *Absorption of 6.4 keV conversion X-rays and 14.4 keV gamma rays in the toroidal detector with different counting gases (0.1 MPa).*

Counting gas	Absorption for 6.4 keV conversion X-rays (%)	Absorption for 14.4 keV gamma rays (%)
90 % Ar + 10 % CH$_4$	80	16
90 % Kr + 10 % CH$_4$	85	91
45 % Ar + 45 % Kr + 10 % CH$_4$	83	73

With respect to reduction of the 1.8 keV escape of krypton, the mixture of argon, krypton and methane is more preferable to register 14.4 keV gamma rays.

Other studies [55, 56] presented a "toroidal" proportional gas flow counter filled with 90 % argon and 10 % methane mixture (0.1 MPa). This detector is a true toroid only from 75 % of its shape. The anode (supported by eight teflon rods) is shifted by 10 % from the center of the diameter of the toroidal cross section towards the symmetry axis of the counter to be closer to the sample. The detector window was made from a metalized plastic foil (mylar) and had flat shape, whereas the windows presented in [53,54] had a curved shape. In fact, the absorber (sample) is a part of the detector and has a limited size [55,56]. The energy resolution of this detector for 14.4 keV gamma rays was determined to be 19 %. The line width for the conversion X-rays Mössbauer spectroscopy was 0.37 mm/s and for the transmission Mössbauer spectroscopy 0.47 mm/s. All of the previous studies [52–56] presented the detectors, whose anode wires are not usually circular but polygonal and stand on insulated support rods, which could have negative impact on the energy resolution of the detector. This effect was in details described by Dudkin et al. in [57].

3.1. Design of the counter

The developed prototype of a toroidal proportional gas flow counter (see Figure 8 (a)) [58] has an ideal toroidal shape (a ring shape in cross section). The outer diameter of the detector is 80 mm. The detector body forms the cathode (ground state) and it was manufactured from the stainless steel EN 1.4404 (AISI 316L) using 3D printing technology. This technology (LaserCUSING, layer thickness of 30-45 μm) allows to create a true toroidal shape with a constant thickness of the cathode wall (in this case, 2.5 mm). The inner diameter of the cathode is 25 mm. In fact, the cathode consists of two parts, which originate from the horizontal cross section of the toroid.
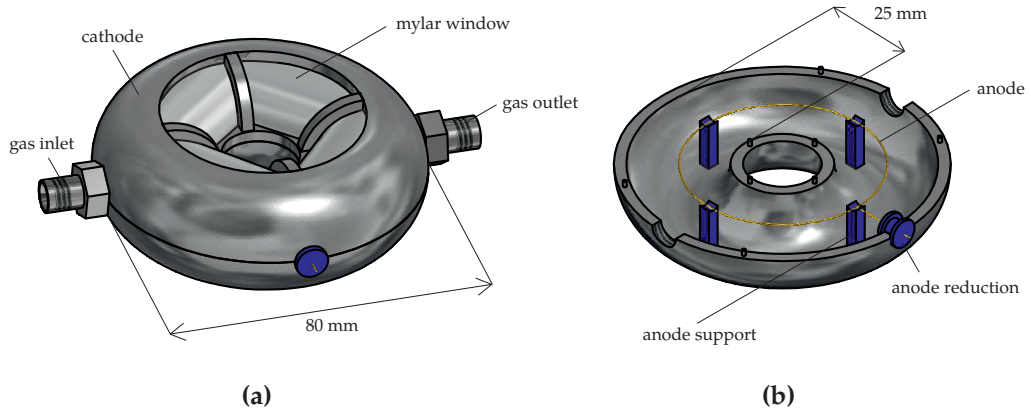
Figure 8 | *(a) Layout of the developed toroidal proportional gas flow counter and (b) anode configuration inside the counter.*

The first part of the cathode includes four gaps for the windows. The selection of window material is crucial as it has a tremendous impact on the detection efficiency of the detector. It has to transmit as much the 6.4 keV X-rays and the 14.4 keV gamma rays as possible. Thus, the absorption coefficient of this material for these two energies has to be as low as possible. Because curved windows are required (see Figure 9), the use of beryllium was rejected by its brittleness, cost and toxicity. The thin aluminum foils can be contaminated by the trace amounts of iron caused by their fabrication; hence, all the Mössbauer spectra observed with these windows will contain a subspectrum of it. Regarding to this, a plastic foil (mylar) with one side aluminized was chosen as an ideal material for windows. The conductive side of the plastic foil is located inside the working volume of the detector. The electrical conductivity between the shell of the detector and the mylar windows is provided via the carbon conductive glue.
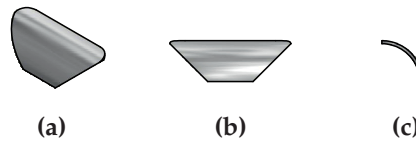

Figure 9 | *Specific shape of mylar window: (a) layout, (b) front view and (c) side view.*

The anode support is mounted in the second part of the cathode. The anode (gold plated tungsten wire with 50 μm diameter) has a circular shape (not polygonal), and it stands on four plastic columns located in the centre of the detector (see Figure 8 (b)). The anode is carried out of the detector through a plastic reduction and soldered to the coaxial cable RG-62A/U (93 ohm, 42.5 pF/m) with crimped SHV connector.

Both cathode parts are assembled together and sealed with a two-components putty (Thorlabs' Vacuum epoxy resin) designed for high vacuum chambers down to 10^{-9} Torr. As shown in Figure 8 (a), the detector is equipped with a gas inlet and gas outlet to fill the detector and for continuous exchange of the counting gas or a mixture.

3.2. Experimental setup

The proposed experimental setup (see Figure 10) was designed to determinate the parameters of the detector (such as energy resolution via multichannel analysis and detection efficiency), where gas management with the precise signal processing and data acquisition were provided. As the detector was tested with different types of counting gases, the pure ones (argon and krypton) were supplied from commercial flashes. However, the gas mixtures (different concentration of argon and methane) were prepared by the gas mixer KM 20-200-3ME (WITT). The whole system of gas tubing (3 mm outer diameter) was fabricated from stainless steel, which does not interact with the methane. For better comparison of different counting gases, the constant gas pressure (approximately 0.1 MPa) and almost the same flow rates of the gases were used.
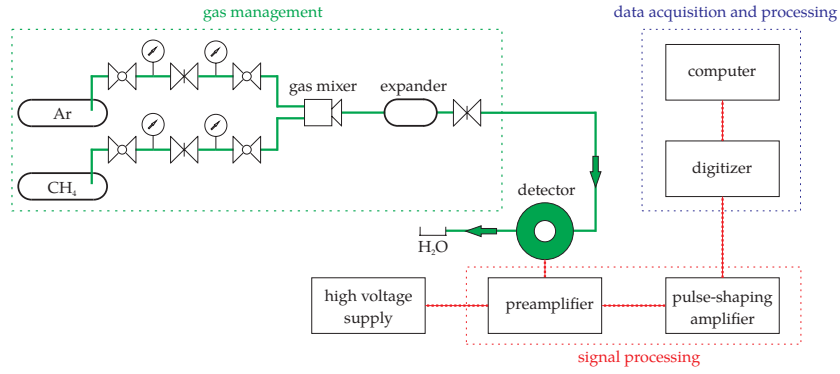
Figure 10 | *Experimental setup used to determinate the parameters of the detector.*

The toroidal proportional gas flow counter was supplied by the programmable high voltage supply HP2.5PAA025 (Applied Kilovolts), which was controlled by the NI USB-6221 card (National Instruments). The analog output of this USB multifunction card provided signal (0-10 V), which set the relevant voltage on the high voltage supply output (0-2500 V). The signal of 1 V (on the analog output of the multifunction card) corresponds to 250 V (voltage provided by the high voltage supply). For keeping better stability of the high voltage supply (crucial parameter), the burn-in process for 24 hours was followed (e.g. long term measurements like obtaining Mössbauer spectra). Considering the time and economy (flowing gas), it was not possible to burn-in the high voltage supply during measuring of the multichannel analysis spectra.

The current pulses with low amplitudes from the detector were converted into the voltage signal with a high signal-to-noise ratio by the 142PC preamplifier (ORTEC). Then the voltage signal was amplified by the 572A amplifier (ORTEC) with the shaping time of the pulses, equal to 1 μs. The fast digitizer NI PCI-5124 (National Instruments) with 8-bits resolution was used to record the data and the LabVIEW™-based user application [18] to process the data. With regard to the shaping time of the pulses, the sampling rate of the detector signal was set to 2 MSa/s. The optimal vertical range of the input channel was set in accordance with the observed pulse amplitudes (shapes of the obtained pulses are shown in Figure 11).
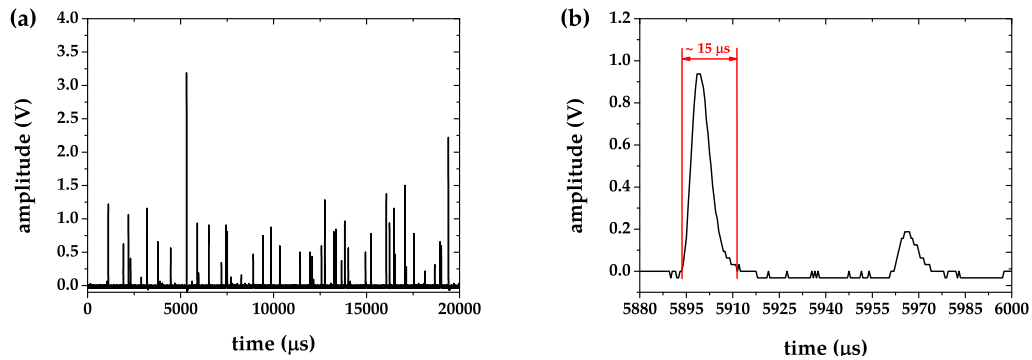

Figure 11 | *(a) Amplified signal from the toroidal proportional gas flow counter using 90.0 % argon and 10.0 % methane mixture (1400 V) as a counting gas, and (b) detailed view of pulse shapes.*

3.3. Multichannel analysis

Multichannel analysis spectra were measured in the transmission geometry ([57]Co radiation source was directed straight into the detector window and no sample was used during the measurements). The lead plate (with a thickness of 8 mm) was used as a collimator with a hole (10 mm in diameter) in the center. The multichannel analysis spectra were measured for pure argon, several mixtures of argon and methane with different concentration and pure krypton. Because the first legible peaks occurred above 1100 V, the high voltage range for every gas or gas mixture was from 1100 V to 1600 V (above this value, the pulse amplitudes were out of vertical range of the

used digitizer) with a step of 50 V. Every single voltage step of the multichannel analysis was measured:

a) **without filters** - all the ionization radiation was detected,

b) **with aluminum filter** (approximate thickness of 40 µm) - this filter shields soft X-rays,

c) **with cooper filter** (approximate thickness of 40 µm) – the cooper filter shields soft X-rays as well as low-energy gamma rays.

The location of these two types of filters between the radiation source and the detector allows to distinguish the type of ionization radiation. Tables 4 and 5 summarize the used input channel vertical ranges of the digitizer NI PCI-5124 for different gases (or gas mixtures) and applied high voltages.

Table 4 | *The used input channel vertical ranges for Kr, Ar and Ar-CH$_4$ mixtures.*

Applied voltage	Kr	Ar	97.5 % Ar, 2.5 % CH$_4$	95.0 % Ar, 5.0 % CH$_4$
1100 V	± 0.4 V	± 0.8 V	± 0.4 V	± 0.4 V
1150 V	± 0.4 V	± 0.8 V	± 0.4 V	± 0.4 V
1200 V	± 0.4 V	± 0.8 V	± 0.8 V	± 0.8 V
1250 V	± 0.8 V	± 0.8 V	± 0.8 V	± 0.8 V
1300 V	± 0.8 V	± 2.0 V	± 2.0 V	± 0.8 V
1350 V	± 0.8 V	± 2.0 V	± 2.0 V	± 2.0 V
1400 V	± 2.0 V	± 2.0 V	± 4.0 V	± 4.0 V
1450 V	± 4.0 V	± 4.0 V	± 4.0 V	± 4.0 V
1500 V	± 4.0 V	± 4.0 V	± 8.0 V	± 8.0 V
1550 V	± 8.0 V	± 8.0 V	± 8.0 V	± 8.0 V
1600 V	± 8.0 V	± 8.0 V	± 8.0 V	± 8.0 V

Table 5 | *The used input channel vertical ranges for Ar-CH$_4$ mixtures.*

Applied voltage	92.5 % Ar, 7.5 % CH$_4$	90.0 % Ar, 10.0 % CH$_4$	87.5 % Ar, 12.5 % CH$_4$	85.0 % Ar, 15.0 % CH$_4$
1100 V	± 0.4 V	± 0.8 V	± 0.4 V	± 0.8 V
1150 V	± 0.4 V	± 0.8 V	± 0.4 V	± 0.8 V
1200 V	± 0.8 V	± 0.8 V	± 0.8 V	± 0.8 V
1250 V	± 0.8 V	± 0.8 V	± 0.8 V	± 0.8 V
1300 V	± 2.0 V	± 2.0 V	± 2.0 V	± 0.8 V
1350 V	± 2.0 V	± 2.0 V	± 2.0 V	± 2.0 V
1400 V	± 4.0 V	± 2.0 V	± 4.0 V	± 2.0 V
1450 V	± 4.0 V	± 2.0 V	± 4.0 V	± 4.0 V
1500 V	± 8.0 V	± 8.0 V	± 8.0 V	± 4.0 V
1550 V	± 8.0 V	± 8.0 V	± 8.0 V	± 8.0 V
1600 V	± 8.0 V	± 8.0 V	± 8.0 V	± 8.0 V

Considering that every vertical range corresponds to 257 channels in the used application [18], the channels were recalculated to voltage values to observe the changes of pulse amplitudes. Because the purity of the gas could also affect the results, the high purity gases were used as counting gases in the detector (see Table 6). Before the measurements started, the detector was washed by the given gas for 15 minutes to keep the purity of every single gas (or a gas mixture).

Table 6 | *Purity of gases used as counting gases in the detector.*

Type of gas	Gas label	Purity (%)
Argon	6.0	≥ 99.9999
Methane	6.0	≥ 99.9999
Krypton	5.0	≥ 99.999

As all measurements were not realized during one day, the activities $A(t)$ of ^{57}Co radiation source (1.85 GBq on 15th of November, 2010) were calculated using the equation 15 for every date of the realized measurement.

$$A(t) = A_0 \left(\frac{1}{2}\right)^{\frac{t}{\tau}},$$ (15)

where A_0 is the initial activity, t is the age of the source and τ is the half-life of the radionuclide. The calculated values of the activities in current day of measurement are shown in Table 7. The uncertainty of $\pm$ 10 % is given by manufacturer of the radioactive isotope (RITVERC) [7].

Table 7 | *Activities of ^{57}Co used to compare different counting gases in the toroidal proportional gas flow counter.*

Date of measurement	Counting gas	Current activity (Bq)
16.3.2018	pure argon	2 005 769 $\pm$ 10 %
4.4.2018	97.5 % Ar, 2.5 % CH_4	1 910 898 $\pm$ 10 %
4.4.2018	95.0 % Ar, 5.0 % CH_4	1 910 898 $\pm$ 10 %
5.4.2018	92.5 % Ar, 7.5 % CH_4	1 906 031 $\pm$ 10 %
31.1.2018	90.0 % Ar, 10.0 % CH_4	2 243 948 $\pm$ 10 %
5.4.2018	87.5 % Ar, 12.5 % CH_4	1 906 031 $\pm$ 10 %
16.3.2018	85.0 % Ar, 15.0 % CH_4	2 005 769 $\pm$ 10 %
6.4.2018	pure krypton	1 901 177 $\pm$ 10 %

As a large amount of data was collected, the multichannel analysis spectra recorded without any filters are presented below. All the multichannel analysis spectra were collected by René Vondrášek, B.Sc. within his bachelor thesis [59] (where L. Kouril was his consultant and laboratory supervisor). The multichannel analysis spectra for the pure argon are shown in Figure 12. The higher voltage applied between the anode and the cathode causes the increase in pulse amplitudes. At 1200 V, only a small amount of 14.4 keV gamma rays peak is observed. However, at and above 1200 V, both energies (6.4 keV X-rays and 14.4 keV gamma rays) are distinguished, and the energy resolution rises with continuous increase in the supplied voltage.
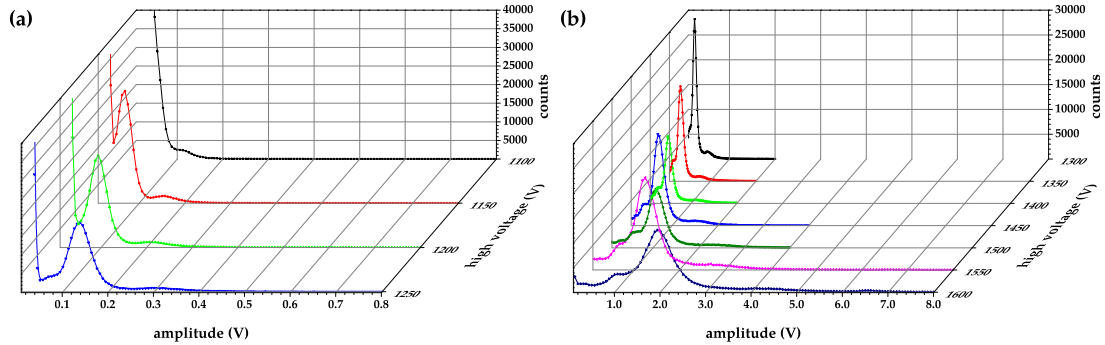

Figure 12 | *Multichannel analysis spectra obtained for pure argon, while applying (a) 1100– 1250 V and (b) 1300-1600 V supply voltage.*

At high voltage with a value of 1350 V, the characteristic escape peak of argon (3.4 keV) starts to be visible. In argon or its mixtures with other gases (such as methane), about 15 % of photoelectric absorptions are followed by the emission of the photon. This secondary photon has a very long mean free path for absorption. Therefore, it can escape from the detection volume. This process produces the characteristic peak of argon [25]. The multichannel analysis spectra obtained for the 97.5 % Ar and 2.5 % CH_4 in a mixture are shown in Figure 13.

As it is shown in Figure 13, the multichannel analysis are almost similar to the ones obtained for pure argon. However, the decrease in vertical range at lower supply voltage (1100-1150 V) and adding of 2.5 % of methane (quenching gas) caused the better resolution of the 14.4 keV gamma rays peak. Repeatedly, the characteristic escape peak of argon starts to be distinguished from 1350 V.
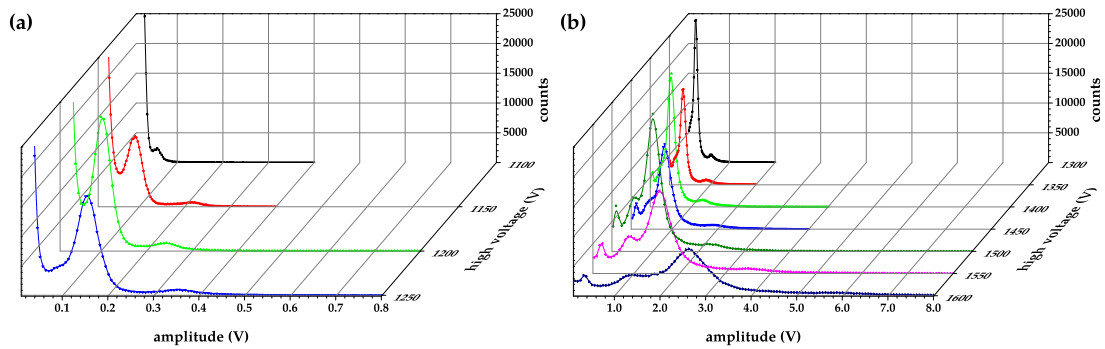
Figure 13 *Multichannel analysis spectra obtained for 97.5 % Ar and 2.5 % CH$_4$ mixture, while applying (a) 1100–1250 V and (b) 1300-1600 V supply voltage.*

Figure 14 demonstrates the multichannel analysis spectra, which have been measured while using 95.0 % Ar and 5.0 % CH$_4$ mixture as a counting gas in the detector. This increase in methane concentration leads to earlier particular visibility of the 6.4 keV X-rays peak (it is nearly visible at 1100 V).
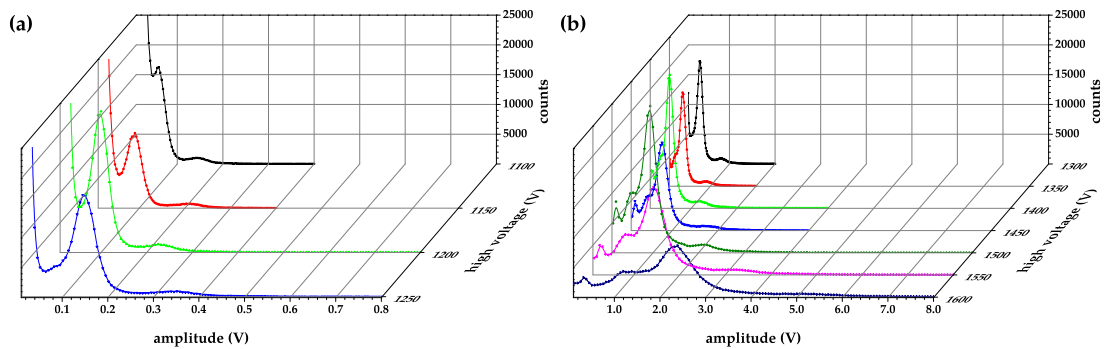

Figure 14 *Multichannel analysis spectra obtained for 95.0 % Ar and 5.0 % CH$_4$ mixture, while applying (a) 1100–1250 V and (b) 1300-1600 V supply voltage.*

As shown in Figure 15 (multichannel analysis for 92.5 % Ar and 7.5 % CH$_4$ in a mixture), the next increase in the energy resolution is observed at 1100 V. Moreover, the characteristic escape peak of argon is barely visible till 1300 V.
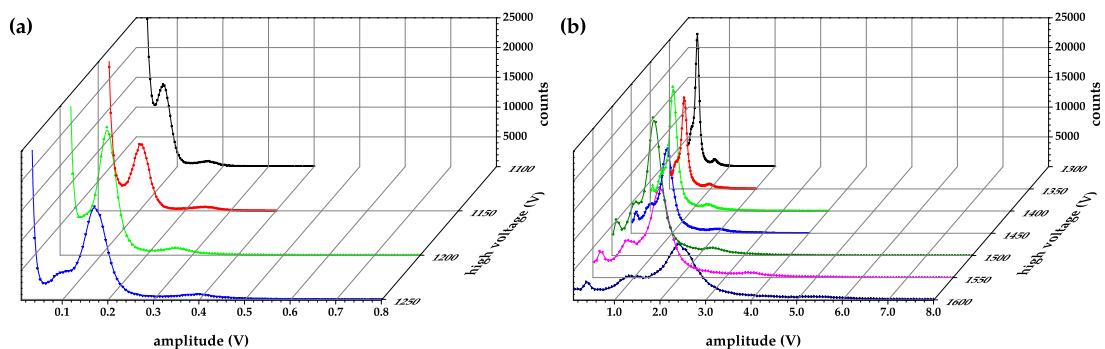

Figure 15 *Multichannel analysis spectra obtained for 92.5 % Ar and 7.5 % CH$_4$ mixture, while applying (a) 1100–1250 V and (b) 1300-1600 V supply voltage.*

The multichannel analysis spectra for the most common gas mixture (90.0 % of Ar and 10.0 % of CH$_4$) used in the area of proportional gas counters are shown in Figure 16. Unfortunately, the inappropriate option of the vertical range of the input channel (for 1100 V and 1150 V supply

24

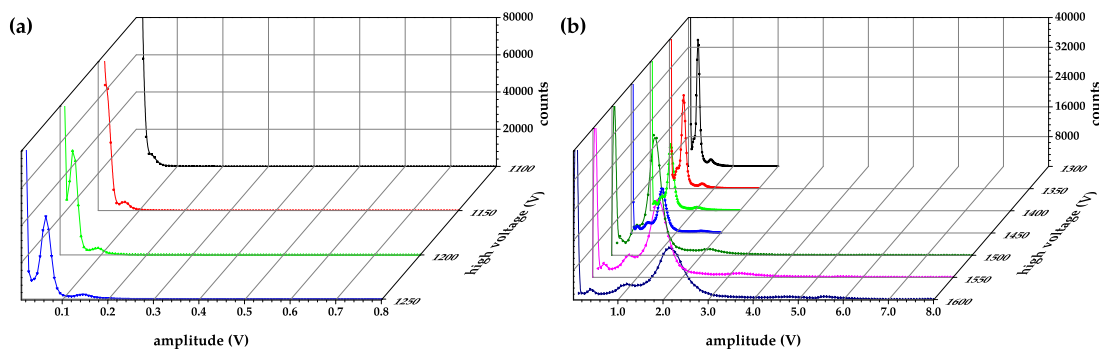voltage) makes the determination of the energy resolution impossible (especially for 6.4 keV X-rays peak).

Figure 16 *Multichannel analysis spectra obtained for 90.0 % Ar and 10.0 % CH$_4$ mixture, while applying (a) 1100–1250 V and (b) 1300-1600 V supply voltage.*

On the other hand, the detector high voltage working area for this gas mixture is probably higher than 1150 V. Figure 17 presents the multichannel analysis spectra for the 87.5 % Ar and 12.5 % CH$_4$ mixture. While using this gas mixture as a counting gas, the first evidence of the characteristic escape peak argon appears at 1200 V.
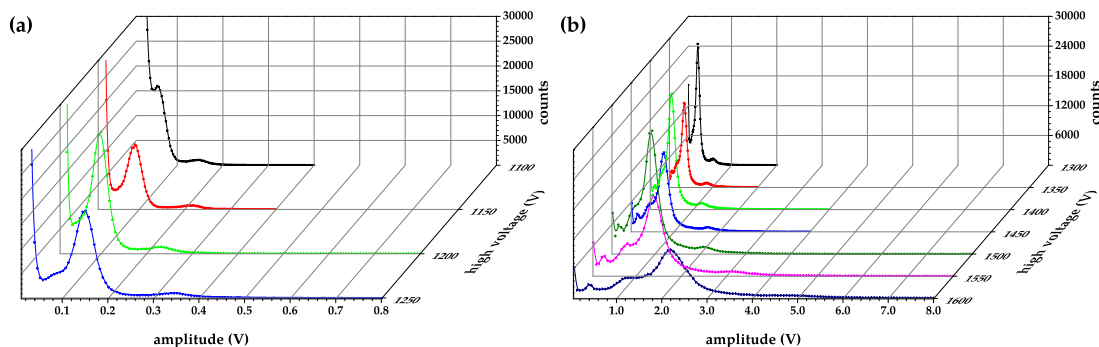

Figure 17 *Multichannel analysis spectra obtained for 87.5 % Ar and 12.5 % CH$_4$ mixture, while applying (a) 1100–1250 V and (b) 1300-1600 V supply voltage.*

The last analyzed gas mixture was 85.0 % of Ar and 15.0 % of CH$_4$. Its multichannel analysis spectra are demonstrated in Figure 18. The results are similar to those, which were observed using the 87.5 % Ar and 2.5 % CH$_4$ mixture. The escape peak is barely visible from 1200 V and the energy resolution increases with the increase in the supplied voltage.
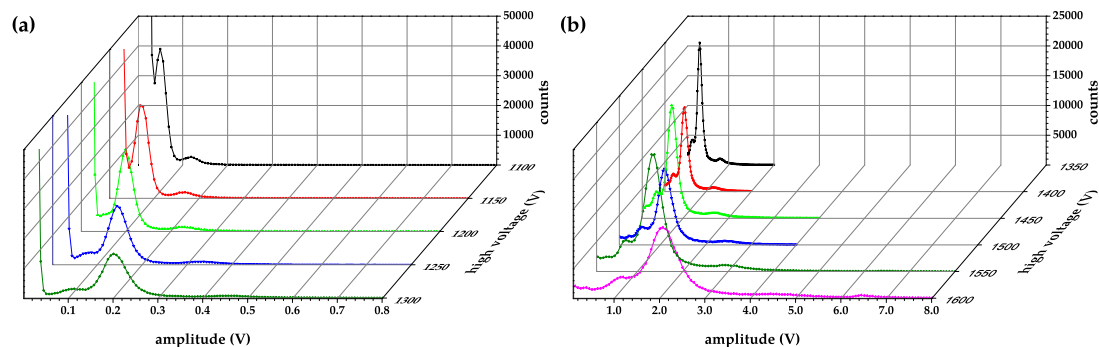

Figure 18 *Multichannel analysis spectra obtained for 85.0 % Ar and 15.0 % CH$_4$ mixture, while applying (a) 1100–1300 V and (b) 1350-1600 V supply voltage.*

Multichannel analysis spectra obtained with pure krypton as counting gas are shown in Figure 19. While the pure krypton is used, the detector achieves higher energy resolution than with pure argon or its mixtures with methane. The first evidence of the characteristic escape peak of krypton (1.8 keV) is at 1400 V supply voltage. The origin of this escape peak is the same as the one for characteristic escape peak of argon, which was described above. All the measured multichannel analysis spectra prove that with an increase of supply high voltage, the amplitudes of the pulses grow. It leads to a strong dependence of pulse amplitudes on the stability of the used high voltage supply, which is supported by the Diethorn expression 10.
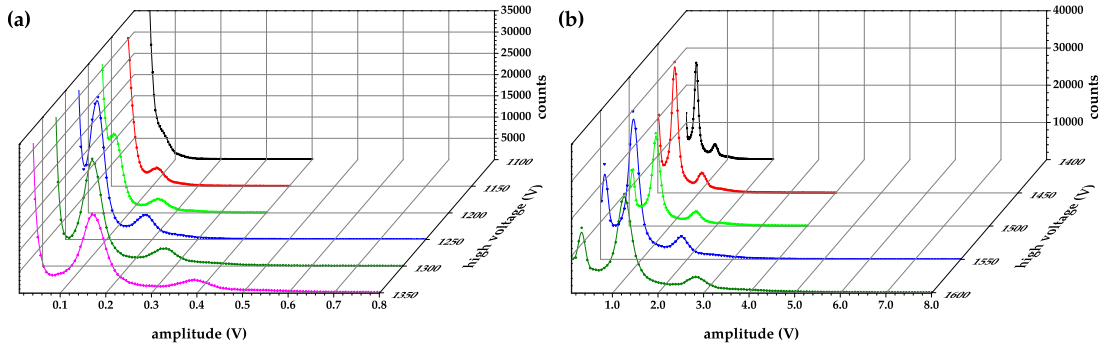

Figure 19 *Multichannel analysis spectra obtained for pure krypton, while applying (a) 1100–1300 V and (b) 1350-1600 V supply voltage.*

3.4. Energy resolution

Energy resolution R_E for different counting gases was determined from the multichannel analysis spectra shown in Figures 12-19. As the energy resolution depends on the *FWHM* (see equation 13) all the observed full energy peaks (6.4 keV and 14.4 keV) were fitted by the classical Gaussian function defined as

$$y = y_0 + Ae^{-\frac{(x-x_c)^2}{2w^2}},$$ (16)

where y_0 is an offset, A is an amplitude, x_c is a center of the peak and w is a width. The *FWHM* was calculated using the equation

$$FWHM = 2w\sqrt{\ln 4}.$$ (17)

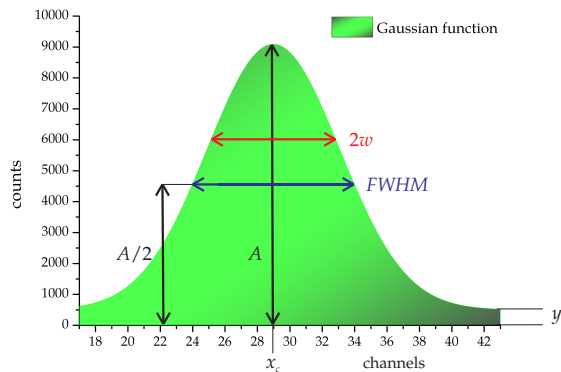All the parameters shown in Figure 20 demonstrates typical Gaussian function.

Figure 20 *Gaussian function parameters of the fitted peak.*

The background compensation was properly provided by the LabVIEW[TM]-based application [60], which is based on the methods used in the commercial spectroscopy systems (ORTEC, CANBERRA). This linear background compensation method is shown in Figure 21 (the 14.4 keV gamma

rays peak obtained with pure krypton at 1350 V). The red line (see Figure 21 (a)) represents the background compensation of the experimental data. Afterwards, the background data are subtracted from the recorded spectra and the corrected experimental data are fitted by the Gaussian function (see Figure 21 (b)). The fit quality could be determined by R^2 value (also known as coefficient of determination; ideal fit gives $R^2 = 1$). R^2 value rises with more parameters introduced, but this does not imply a better fit. The adjusted $R^2_{\text{adj.}}$ value accounts for the degrees of freedom and it is a better measure of the fit precision. Hence, this parameter is used for determination of fit qualities below. In this case, the $R^2_{\text{adj.}}$ value is 0.99545, which means that the residual data (residual sum of squares) of the fit are 0.455 %. For all calculations, the Origin$^{\text{TM}}$-software was used.
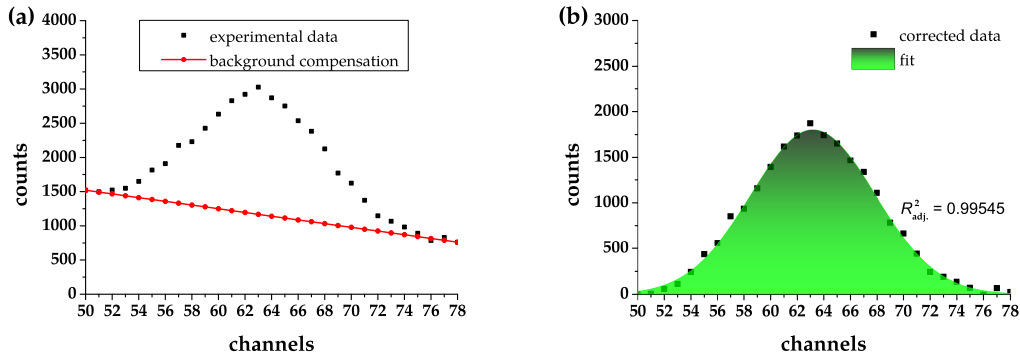

Figure 21   *Full energy peak of the 14.4 keV gamma rays obtained for krypton at 1350 V: (a) linear background compensation and (b) fit of the corrected data.*

Whereas the full energy 14.4 keV gamma peak is simple to fit by one Gaussian function, the ^{57}Fe X-rays full energy peak theoretically consists of three Gaussian functions in the obtained multichannel analysis spectra. The probability of different X-rays emissions and their energies are determined by the decay scheme of ^{57}Fe (see Table 8) [7].

Table 8   *Probabilities of X-rays emissions from ^{57}Fe.*

Type of X-rays	Energy (keV)	Probability of emission
Fe $X_{K\alpha 1}$	6.40384	16.8 ± 0.3 %
Fe $X_{K\alpha 2}$	6.39084	33.2 ± 0.5 %
Fe $X_{K\beta}$	$7.058 - 7.108$	7.1 ± 0.2 %

Basically, it is impossible to achieve enough high energy resolution for distinguishing these low energy differences by using the proportional gas counters. However, their presence affects the fit quality $R^2_{\text{adj.}}$ value. Thus, it is necessary to fit the X-rays full energy peak area at least by using two Gaussian functions. The Fe $X_{K\alpha 1}$ and Fe $X_{K\alpha 2}$ energies are very close (the difference between them is only 0.013 keV) and their centers correspond to almost same channels in multichannel analysis spectra. On the other hand, the energy difference between Fe $X_{K\beta}$ and Fe $X_{K\alpha 2}$ is in the range from 0.66716 keV to 0.71716 keV, so the Fe $X_{K\beta}$ can affect the right side of the total fit. Moreover, at 1200 V and above (for argon and its mixtures), a next peak has to be added to the fitted data, because the escape peak of argon (3.4 keV, created by Fe $X_{K\alpha}$) starts to occur. The argon gamma rays absorption probability (see Table 3) and K fluorescence yield of argon (ω_K is in the range from 0.08 to 0.14 [61]) are low, so escape peak created by gamma rays was not observed in the multichannel analysis spectra. In fact, K fluorescence yield ω_K determinates the probability of escape peak creation. The krypton escape peak (ω_K is in the range from 0.62 to 0.67 [62]) has lower energy (1.8 keV, created by the 14.4 keV gamma rays) and is not included in the fitting data. The condition for the escape peak production is that ionization rays energy has to be higher than the absorption edge of the given gas. The K absorption edge of krypton is 14.32 keV (3.20 keV for argon), so no escape peak is created by Fe $X_{K\alpha}$. Figure 22 (a) demonstrates theoretical fit distribution (including argon escape peak) of different X-rays types in the recorded multichannel analysis spectrum for 95.0 % Ar and 5.0 % CH$_4$ mixture at 1450 V. Subsequently, Figure 22 (b) shows real fit of this spectrum using three Gaussian functions, which were used to determine energy resolution of the toroidal proportional gas counter for X-rays detection.
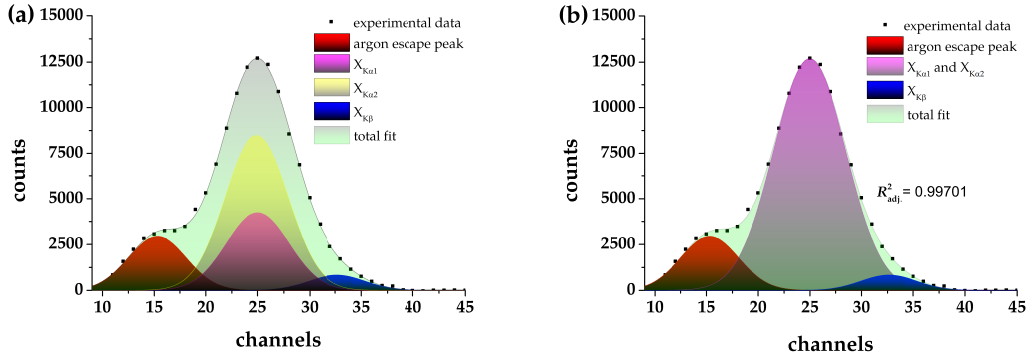
Figure 22   *(a) Theoretical fit distribution of the multichannel analysis spectrum obtained for 95.0 % Ar and 5.0 % CH$_4$ mixture at 1450 V and (b) real fit by using three Gaussian functions.*

Energy resolution of the detector was determined separately for the X-rays (Fe X$_{K\alpha 1}$ and Fe X$_{K\alpha 2}$, counted at 6.4 keV) and for the full peak of 14.4 keV gamma rays. The energy resolution R_E values together with the $R^2_{adj.}$ values calculated for pure argon are shown in Figure 23.
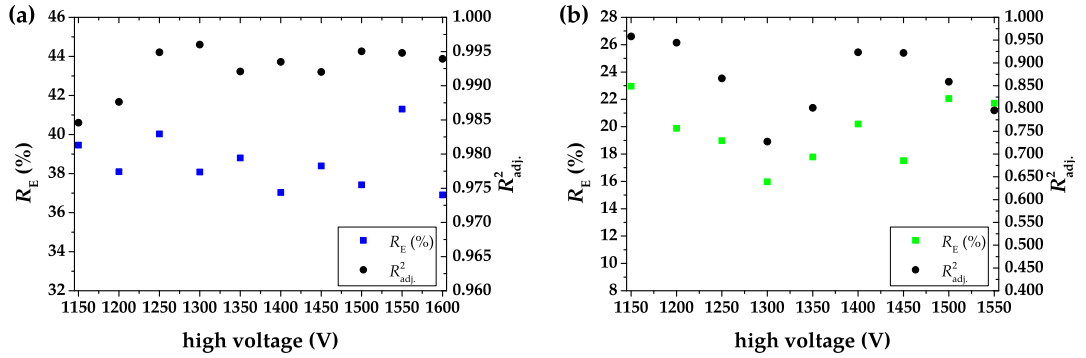

Figure 23   *Energy resolution R_E and quality of the fit $R^2_{adj.}$ while using pure argon as a counting gas for (a) the 6.4 keV X-rays and (b) the 14.4 keV gamma rays.*

Unfortunately, the Gaussian fits qualities (especially for 14.4 keV) were very low. It is given by the non-stability of pure argon as a counting gas. The quenching gas is usually added to this noble gas to ensure each pulse discharge termination. As it is shown in Figure 24 (the energy resolution and appropriate $R^2_{adj.}$ values for 97.5 % Ar and 2.5 % CH$_4$ mixture), adding of the quenching gas also decreases the energy resolution value.

It is necessary to mention that some data (especially for 1100 V and 1600 V) are missing. It is caused by the low value of high voltage, which does not provide enough electron-ion pairs for signal creation or by the high influence of the noise to the signal. The energy resolution values with appropriate $R^2_{adj.}$ values for 95.0 % Ar and 5.0 % CH$_4$ mixture are shown in Figure 25.

From the calculated energy resolution values, it is clear that high voltage has a big impact on them. An increase in supplying high voltage leads to the drop of energy resolution value. Some deviation between the high voltage steps are caused by changing of the digitizer input channel vertical range, which was considered as an experimental error. Each increase in the vertical range causes an artificial increase of the energy resolution value. Because the number of channels was always constant (257, in the range of ± 128 channels), the coefficient of the voltage value per channel grows with widening the vertical range. This fact has a negative impact on all the recorded multichannel analysis spectra. Figure 26 presents the energy resolution values and the $R^2_{adj.}$ values calculated for 92.5 % Ar and 7.5 % CH$_4$ in a mixture.

The fit quality of the 6.4 keV X-rays (given by $R^2_{adj.}$ value) is basically higher than the one obtained for the 14.4 keV gamma rays. One of the possible reasons is that Compton scattering becomes dominant at descending edge of the 14.4 keV gamma rays peak and Compton edge has a negative effect on the resultant fit. This phenomena was observed in all the recorded multichan-
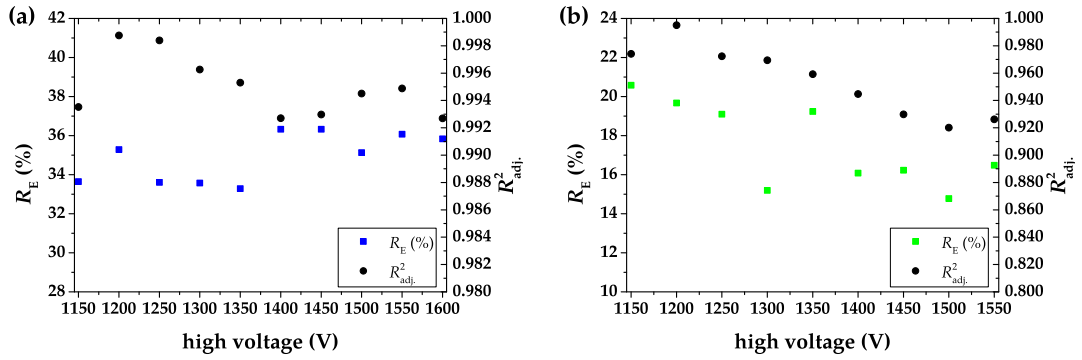
Figure 24   *Energy resolution R_E and quality of the fit $R^2_{adj.}$ while using 97.5 % Ar and 2.5 % CH$_4$ mixture as a counting gas for (a) the 6.4 keV X-rays and (b) the 14.4 keV gamma rays.*

Figure 25   *Energy resolution R_E and quality of the fit $R^2_{adj.}$ while using 95.0 % Ar and 5.0 % CH$_4$ mixture as a counting gas for (a) the 6.4 keV X-rays and (b) the 14.4 keV gamma rays.*
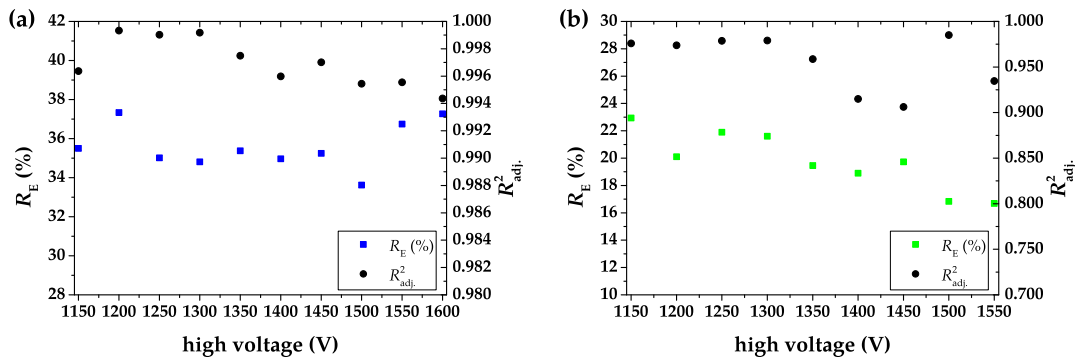

Figure 26   *Energy resolution R_E and quality of the fit $R^2_{adj.}$ while using 92.5 % Ar and 7.5 % CH$_4$ mixture as a counting gas for (a) the 6.4 keV X-rays and (b) the 14.4 keV gamma rays.*
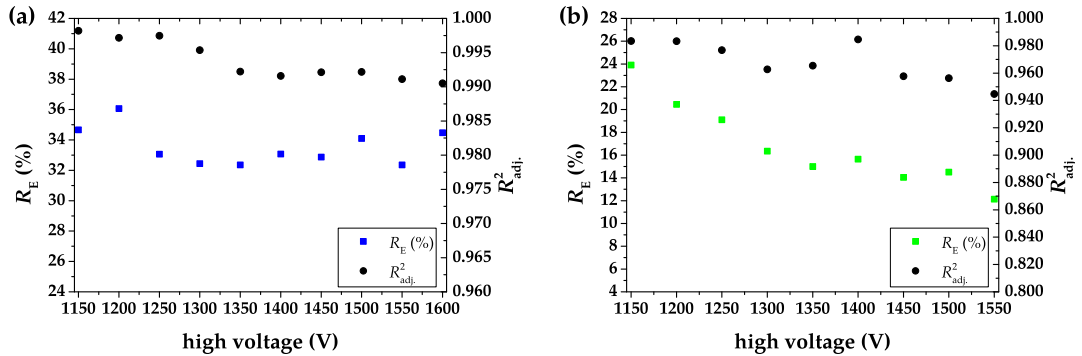
nel analysis spectra. The energy resolution values with appropriate $R^2_{adj.}$ values of the fit for the 90.0 % Ar and 10.0 % CH$_4$ gas mixture are shown in Figure 27.

The increase in the methane concentration (up to 10.0 %) in the Ar-CH$_4$ gas mixtures leads to the decrease in energy resolution values. The comparison of energy resolution values in Figures 27, 28 (87.5 % Ar and 12.5 % CH$_4$), and 29 (85.0 % Ar and 15.0 % CH$_4$) proves that additional increase in the methane concentration (over 10.0 %) slightly increases the energy resolution values (especially for the 6.4 keV X-rays).
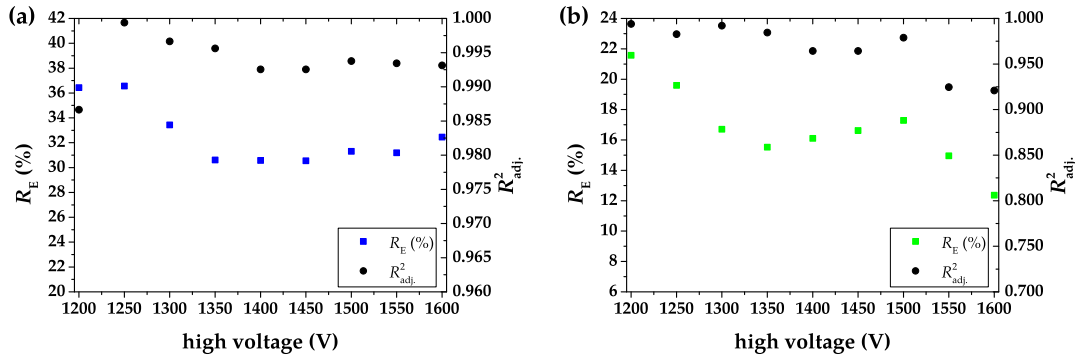
Figure 27   *Energy resolution R_E and quality of the fit $R^2_{adj.}$ while using 90.0 % Ar and 10.0 % CH$_4$ mixture as a counting gas for (a) the 6.4 keV X-rays and (b) the 14.4 keV gamma rays.*

Figure 28   *Energy resolution R_E and quality of the fit $R^2_{adj.}$ while using 87.5 % Ar and 12.5 % CH$_4$ mixture as a counting gas for (a) the 6.4 keV X-rays and (b) the 14.4 keV gamma rays.*

Figure 29   *Energy resolution R_E and quality of the fit $R^2_{adj.}$ while using 85.0 % Ar and 15.0 % CH$_4$ mixture as a counting gas for (a) the 6.4 keV X-rays and (b) the 14.4 keV gamma rays.*
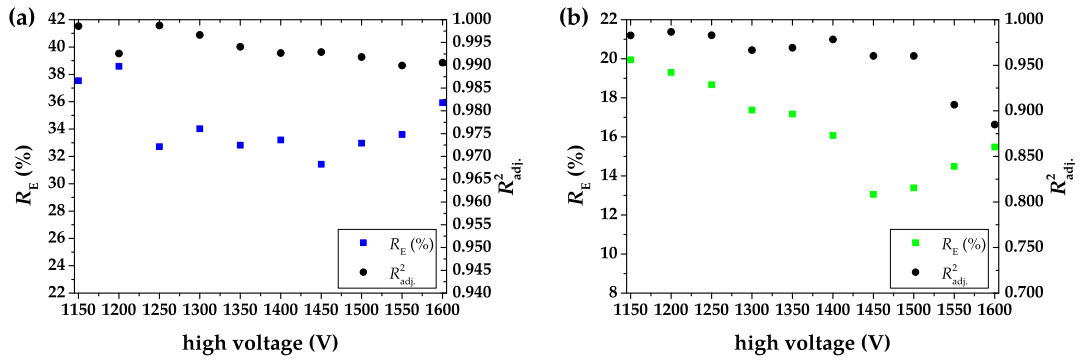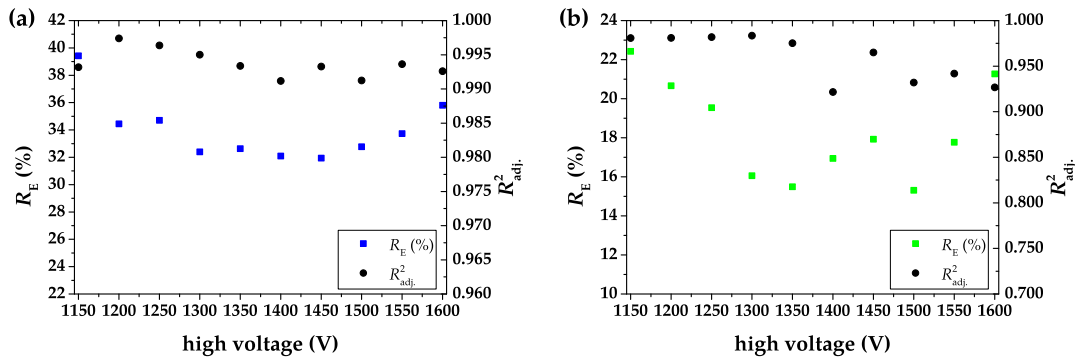
While the $R^2_{adj.}$ values of the Gaussian fit for argon and its mixtures with methane were typically in the range from 0.9000 to 0.9800 (the full energy 14.4 keV gamma rays peak), the $R^2_{adj.}$ values appropriating to the same energy peak obtained for krypton as a counting gas were always higher than 0.9800 (see Figure 30). It is probably caused by a higher absorption probability of the 14.4 keV gamma rays (see Table 3). Other reason could be a lower energy resolution values leading to better distinction of Compton edge. Thus, it can be excluded from full energy peak and has no influence on the fit.
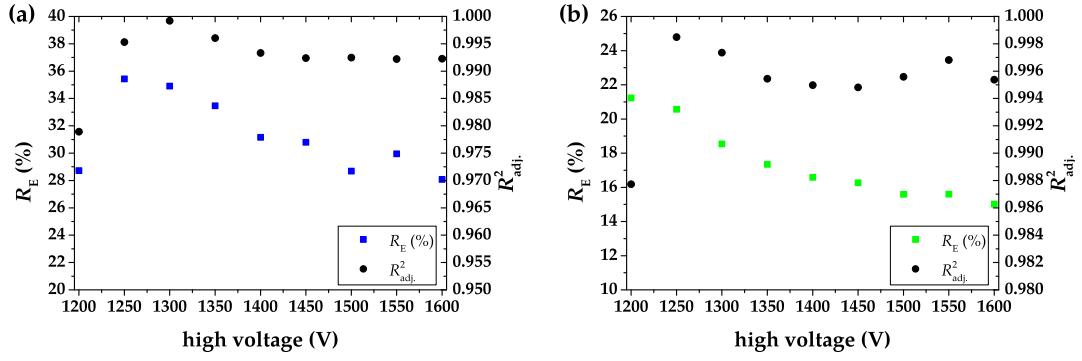
30

Figure 30 | *Energy resolution R_E and quality of the fit $R^2_{adj.}$ while using pure krypton as a counting gas for (a) the 6.4 keV X-rays and (b) the 14.4 keV gamma rays.*

There is a decreasing trend of all energy resolution values with increasing high voltage value. Generally, the quality of the fit $R^2_{adj.} > 0.99$ for the 6.4 X-rays fit was reached in almost all the cases. This means that the amount of the residual data excluding the fit were lower than 1 %. The same fit quality was achieved for 14.4 keV gamma rays peak (only when krypton was used as a counting gas). Table 9 summarizes minimum reached energy resolution values R_X (for 6.4 keV X-rays) and R_γ (for 14.4 keV gamma rays) with appropriate $R^2_{adj.}$ values for all the tested counting gases.

Table 9 | *Minimum reached energy resolution values R_X and R_γ with appropriate $R^2_{adj.}$ values for all tested counting gases.*

Counting gas	R_X	$R^2_{adj.}$ (for R_X)	R_γ	$R^2_{adj.}$ (for R_γ)
pure argon	37 %	0.99350	16 %	0.72751
97.5 % Ar, 2.5 % CH$_4$	33 %	0.99530	15 %	0.96948
95.0 % Ar, 5.0 % CH$_4$	34 %	0.99545	17 %	0.98508
92.5 % Ar, 7.5 % CH$_4$	32 %	0.99536	**12 %**	0.94471
90.0 % Ar, 10.0 % CH$_4$	**31 %**	0.99561	**12 %**	0.92100
87.5 % Ar, 12.5 % CH$_4$	**31 %**	0.99292	13 %	0.96031
85.0 % Ar, 15.0 % CH$_4$	32 %	0.99501	15 %	0.97527
pure krypton	**28 %**	0.99227	**15 %**	0.99538

While the minimum achieved energy resolution value for 6.4 keV X-rays ($R_X = 28$ %) was reached when the pure krypton was used as a counting gas, the maximum value ($R_X = 37$ %) was determined for pure argon. Adding quenching gas (methane) to argon decreases this value and the lowest energy resolution value ($R_X = 31$ %) was obtained when the gas mixture was 90.0 % of Ar and 10.0 % of CH$_4$. This gas mixture ratio was found as the best one as in [56,58,63]. The same energy resolution value for 6.4 keV X-rays was reached when using the 87.5 % Ar and 12.5 % CH$_4$ mixture as a counting gas. On the other hand, minimum energy resolution value for the 14.4 keV gamma rays ($R_\gamma = 12$ %) was observed when 92.5 % Ar and 7.5 % CH$_4$ in a mixture (the same value for 90 % Ar, 10 % CH$_4$ mixture) was used as a counting gas. The lowest energy resolution value for krypton was $R_\gamma = 15$ %. The published toroidal proportional counters [53,55,56] have energy resolution for the 14.4 keV gamma rays (energy resolution values for the 6.4 keV X-rays are not mentioned) in the range from 25 % to 19 %. The toroidal proportional gas flow counter developed within this dissertation thesis reached energy resolution values for the same energy peak in the range from 17 % to 12 %, while various types of gases were used as counting gases.

3.5. Energy proportionality

The characteristic escape peak of argon (at 1250-1300 V and above, see Figures 12-18) appears in the multichannel analysis spectra, and its energy of 3.4 keV is commonly known [25]. For krypton, the escape peak has lower energy i.e., 1.8 keV [54], and it starts to appear at 1450 V and above (see Figure 19). With respect to this fact, energy proportionality of the detector could be beneficially determined by using one radiation source (in this case, ^{57}Co). The peak maximum channel

positions were obtained from the previous Gaussian fits (chapter 3.4). These values correspond to the energies given by the ^{57}Co decay scheme (i.e., the 6.4 keV X-rays, the 14.4 keV gamma rays and relevant escape peaks of used counting gas). Because energy distribution should be proportional, pulse amplitudes (represented by the channel number) the dependence of on energy values has to be linear. Therefore, the data were fitted by using the simple equation

$$y = a + bx, \tag{18}$$

where the a is y-intercept and b is line slope. The linear regressions of the energy distribution for pure argon and a 97.5 % Ar and 2.5 % CH$_4$ mixture are shown in Figure 31. In fact, energy proportionality is determined by the $R^2_{\text{adj.}}$ value, which represents the linear regression quality (perfect one with $R^2_{\text{adj.}} = 1$).
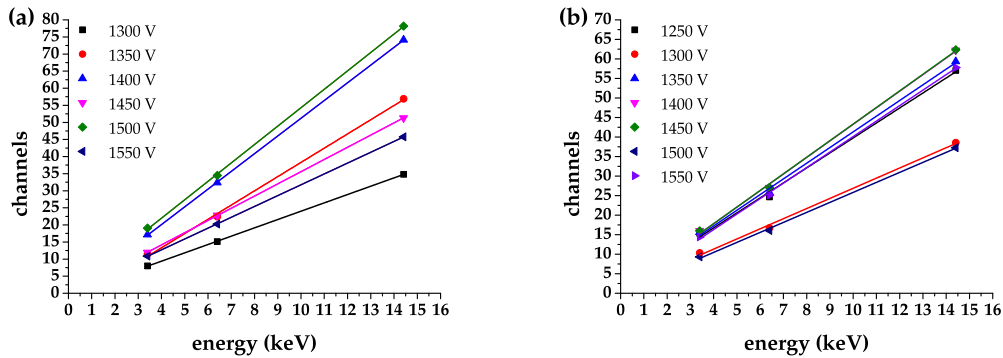

Figure 31 | *Linear regression of energy distribution for (a) pure argon and (b) 97.5 % Ar and 2.5 % CH$_4$ mixture.*
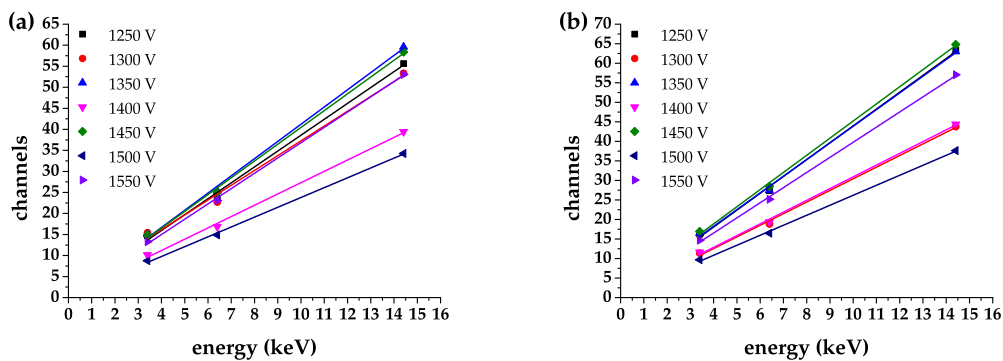

Figure 32 | *Linear regression of energy distribution for (a) 95.0 % Ar, 5.0 % CH$_4$ mixture and (b) 92.5 % Ar, 7.5 % CH$_4$ mixture.*

When using pure argon or its mixture with 2.5 % of methane, energy proportionality deviation never exceeded 0.5 %. The same non-linearity was achieved by using the 92.5 % Ar and 7.5 % CH$_4$ mixture (see Figure 32 (b)). For the 95.0 % Ar and 5.0 % CH$_4$ gas mixture (see Figure 32 (a)), this deviation was in the range from 0.5 % to 1.5 %. These energy proportionality deviations $R^2_{\text{adj.}}$ are shown in Figure 33.

The linear regression for the applied voltage of 1600 V is not presented in Figures 31-33, because the residual data of Gaussian fit reached high values and maximum positions were loaded by high deviation. The linear regressions of energy distribution obtained for the 90.0 % Ar, 10.0 % CH$_4$ and 87.5 % Ar , 12.5 % CH$_4$ gas mixtures are shown in Figure 34.

Figure 35 (a) presents the linear regression of the energy distribution when the 85.0 % Ar and 15.0 % CH$_4$ gas mixture was used as a counting gas. Because the characteristic escape peak of krypton appears at a high voltage equal to 1450 V and above, the linear regression of energy distribution is presented only in the range from 1450 V up to 1600 V for pure krypton (see Figure 35 (b)). The lowest energy proportionality deviations from all the tested counting gases were achieved for pure krypton ($R^2 > 0.999$, see Figure 36 (b)).
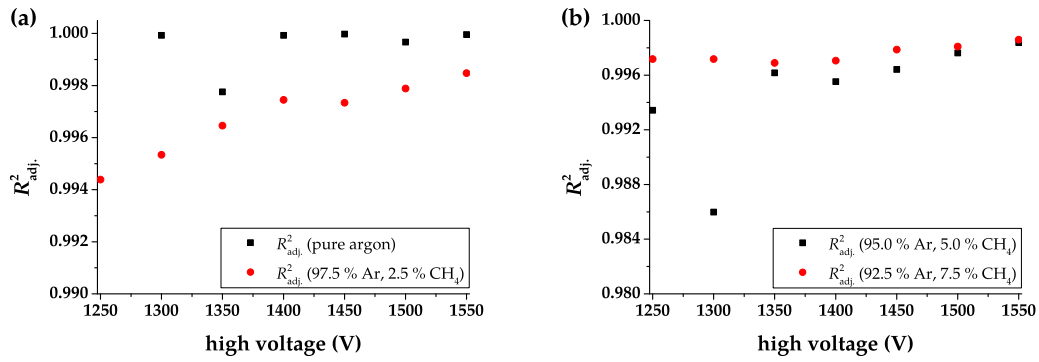
32

Figure 33   *Energy proportionality deviations for (a) pure argon and 97.5 % Ar, 2.5 % CH$_4$ mixture and (b) 95.0 % Ar, 5.0 % CH$_4$ and 92.5 % Ar, 7.5 % CH$_4$ mixtures.*
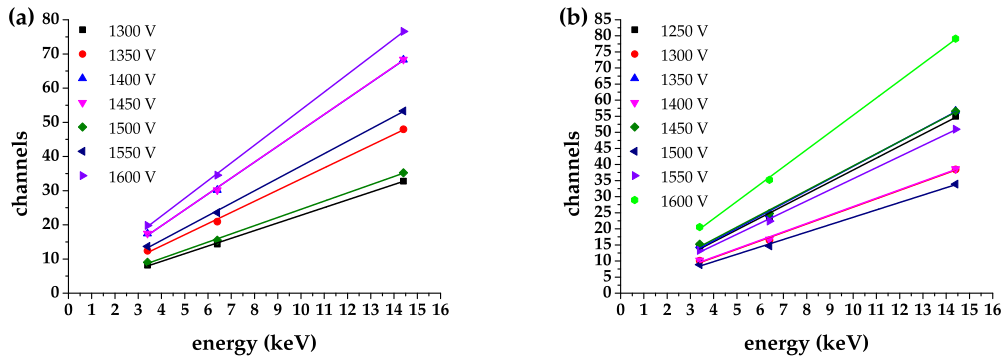

Figure 34   *Linear regression of energy distribution for (a) 90.0 % Ar, 10.0 % CH$_4$ and (b) 87.5 % Ar, 12.5 % CH$_4$ mixtures.*
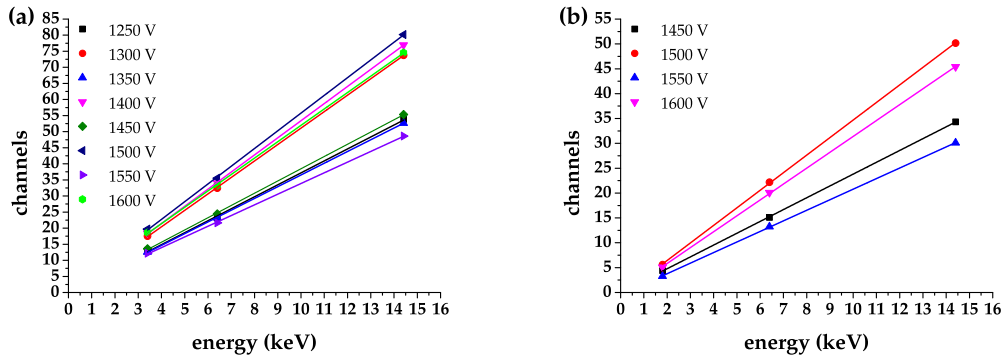

Figure 35   *Linear regression of the energy distribution for (a) 85.0 % Ar, 15.0 % CH$_4$ mixture and (b) pure krypton.*

Free gap occurred in all calculated linear regressions between larger individual voltage steps. It was caused by the vertical range change, which was necessary to perform for all required peaks observation. The developed toroidal proportional gas flow counter achieved high proportionality in the energy region from 1.8 keV to 14.4 keV, where the energy proportionality deviation was in almost all cases lower than 1 % for pure argon and its mixtures with methane (0.1 % for pure krypton). Due to this, the detector is able to work properly in the spectroscopic mode, which requires high energy proportionality.
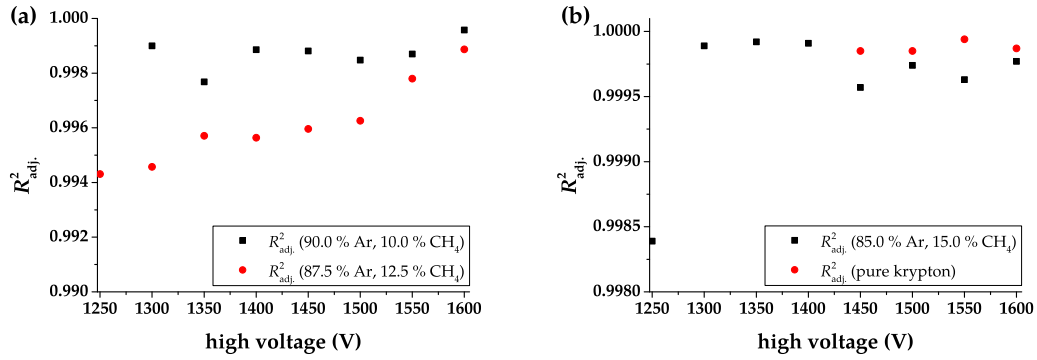
Figure 36 | *Energy proportionality deviations for (a) 90.0 % Ar, 10.0 % CH$_4$ and 87.5 % Ar, 12.5 % CH$_4$ mixtures and (b) 85.0 % Ar, 15.0 % CH$_4$ mixture and pure krypton.*

3.6. Detection efficiency

Detection efficiency ϵ_d of every radiation detector is defined as a ratio of the registered photon events number (sum of counts in the given discrimination window N_c) and the theoretical number of emitted photons N_e incidental on the detector window (see equation 12). The detection efficiency values were calculated via processing the data collected in the chapter 3.3. Firstly, the theoretical numbers of emitted photons N_{eX} and $N_{e\gamma}$ were calculated for every analyzed counting gas. The number of emitted photons was calculated by using the source activities presented in Table 8 and probabilities of different photon emissions (a sum of emission probabilities is shown in Table 8 for the 6.4 keV X-rays including the 7.0 keV X-rays, and probability of the 14.4 keV gamma photon emission is 9.15 ± 0.17 % [7]). Because of the used geometry for recording the multichannel analysis spectra (see Figure 37), the simple point source approximation was calculated to correct the emitted photon number incidental on the counter.
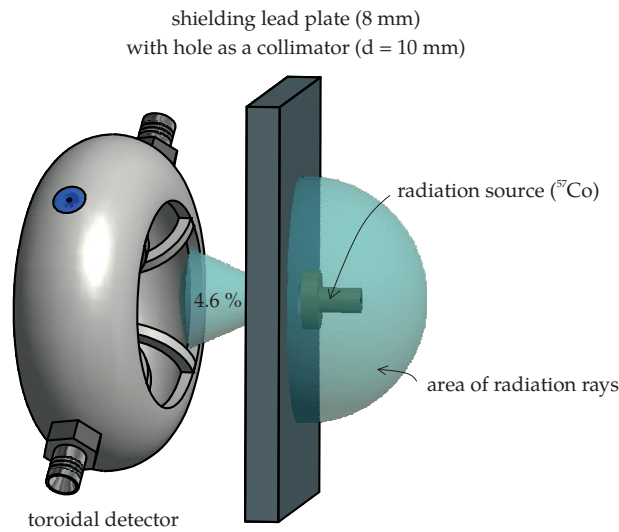

Figure 37 | *Layout of the geometry used for recording the multichannel analysis spectra, with approximate percentage of incidental photons on the counter window (4.6 %).*

All the multichannel analysis spectra were recorded during 50 s (real time). The summary of N_{eX} and $N_{e\gamma}$ for all used counting gases is shown in Table 10.

The number of registered photon events was calculated as the sum of the counts in the relevant discrimination window. For argon and its mixtures, the 6.4 keV X-rays discrimination windows also cover the escape peak (if observed), as it should be a valid detection of X-ray photon. The krypton 1.8 keV escape peak was added to valid detection of the 14.4 keV gamma rays. Detection efficiencies were calculated for manually determined discrimination windows (total sum of counts in the relevant window, see Figure 38 (a)) and also for the same window with the linear background

Table 10 | *Theoretical number of emitted photons N_{eX} and $N_{e\gamma}$ for all tested counting gases.*

Counting gas	N_{eX}	$N_{e\gamma}$
pure argon	$2634176 \pm 10\%$	$419807 \pm 10\%$
97.5 % Ar, 2.5 % CH$_4$	$2509582 \pm 10\%$	$399951 \pm 10\%$
95.0 % Ar, 5.0 % CH$_4$	$2509582 \pm 10\%$	$399951 \pm 10\%$
92.5 % Ar, 7.5 % CH$_4$	$2503191 \pm 10\%$	$398932 \pm 10\%$
90.0 % Ar, 10.0 % CH$_4$	$2946977 \pm 10\%$	$469658 \pm 10\%$
87.5 % Ar, 12.5 % CH$_4$	$2503191 \pm 10\%$	$398932 \pm 10\%$
85.0 % Ar, 15.0 % CH$_4$	$2634176 \pm 10\%$	$419807 \pm 10\%$
pure krypton	$2496815 \pm 10\%$	$397916 \pm 10\%$

compensation (sum of the background counts were subtracted from the total sum of counts, see Figure 38 (b)).
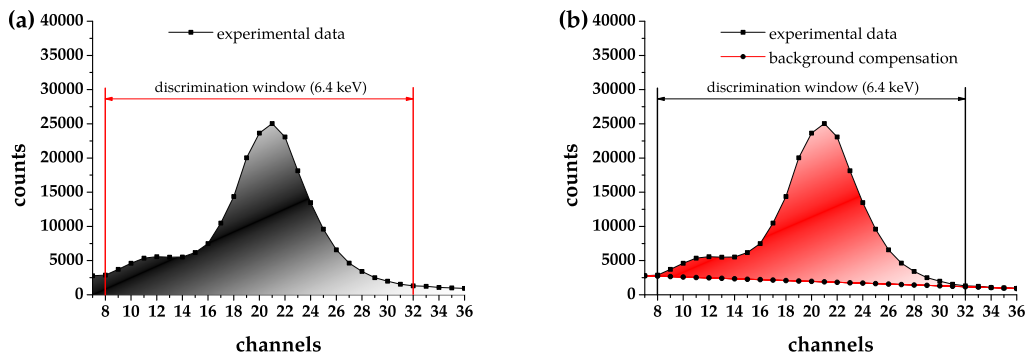

Figure 38 | *The 6.4 keV X-rays discrimination window (90.0 % Ar, 10.0 % CH$_4$, including argon escape peak) for calculating detection efficiency using (a) all counts in the window and (b) linear background compensation to correct the counts number.*

Detection efficiencies were determined for the whole range of supplying high voltage (usually in the interval of 1150-1600 V, if both peaks were observed). The detection efficiencies for pure argon and its mixture with 2.5 % methane are shown in Figure 39.
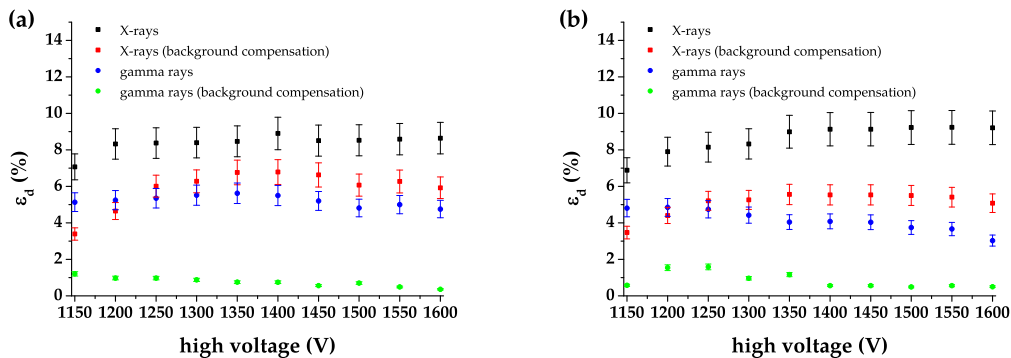

Figure 39 | *Detection efficiency for (a) pure argon and (b) 97.5 % Ar and 2.5 % CH$_4$ mixture.*

In both cases the detection efficiency values grows with the increase of the supplying high voltage. It is also obvious that even a small addition of quenching gas (methane) has a positive impact on the X-rays detection efficiency value (when all counts are summed in the discrimination window). However, this effect is achieved by applying higher supplying voltage (1350 V and above). There is also a rapid decrease in the detection efficiency, when the linear background compensation is applied for all the tested counting gases. Detection efficiency of the 14.4 keV gamma rays was basically much lower than the one obtained for the 6.4 keV X-rays. The detection efficiencies for 95.0 % Ar, 5.0 % CH$_4$ and 92.5 % Ar, 7.5 % CH$_4$ mixtures are shown in Figure 40.
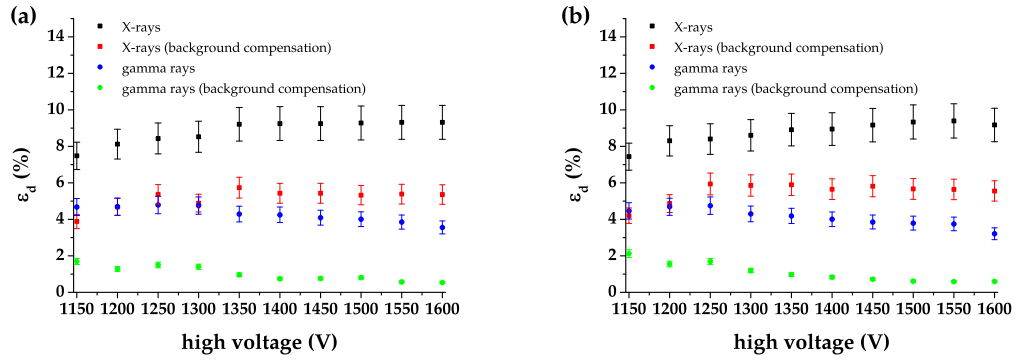
Figure 40 | *Detection efficiency for (a) 95.0 % Ar, 5.0 % CH$_4$ and (b) 92.5 % Ar, 7.5 % CH$_4$ mixtures.*

Generally, detection efficiency values of the 14.4 keV gamma rays decreases with higher supplying voltage. This effect could be explained by a lower energy resolution, so a part of the Compton scattering edge is included in the discrimination window. Figure 41 displays calculated detection efficiencies for 90.0 % Ar, 10.0 % CH$_4$ and 87.5 %, 12.5 % CH$_4$ mixtures.
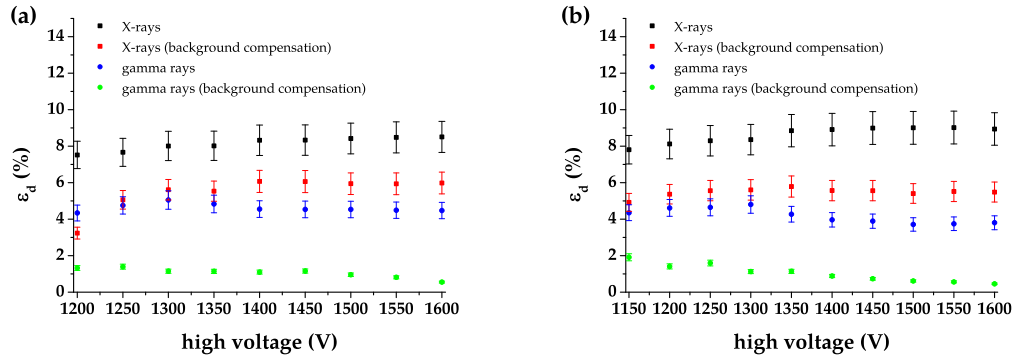
Figure 41 | *Detection efficiency for (a) 90.0 % Ar, 10.0 % CH$_4$ and (b) 87.5 % Ar, 12.5 % CH$_4$ mixtures.*

Further addition of the quenching gas improves the stability of detection efficiency. Especially, if the lower methane concentrations ($2.5 - 7.5$ %) are used, the initial detection efficiency value fluctuations are not so significant. Figure 42 demonstrates detection efficiencies for 85.0 % Ar, 15.0 % CH$_4$ mixture and pure krypton.
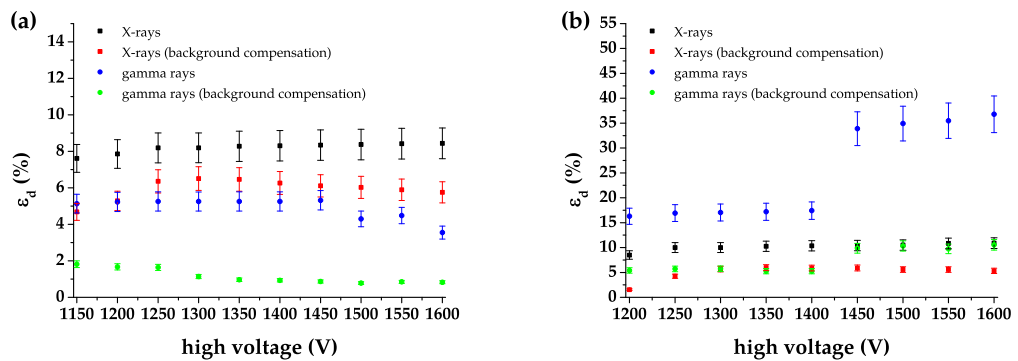
Figure 42 | *Detection efficiency for (a)85.0 % Ar, 15.0 % CH$_4$ mixture and (b) pure krypton.*

As it can be deduced from Table 3, pure krypton has the highest detection efficiency for both ionization rays from all the tested counting gases. The 1.8 keV krypton escape peak was completely hidden in the noise till 1400 V. However, its appearance at 1450 V causes a rapid increase of the

14.4 keV gamma rays detection efficiency. Table 11 provides a summary of the highest calculated detection efficiencies ϵ_d and detection efficiencies with background compensation $\epsilon_{d'}$.

Counting gas	ϵ_{dX} (%)	$\epsilon_{d\gamma}$ (%)	$\epsilon_{d'X}$ (%)	$\epsilon_{d'\gamma}$ (%)
pure argon	8.9	**5.6**	**6.8**	1.2
97.5 % Ar, 2.5 % CH$_4$	9.2	4.8	5.5	1.6
95.0 % Ar, 5.0 % CH$_4$	9.3	4.8	5.7	1.7
92.5 % Ar, 7.5 % CH$_4$	**9.4**	4.7	5.9	**2.1**
90.0 % Ar, 10.0 % CH$_4$	8.5	5.1	6.1	1.4
87.5 % Ar, 12.5 % CH$_4$	9.0	4.8	5.8	1.9
85.0 % Ar, 15.0 % CH$_4$	8.4	5.3	**6.5**	1.8
pure krypton	**10.9**	**36.8**	5.9	**10.6**

The determined accuracy for all the detection efficiency values was ± 10 % from the calculated value. In fact, this accuracy value eliminates any possibility to determine the best counting gas for X-rays regarding the detection efficiency. However, optimal counting gas for the 14.4 keV gamma rays detection is definitely pure krypton reaching up to seven times higher detection efficiency value than pure argon or any of its mixtures with methane.

3.7. Utilization in Mössbauer spectroscopy

The toroidal proportional gas flow counter has been primarily designed for the purpose of the conversion X-rays ^{57}Fe Mössbauer spectroscopy (especially for analysis of the bulk material surfaces). On the other hand, it is also possible to use it for the transmission Mössbauer spectroscopy, when the 14.4 keV gamma rays are registered. In both cases, the experimental setup was modified by adding the velocity driver and the analog feedback [20]. The rest of the experimental setup remains the same as shown in Figure 10. The detection parts of the assembled Mössbauer spectrometers in both geometries are demonstrated in Figure 43.
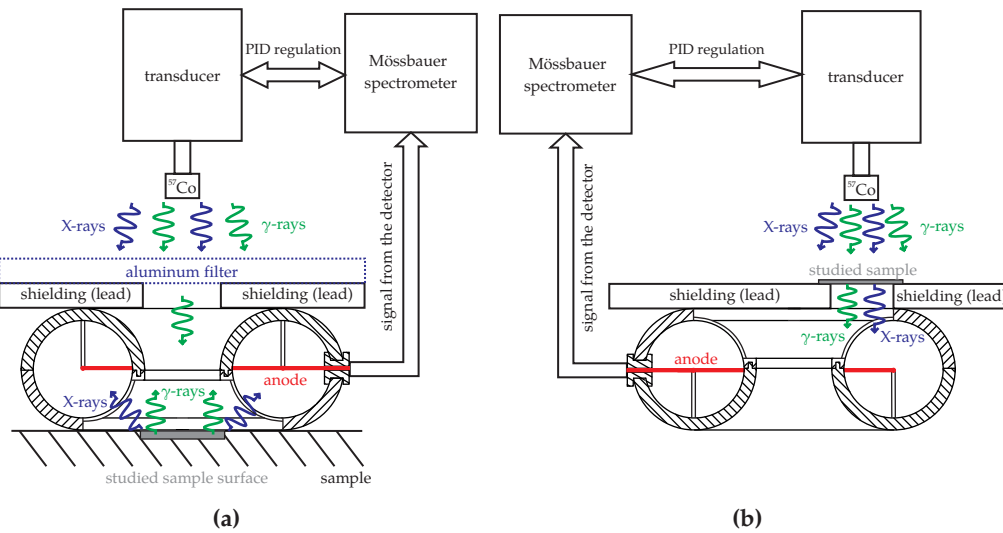
Figure 43 | *Detection part of the Mössbauer spectrometer in the (a) backscattering geometry and (b) transmission geometry.*

As the counting gas, the 90.0 % argon and 10.0 % methane gas mixture was used as it is less expensive compared to the krypton usage. This selected mixture of gases provides the best energy resolution (31 % for the 6.4 keV X-rays and 12 % for the 14.4 keV gamma rays, see chapter 3.4). The gas pressure was approximately 0.1 MPa (identical as in all the multichannel analysis measured in chapter 3.3).

It was verified that the optimal high voltage value is 1400 V (compromise between energy resolution and detection efficiency). Before first ^{57}Fe Mössbauer spectrum recording, multichannel

analysis spectra (see Figure 44) were measured in both geometries using aluminum and copper foil filters. Multichannel analysis spectrum in the backscattering geometry (see Figure 44 (b)) was recorded when a block of the austenitic stainless steel EN 1.4541 (AISI 321) was used as a sample. In this case, the filters were placed on all four detector windows.
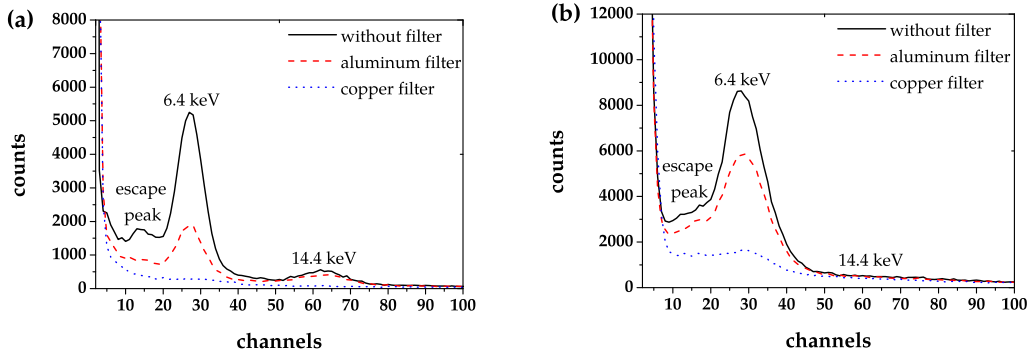

Figure 44 | *Multichannel analysis spectra in the (a) transmission geometry and (b) backscattering geometry.*

Aluminum filters are commonly used in the area of CXMS to reduce the number of lower energy X-rays emitted from the source. These low-energy X-rays are non-resonant and decrease the resonance effect ϵ and the statistical quality Q of the recorded Mössbauer spectrum. The statistical quality Q is given by the equation

$$Q = \frac{\epsilon^2}{\epsilon + 2} N(\infty),$$ (19)

where $N(\infty)$ is the number of counts far from the resonance [64]. A series of aluminum filters with different thicknesses d were placed behind the radiation source (see Figure 43) to evaluate the influence of resonant and non-resonant X-rays. The backscattering ^{57}Fe Mössbauer spectra were obtained for the same period of time (1 hour) for the same sample (a block of the austenitic stainless steel EN 1.4541 (AISI 321)). Then, the data were processed via the MossWinn fitting software [65]. Figure 45 shows the dependence of the calculated effect, statistical quality and the count rate on the thickness of the aluminum filter.
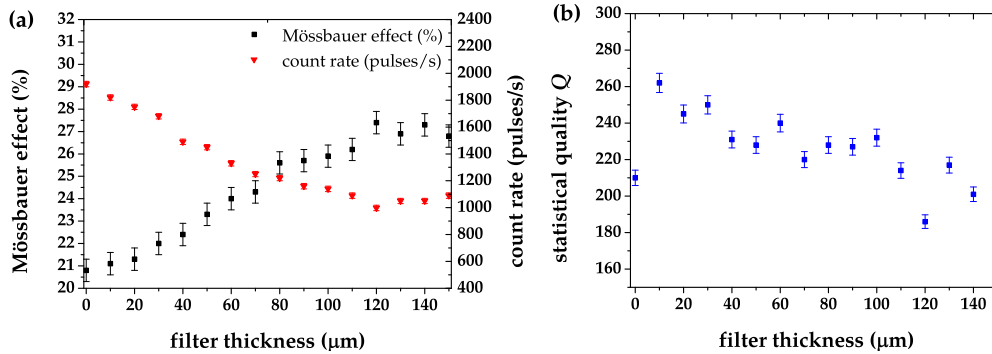
Figure 45 | *The dependence of the (a) Mössbauer effect and count rate and (b) statistical quality on the aluminum filter thickness.*

For increasing the resonant effect and the statistical quality for the practical applications, it is necessary to choose the optimal thickness of the filter. To keep the high count rate and the filtration of some non-resonant X-rays, a 10 μm thick aluminum filter was used for the following measurements in the backscattering geometry.

Figure 46 (a) represents the ^{57}Fe Mössbauer spectrum of the calibration sample α-Fe, whereas the conversion X-rays (6.4 keV) were registered. The line width was determined as 0.258 mm/s and the resonance effect was 9.3 ± 0.5 %. The obtained spectrum of the austenitic stainless steel

block EN 1.4541 (AISI 321) is shown in Figure 46 (b) with the resonance effect of 22.8 ± 0.5 %. Both spectra were recorded for 24 hours.
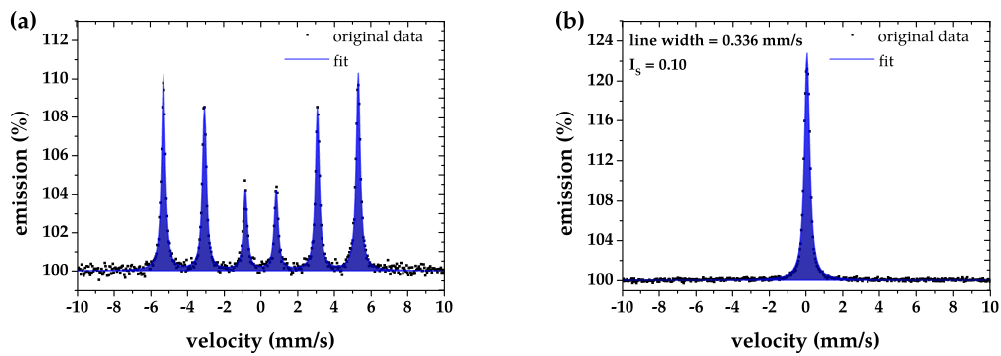
Figure 46 ^{57}*Fe Mössbauer spectra obtained by registration of the 6.4 keV conversion X-rays using the toroidal detector of the (a) α-Fe and (b) austenitic stainless steel EN 1.4541 (AISI 321).*

Figures 47 (a) and (b) demonstrate that the developed detector also allows to register low energy gamma rays. However, the resonance effect was very low, i.e., 3.2 ± 0.5 % in the backscattering geometry (72 hours spectrum) and 17.3 ± 0.5 % in the transmission geometry (1 hour spectrum). Both spectra were obtained for the calibration sample α-Fe.
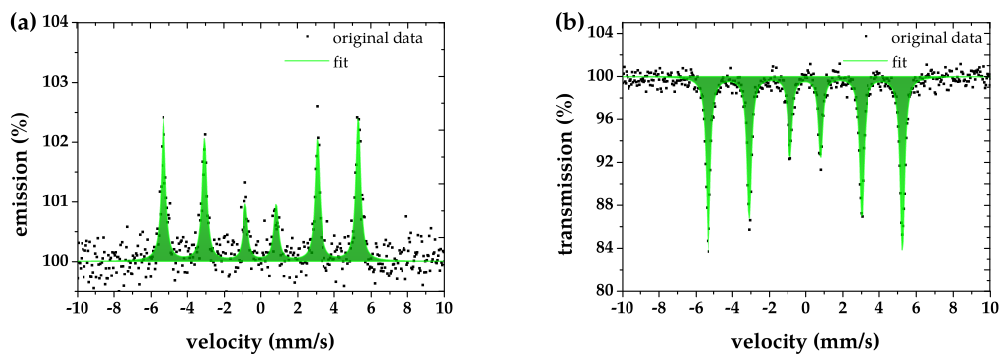

Figure 47 ^{57}*Fe Mössbauer spectra of the α-Fe obtained by registration of the low energy gamma rays (14.4 keV) using the toroidal detector in the (a) backscattering geometry and (b) transmission geometry.*

4. Cylindrical proportional gas counter

As the toroidal shaped proportional gas flow counter (described in the previous chapter 3) is not a very appropriate choice for the purpose of the transmission Mössbauer spectroscopy (only one of four counter windows is used), a cylindrical counter geometry can substitute unnecessarily complicated toroidal shape. The simplest cylindrical proportional counter design has been already described in Figure 5 (see chapter 2).

4.1. Design of the cylindrical counter

The cylindrical proportional gas counter (see Figure 48) was formed by 120 mm long aluminum cylindrical cathode (with an outer diameter of 40 mm, inner diameter of 24 mm). It enclosed central anode (gold plated tungsten wire with a diameter of 50 µm). The anode was supported only by one ABS plastic column (its distance from counter window was approximately 12 mm), as the anode central position was fixed by the ABS plastic reduction located in the rear counter cover. The anode wire was soldered to the coaxial cable RG-62A/U (93 ohm, 42.5 pF/m) with crimped SHV female connector. Front and rear cylindrical cathode sides included grooves for O-rings (26x1, where the inner diameter was 26 mm and the ring thickness was 1 mm) for better counter sealing. The detector window had lateral location and was made from aluminized mylar foil. This window was curved for keeping the cylindrical counter shape (90° sector) and was 40 mm long. In fact, the mylar foil copied the inner wall shape of the cylindrical cathode. The conductive mylar window layer was located in the counter working volume. Electrical conductivity between the aluminum cylinder and the mylar window was provided by the carbon conductive glue. The counter window was sealed with a two-components putty (Thorlabs' Vacuum epoxy resin) to prevent gas leakages. Both (rear and front) covers were fixed by using four M3 screws for properly O-rings work. Due to the possibility of some gas leakages, this proportional gas counter was designed to work in the continuous flow mode using the gas inlet and outlet.

Figure 48 | *Designed cylindrical proportional gas counter: (a) basic layout and (b) cross section.*

4.2. Experimental setup and basic parameters

With respect to the observation and experiences obtained with toroidal proportional gas flow counter in chapter 3, the experimental setup was modified for testing the cylindrical proportional gas flow counter. As most possible utilization of this counter is in the area of the transmission Mössbauer spectroscopy, pure krypton (approximate pressure of 0.1 MPa) was chosen as a counting gas (best detection efficiency for low gamma rays from the tested gases – see chapter 3.6). The detector was supplied by the very stable high voltage supply 556 (ORTEC). The current pulses were converted into the voltage signal with a high signal-to-noise ratio by the 142PC preamplifier (ORTEC). Consequently, the low voltage signal was amplified (the gain was set to ×5 and the shaping time 0.5 µs) by the 575A amplifier (ORTEC). The amplified signal was recorded by the

fast digitizer NI PCI-5124 (National Instruments) and processed by the LabVIEW™-based user application [18]. The proposed experimental setup is shown in Figure 49.

Figure 49 | *Experimental setup for testing cylindrical proportional gas flow counter.*

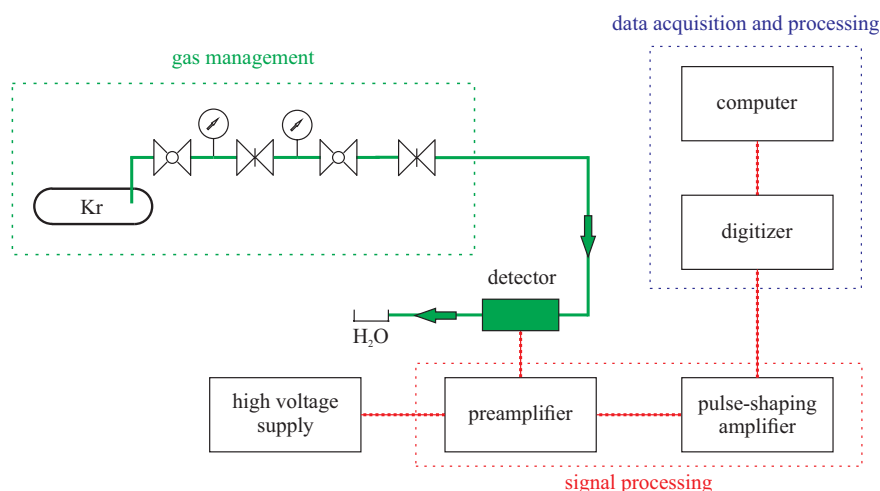As no quenching was added to pure krypton, registered pulses from the detector were slightly longer (see Figure 50) than the ones obtained using the toroidal proportional gas counter filled with a mixture of argon and methane (see Figure 11 in chapter 3.2).
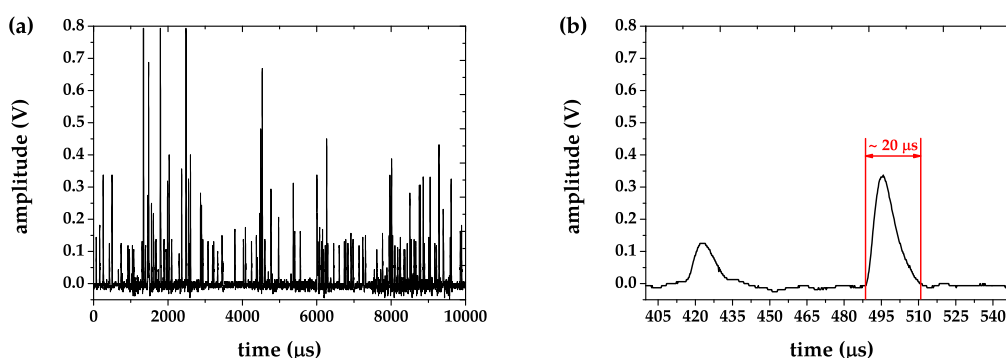

Figure 50 | *(a) Amplified signal from the cylindrical proportional gas flow counter using pure krypton (1550 V) as a counting gas, and (b) detailed view of pulse shapes.*

Multichannel analysis spectra were recorded in the transmission geometry, while ^{57}Co radiation source (1.85 GBq on 18th October, 2013 with a current activity of approximately 22 MBq) was directed straight to the detector window. No samples were used during these measurements. The real time period of the sampled signal was 25 s. Brass disc (with a thickness of 10 mm) was used as collimator with 10 mm diameter hole. Aluminum and copper filters were used to determine the energy arrangement. High voltage supply range was from 1200 V to 1750 V with a step of 50 V. As shown in Figure 51 (a), the low energy gamma rays full energy peak started to appear exactly at 1200 V with a very dominant Compton edge. With further high voltage supply increase, the 6.4 keV X-rays started to be visible (vaguely at 1250 V, clearly at 1300 V and above). The first evidence of the 1.8 keV krypton escape peak was at 1450 V. Next increase of the supplying high voltage caused better krypton escape peak resolution. The digitizer vertical range was constantly set to ±0.8 V for multichannel analysis spectra recording shown in Figure 51 (a). In the high voltage supply range of 1600-1650 V (1700-1750 V respectively), the digitizer vertical range was ±2 V (±4 V respectively). The multichannel analysis spectra obtained in these ranges are shown in Figure 51 (b). Because of the large amount of data collected, only the multichannel analysis spectra recorded without filters are presented below.
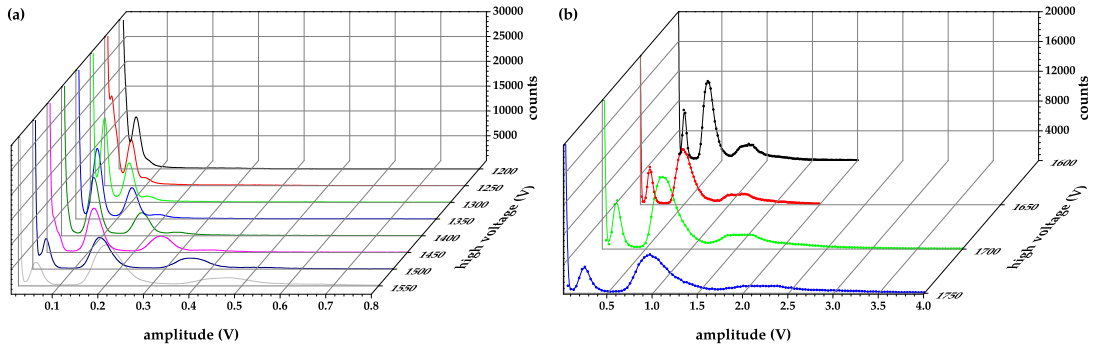
Figure 51 | *Multichannel analysis spectra recorded using the cylindrical proportional gas flow counter with krypton as a counting gas, while applying (a) 1200-1550 V and (b) 1600-1750 V supply voltage.*

Figure 52 shows multichannel analysis spectra at 1500 V using aluminum and copper filter (located between radiation source and cylindrical proportional gas flow counter), where the spectrum recorded with aluminum filter confirms the energy arrangement and the 1.8 keV krypton escape peak gamma registration validity.
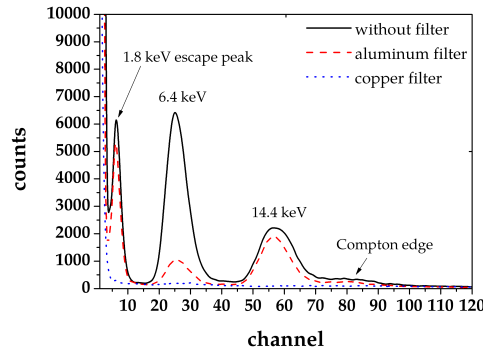

Figure 52 | *Multichannel analysis spectra at 1500 V recorded with aluminum and copper filter.*

Energy resolution R_E values were determined for both types of ionization rays (the 6.4 keV X-rays and the 14.4 keV gamma rays). All the experimental data were corrected by the linear background compensation presented in chapter 3.6. Consequently, the full energy peaks were fitted by the Gaussian function and the *FWHM* parameters were calculated. The energy resolution values for X-rays with appropriate $R^2_{adj.}$ values are shown in Figure 53 (a) (in Figure 53 (b) for gamma rays respectively).

The minimum achieved energy resolution value for the 6.4 keV X-rays was 26 % ($R^2_{adj.} = 0.99877$). This value is 2 % lower in comparison with the minimum value obtained for toroidal proportional gas flow counter in chapter 3.4 ($R_X = 28$ %, $R^2_{adj.} = 0.99227$). On the other hand, the minimum energy resolution value for the 14.4 keV ($R_\gamma = 19$ %, $R^2_{adj.} = 0.99741$) was 4 % higher than the one obtained for the toroidal detector ($R_\gamma = 15$ %, $R^2_{adj.} = 0.99538$). As another high voltage supply was used in this experimental setup, this energy resolution value increase could be caused by longer high voltage supply stabilization. Pulse amplitudes strongly depend on the high voltage and even small high voltage shift can change the amplitude and widen the full energy peak in the multichannel analysis spectrum.

For choosing optimal high voltage supply, detection efficiency was presented via count rates in the discrimination windows corresponding to different energies in Figure 54. Because the 1.8 keV krypton escape peak should be a valid detection of the 14.4 keV gamma photon, it is recommended to use high voltage supply ≥ 1500 V (≥ 1550 V in case of the 6.4 keV X-rays registration, for which an enormous count rate increase is observed).

42
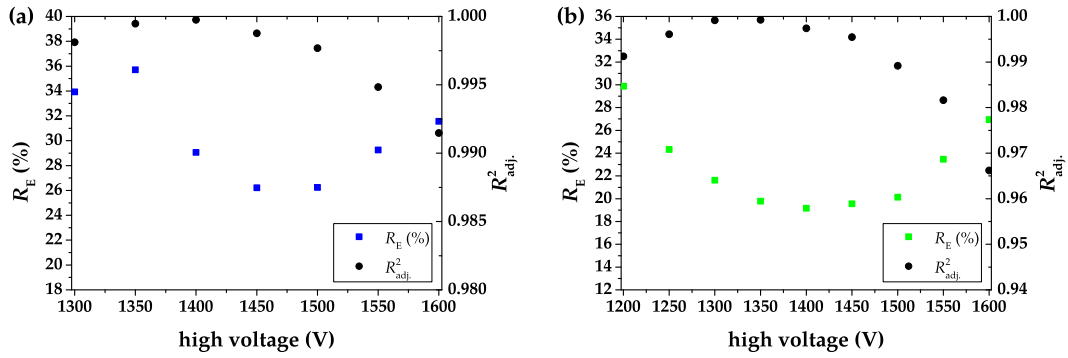
Figure 53   *Energy resolution R_E and quality of the fit $R^2_{adj.}$ while using pure krypton as a counting gas in the cylindrical proportional gas flow counter for (a) the 6.4 keV X-rays and (b) the 14.4 keV gamma rays.*
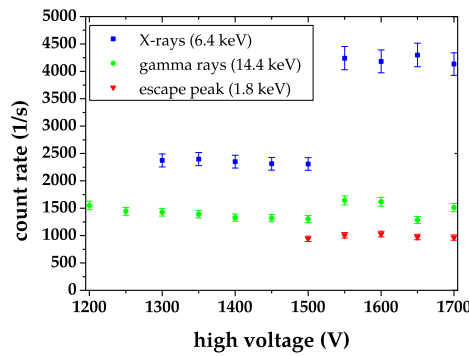
Figure 54   *Count rates for the 6.4 keV X-rays, the 14.4 keV gamma rays, and the 1.8 keV krypton escape peak.*

As it is shown in Figure 54, the 1.8 keV krypton escape peak forms a significant gamma photon registration part (approximately 40 % of the total gamma rays registration). Table 12 demonstrates percentage representation of the 14.4 keV full energy gamma photon peak and the 1.8 keV krypton escape peak in total gamma registration.

Table 12   *Percentage representation of the 14.4 keV gamma full energy gamma photon peak and the 1.8 keV krypton escape peak in total gamma registration.*

high voltage (V)	1.8 keV escape peak	14.4 keV gamma full energy peak
1500	42 %	58 %
1550	38 %	62 %
1600	39 %	61 %
1650	43 %	57 %
1700	39 %	61 %

4.3. Escape peak influence on the Mössbauer spectrum

For completing the transmission Mössbauer spectrometer, the experimental setup (see Figure 49) was modified by adding velocity driver, PID controller [20], and the function generator 33521A (Agilent Technologies). Complete transmission Mössbauer spectrometer experimental setup using a cylindrical proportional gas flow counter is shown in Figure 55. The other parts of the experimental setup remains the same as shown in Figure 49.

Three ^{57}Fe Mössbauer spectra of the α-iron (with different discrimination windows shown in Figure 56) were recorded simultaneously for the same period of time (116 hours). The first

discrimination window (1) covers 1.8 keV krypton escape peak pulse amplitudes, the second one (2) 14.4 keV gamma full energy peak and the third one (3) uses both of them (sum of (1) and (2)).
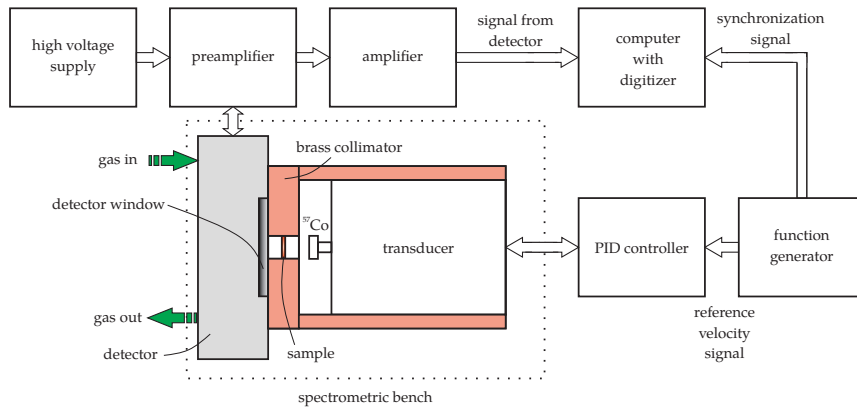
Figure 55 | *Transmission Mössbauer spectrometer using the cylindrical proportional gas flow counter.*
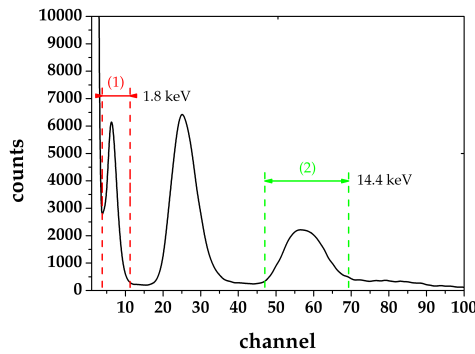
Figure 56 | *The 1.8 keV krypton escape peak discrimination window (1) and the 14.4 keV full energy gamma peak discrimination window (2).*

Figure 57 (a) demonstrates the ^{57}Fe Mössbauer spectrum of the calibration sample α-Fe, while the discrimination window (1) covers counts corresponding to the 1.8 keV krypton escape peak. The line width was determined to be 0.306 mm/s and the resonance effect was 30.4 ± 0.5 %. Simultaneously recorded ^{57}Fe Mössbauer spectrum using the 14.4 keV gamma full energy peak discrimination window (2) is shown in Figure 57 (b). In this case, the line width was 0.289 mm/s and the resonance effect was 31.7 ± 0.5 %.
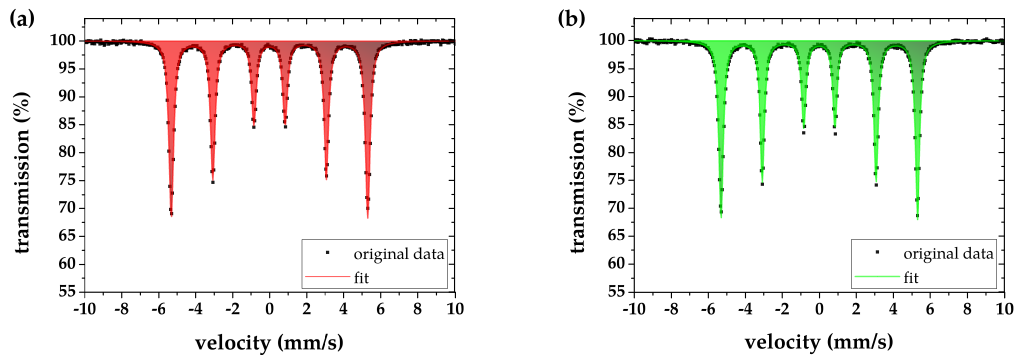
Figure 57 | *^{57}Fe Mössbauer spectra of the α-Fe obtained with cylindrical proportional gas flow counter while using (a) the 1.8 keV krypton escape peak discrimination window and (b) the 14.4 keV gamma full energy peak discrimination window.*

The last ^{57}Fe Mössbauer spectrum (see Figure 58) was recorded when both discrimination windows were used for registering the gamma rays. The line width was 0.306 mm/s and the resonance effect was 30.9 ± 0.5 %.
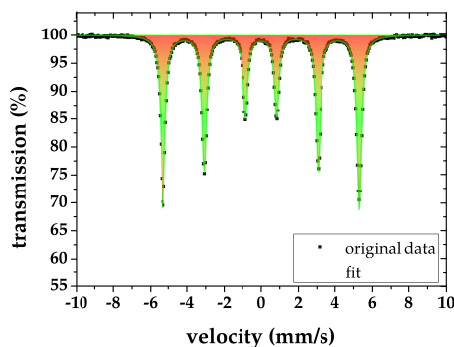
^{57}Fe Mössbauer spectrum of the α-Fe obtained with cylindrical proportional gas flow counter while both discrimination windows were used.

Table 13 summarizes the line widths (LW), resonance effects ϵ, statistical qualities Q (see equation 19), count rates, and base lines of the presented ^{57}Fe Mössbauer spectra in Figures 57 and 58. To conclude, if the studied sample contains low amount of iron, it is recommended to use both discrimination windows (higher count rate). However, if more precise resolution is required, it is better to use only the 14.4 keV gamma full energy peak discrimination window. This long term measurement also proves that about 48 % of the 14.4 keV gamma photon registration is followed by creation of the 1.8 keV krypton escape peak.

Table 13 *Parameters of the α-Fe Mössbauer spectra recorded while using different discrimination windows.*

discrimination window	LW (mm/s)	ϵ (%)	Q	count rate (1/s)	base line (counts)
1.8 keV	0.306	30.4	17838	328	276734
14.4 keV	0.289	31.7	17026	348	292570
1.8 keV and 14.4 keV	0.306	30.9	34828	676	569416

Conclusion

The presented toroidal proportional gas flow counter has been primarily designed for the purpose of the conversion X-rays Mössbauer spectroscopy for analyzing the surfaces of the bulk materials. With respect to the toroidal shape of the detector, it is able to register soft energy X-rays and low-gamma rays in almost 2π geometry with sufficient efficiency.

Several proportional gas counter parameters were determined for different counting gases. The 90.0 % argon and 10.0 % methane mixture provides the lowest energy resolution value ($R_X = 31$ % and $R_\gamma = 12$ %) from the whole tested argon-methane mixture spectrum. Regarding the error levels of detection efficiency values calculation, it is impossible to determine the optimal gas mixture for the 6.4 keV X-rays registration. On the other hand, pure krypton offers the lowest energy resolution value for X-rays ($R_X = 28$ %) from all tested counting gases. It was also proved that pure krypton is the most efficient counting gas (from the tested group of gases) for both ionization rays, especially for the 14.4 keV gamma rays, where detection efficiency is approximately seven times higher than in the case of argon or any of its mixtures with methane. Generally, pure noble gases are not very appropriate choices as counting gases, because detector pulses are quite long. It is more advantageous to add some more complex gases (like methane) to ensure that every pulse discharge was successfully terminated. This leads to detector pulse shortening, which can be considered as an advantage when high active radiation sources are used. On the other hand, it could also lead to detection efficiency value decrease (it can reduce the number of created pulse discharges).

The energy arrangement was confirmed by recording some ^{57}Fe Mössbauer spectra in chapter 3.7. It was also verified that usage of an aluminum filter (at least 10 µm) can improve the statistical quality of the backscattering Mössbauer spectra. The utilization of the lead shielding (see Figure 43 (a)) was observed as a crucial task as it reduces the saturation of the detector and increases the energy resolution of the detector. However, more optimized solution of stacked plate shielding arrangement [54] would probably improve its performance.

The presented detector is easy to handle and its main advantage is that it does not require any sample preparations to measure backscattering Mössbauer spectra. The detector could be also used to register low-energy gamma rays. In this case it could find an application in the transmission Mössbauer spectroscopy or the backscattering gamma Mössbauer spectroscopy.

This detector is also an essential part of the ''Austenitemeter'' device, which enables fast and non-destructive determination of residual austenite amount in steels. Because of this, the detector is still upgraded to achieve the highest performance. The actual version (its technical drawing in Czech language and 3D model - available only in electronic version - are shown in appendixes 1-3) is made from dural using the CNC technology. As it contains two O-rings between both cathode parts, it prevents more gas leakages. Nowadays, this version already successfully operates in the laboratories of the Department of Experimental Physics (Palacký University in Olomouc). Next step of the development will be focused on the detector and the whole Austenitemeter shielding to enhance its implementation by private companies.

For the purpose of the transmission Mössbauer spectroscopy, it is more optimal using the cylindrical proportional gas flow counter. The calibration sample α-Fe Mössbauer spectra recorded when using this detector proved 1.8 keV krypton escape peak being a valid detection of 14.4 keV gamma photon. In this case, it could be successfully used to improve the statistical spectra quality and count rate. On the other hand, it slightly decreases the resonance effect and increases the line width. This is probably caused by a higher noise influence, as pulse amplitudes corresponding to 1.8 keV krypton escape peak are lower than the pulses belonging to 14.4 keV gamma full energy peak. This advantage of escape peak could be also exploited by using argon or its mixtures in the conversion X-rays Mössbauer spectroscopy (e.g. when using the toroidal proportional gas flow counter).

Stručné shrnutí v českém jazyce

Prezentovaný průtokový toroidní proporcionální plynový detektor byl primárně navržen pro účely Mössbauerovy spektroskopie konverzního RTG záření, která slouží k analýze povrchu objemných vzorků. Díky svému toroidnímu tvaru je detektor schopen registrovat měkké RTG záření a nízkoenergetické gama záření téměř v 2π geometrii s dostatečnou účinností.

Detektor byl testován s různými plynovými náplněmi, pro které bylo následně určeno několik provozních parametrů detektoru. Minimální hodnota energetického rozlišení pro RTG záření 6,4 keV $R_X = 31$ % a pro gama záření 14,4 keV $R_\gamma = 12$ % byla určena pro směs 90.0 % argonu a 10.0 % metanu (ze skupiny směsí argonu s metanem, případně čistého argonu). Z pohledu detekční účinnosti nebylo možné určit nejoptimálnější směs plynů pro registraci konverzního RTG záření (6,4 keV) především díky velké chybě při určování hodnot detekční účinnosti. S čistým kryptonem bylo dosaženo nejnižší hodnoty energetického rozlišení RTG záření ($R_X = 28$ %) ze všech testovaných plynů (směsí). Bylo také prokázáno, že právě použitím kryptonu lze dosáhnout nejvyšší detekční účinnosti (ze skupiny všech testovaných plynů) pro oba druhy ionizujícího záření, především však pro nízkoenergetické gama záření, kde byla dosažena přibližně sedmkrát vyšší hodnota detekční účinnosti než u argonu případně jakékoliv jeho směsi s metanem. Obecně však vzácné čisté plyny nejsou příliš vhodnou volbou pro plnění detektorů, jelikož délky impulzů z detektoru jsou relativně dlouhé. Je mnohem výhodnější přidat k jednoduchým molekulám vzácného plynu složitější molekuly zhášecího plynu (např. metanu). Tento zhášecí plyn při správné koncentraci dokáže zajistit, aby každý pulzní výboj byl řádně ukončen. Tento efekt vede ke zkrácení událostí (impulzů) v detektoru, které je žádoucí především při použití aktivnějších zdrojů ionizujícího záření. Na druhou stranu, tento efekt může samozřejmě zabránit vzniku některých sekundárních ionizací a tím tak snížit účinnost detektoru.

Naměřená mössbauerovská spektra jednoznačně potvrzují správné určení jednotlivých energií v mnohokanálových spektrech. Bylo také ověřeno, že použití hliníkového filtru (tloušťky alespoň 10 μm) pozitivně ovlivní statistickou kvalitu mössbauerovského spektra v geometrii zpětného rozptylu. Velmi významnou roli hraje také olověné stínění, jelikož zabraňuje přesycení detektoru a také zvyšuje energetické rozlišení detektoru. Nicméně skládané destičkové stínění podle Schaafa [54] by mohlo ještě více vylepšit vlastnosti detektoru.

Hlavní výhodou prezentovaného detektoru je, že pro měření mössbauerovských spekter ve zpětném rozptylu není potřeba měřené vzorky nijak připravovat. Kromě toho je možné detektor použít i v transmisní Mössbauerově spektroskopii k registraci nízkoenergetického gama záření.

Tento detektor tvoří velmi významnou část zařízení "Astenitometr", které umožňuje rychlé a nedestruktivní určení zbytkového austenitu v ocelích. Z tohoto důvodu je tento detektor stále vylepšován za účelem dosáhnutí nejlepších parametrů. Aktuální verze je vyrobena z duralu pomocí CNC obráběcích strojů. Mezi oběma částmi katody jsou umístěny navíc dva O-kroužky, které zabraňují větším únikům detekčního plynu. V této době je tato verze již plně využívána v laboratořích Katedry experimentální fyziky (Univerzita Palackého v Olomouci). Další krok vývoje bude zaměřen na stínění detektoru a samotného Austenitometru pro jeho širší využití v komerční sféře.

Výhodnější volbou pro účely transmisní Mössbauerovy spektroskopie je použití průtokového válcového proporcionálního plynového detektoru. Měření kalibračních mössbauerovských spekter α-Fe prokázala, že uníkový pík kryptonu (1,8 keV) je platnou detekcí gama fotonu o energii 14,4 keV. V tomto případě jej lze výhodně použít a zvýšit tak statistickou kvalitu spektra a čítací rychlost. Na druhou stranu využití úníkového píku mírně snižuje rezonanční efekt a také zvyšuje šířku čáry (snižuje rozlišení spektrometru). To je pravděpodobně způsobeno větším vlivem šumu na signál, jelikož amplitudy impulzů odpovídající úníkovému píku kryptonu (1.8 keV) jsou nižší než ty, které odpovídají píku úplné absorpce gama záření o energii 14,4 keV. Výhody úníkového píku mohou být využity i při použití argonu (případně jeho směsí) v Mössbauerově spektroskopii zpětného rozptylu (např. při použití průtokového toroidního proporcionálního plynového detektoru).

References

[1] N. N. Greenwood and T. C. Gibb, *Mössbauer Spectroscopy*. London: Chapman and Hall, 1971.

[2] M. Mašláň, *Mössbauerova spektroskopie*. Olomouc: Vydavatelství UP Olomouc, 1992.

[3] J. Danon, *Lectures on the Mössbauer effect*. New York: Gordon and Breach, 1968.

[4] A. Vértes, L. Korecz, and K. Burger, *Mössbauer spectroscopy*. Amsterdam: Elsevier Scientific Pub. Co., 1979.

[5] R. L. Mössbauer, "Kernresonanzfluoreszenz von Gammastrahlung in Ir191," *Zeitschrift für Physik*, vol. 151, no. 2, pp. 124–143, apr 1958.

[6] G. Klingelhöfer, R. V. Morris, B. Bernhardt, D. Rodionov, P. A. de Souza, S. W. Squyres, J. Foh, E. Kankeleit, U. Bonnes, R. Gellert, C. Schröder, S. Linkin, E. Evlanov, B. Zubkov, and O. Prilutski, "Athena MIMOS II Mössbauer spectrometer investigation," *Journal of Geophysical Research: Planets*, vol. 108, no. E12, pp. 8067–8084, dec 2003.

[7] RITVERC, "Mössbauer sources: Cobalt-57 / Co-57." [Online]. Available: http://www.ritverc.com/products/detail.php?ID=1691

[8] J. Tuček, L. Machala, J. Frydrych, J. Pechoušek, and R. Zbořil, "Mössbauer Spectroscopy in Study of Nanocrystalline Iron Oxides From Thermal Processes," in *Mössbauer Spectroscopy: Applications in Chemistry, Biology, and Nanotechnology*, V. K. Sharma, G. Klingelhöfer, and T. Nishida, Eds. Hoboken, New Jersey, USA: John Wiley & Sons, Inc., oct 2013, pp. 349–392.

[9] J. R. Gancedo, M. Gracia, and J. F. Marco, "CEMS methodology," *Hyperfine Interactions*, vol. 66, no. 1-4, pp. 83–93, nov 1991.

[10] K. Sisson and P. Boolchand, "A microcomputer system for the analysis of mössbauer spectra," *Nuclear Instruments and Methods in Physics Research*, vol. 198, no. 2-3, pp. 317–320, jul 1982.

[11] T. Sundqvist and R. Wäppling, "A microcomputer controlled Mössbauer spectrometer," *Nuclear Instruments and Methods in Physics Research*, vol. 205, no. 3, pp. 473–478, feb 1983.

[12] J. Jing, S. J. Campbell, and J. Pellegrino, "A stand-alone Mössbauer spectrometer based on the MC68008 microprocessor," *Measurement Science and Technology*, vol. 3, no. 1, pp. 80–84, jan 1992.

[13] P. Schaaf, T. Wenzel, K. Schemmerling, and K. P. Lieb, "A simple six-input multichannel system for Mössbauer spectroscopy," *Hyperfine Interactions*, vol. 92, no. 1, pp. 1189–1193, dec 1994.

[14] R. Zhou, F. Li, and Z. Zhang, "A microcomputer system for data-acquisition, fitting and plotting of Mössbauer spectra," *Hyperfine Interactions*, vol. 42, no. 1-4, pp. 1181–1184, feb 1988.

[15] G. Faigel, P. Haustein, and D. Siddons, "An IBM PC based Mössbauer spectrometer and data analysis system," *Nuclear Instruments and Methods in Physics Research Section B: Beam Interactions with Materials and Atoms*, vol. 17, no. 4, pp. 363–367, nov 1986.

[16] J. Pechousek and M. Mashlan, "Mössbauer spectrometer as a virtual instrument in the PXI/Compact PCI modular system," *Czechoslovak Journal of Physics*, vol. 55, no. 7, pp. 853–863, jul 2005.

[17] J. Pechousek, R. Prochazka, D. Jancik, and M. Mashlan, "Fully-LabVIEW Powered Mössbauer Spectrometer," *International Journal of Online Engineering (iJOE)*, vol. 5, no. 5, pp. 61–64, jul 2006.

[18] J. Pechousek, R. Prochazka, D. Jancik, J. Frydrych, and M. Mashlan, "Universal LabVIEW-powered Mössbauer spectrometer based on USB, PCI or PXI devices," *Journal of Physics: Conference Series*, vol. 217, no. 1, mar 2010.

[19] L. Kouřil, P. Kohout, P. Novák, J. Navařík, and J. Pechoušek, "Setup of the Mössbauer spectrometer based on stand-alone instruments - A case study," in *AIP Conference Proceedings*, vol. 1622, no. 1, oct 2014, pp. 58–66.

[20] V. Evdokimov, M. Mashlan, D. Zak, A. Fyodorov, A. Kholmetskii, and O. Misevich, "Mini and micro transducers for Mössbauer spectroscopy," *Nuclear Instruments and Methods in Physics Research Section B: Beam Interactions with Materials and Atoms*, vol. 95, no. 2, pp. 278–280, feb 1995.

[21] P. Kohout, L. Kouřil, J. Navařík, P. Novák, and J. Pechoušek, "Optimized linear motor and digital PID controller setup used in Mössbauer spectrometer," in *AIP Conference Proceedings*, J. Tuček and M. Miglierini, Eds., vol. 1622, no. 1, oct 2014, pp. 50–57.

[22] J. Pechousek, R. Prochazka, M. Mashlan, D. Jancik, and J. Frydrych, "Digital proportional-integral-derivative velocity controller of a Mössbauer spectrometer," *Measurement Science and Technology*, vol. 20, no. 1, p. 017001, jan 2009.

[23] J. Navařík, P. Novák, J. Pechoušek, L. Machala, D. Jančík, and M. Mašláň, "Precise Compact System For Ionizing Radiation Detection And Signal Processing With Advanced Components Integration And Electronic Control," *Journal of Electrical Engineering*, vol. 66, no. 4, pp. 220–225, sep 2015.

[24] C. Stéphan, "Gas Filled Detectors," in *Experimental Techniques in Nuclear Physics*, D. N. Poenaru and W. Greiner, Eds. Berlin, Boston: DE GRUYTER, 1997, pp. 11–58.

[25] F. Sauli, "Principles of operation of multiwire proportional and drift chambers," CERN/77-09, CERN/77-09, Geneva, Tech. Rep., 1977.

[26] J. Gerndt, *Detektory ionizujícího záření*. Praha: ČVUT, 1994.

[27] J. S. E. Townsend, *Electrons in gases*. London: Hutchinson, 1947.

[28] E. D. Klema and J. S. Allen, "Drift velocities of electrons in argon, nitrogen, and argon-nitrogen mixtures," *Physical Review*, vol. 77, no. 5, pp. 661–665, 1950.

[29] V. Lisovskiy, J.-P. Booth, K. Landry, D. Douai, V. Cassagne, and V. Yegorenkov, "Electron drift velocity in argon, nitrogen, hydrogen, oxygen and ammonia in strong electric fields determined from rf breakdown curves," *Journal of Physics D: Applied Physics*, vol. 39, no. 4, pp. 660–665, feb 2006.

[30] L. Foreman, P. Kleban, L. D. Schmidt, and H. T. Davis, "Drift velocities of electrons in methane-inert-gas mixtures," *Physical Review A*, vol. 23, no. 3, pp. 1553–1557, mar 1981.

[31] W. Diethorn, "A methane proportional counter system for natural radiocarbon measurements (thesis)," Carnegie Inst. of Tech., Carnegie Inst. of Tech., Pittsburgh, USA, Tech. Rep. NYO-6628, Ph.D. dissertation, mar 1956.

[32] R. W. Kiser, "Characteristic parameters of gas-tube proportional counters," *Applied Scientific Research, Section B*, vol. 8, no. 1, pp. 183–200, dec 1960.

[33] A. Zastawny, "Gas amplification in a proportional counter with carbon dioxide," *Journal of Scientific Instruments*, vol. 43, no. 3, pp. 179–181, mar 1966.

[34] R. Hendricks, "The gas amplification factor in xenon filled proportional counters," *Nuclear Instruments and Methods*, vol. 102, no. 2, pp. 309–312, jul 1972.

[35] G. F. Knoll, *Radiation detection and measurement*. New York, USA: John Wiley & Sons, Inc., 1979.

[36] R. S. Wolff, "Measurement of the gas constants for various proportional-counter gas mixtures," *Nuclear Instruments and Methods*, vol. 115, no. 2, pp. 461–463, mar 1974.

[37] R. Hendricks, "A pulse-matching method for estimating the gas amplification factor in proportional counters," *Nuclear Instruments and Methods*, vol. 106, no. 3, pp. 579–588, feb 1973.
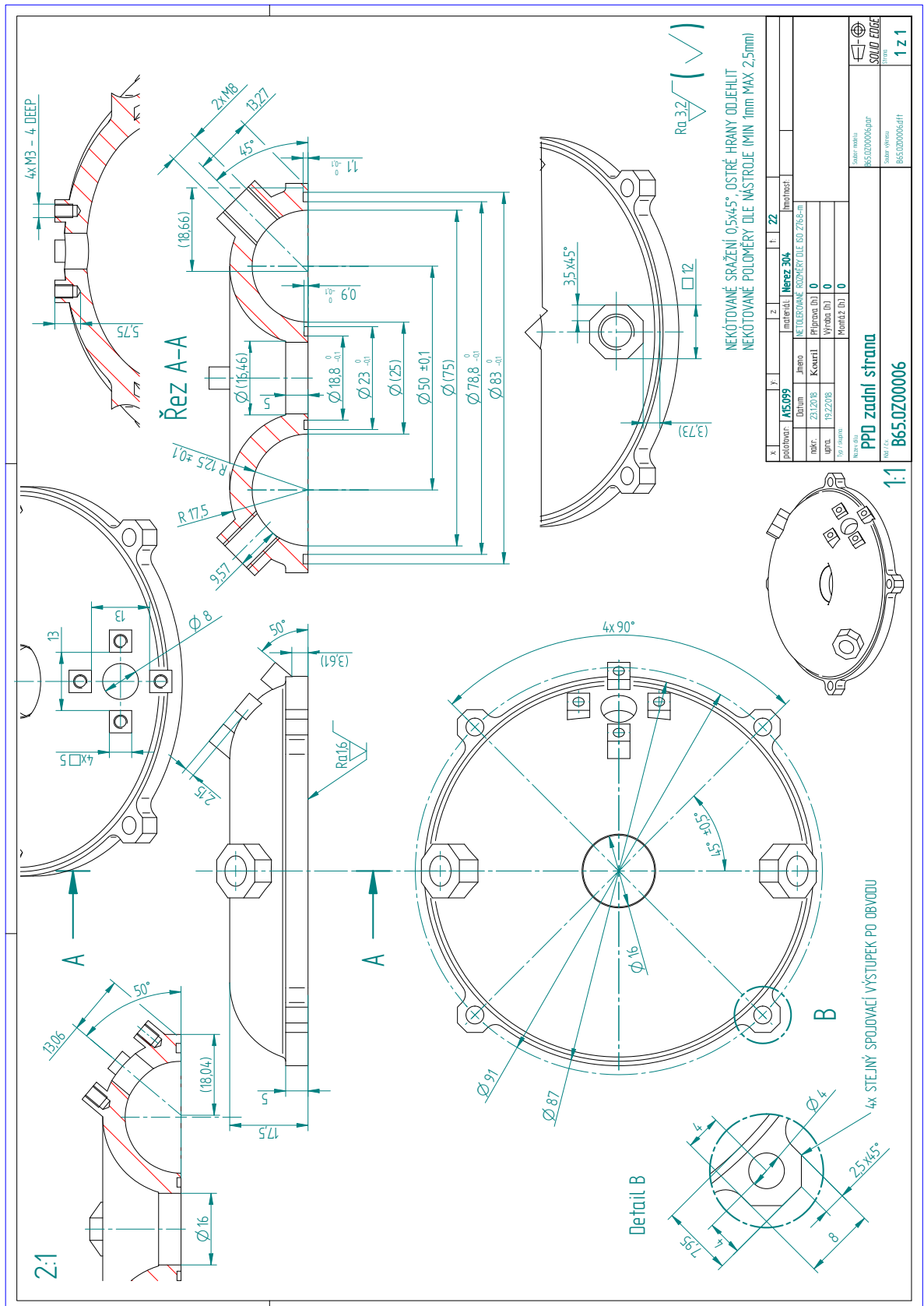
[38] J. H. Hubbell and S. M. Seltzer, "Tables of X-Ray Mass Attenuation Coefficients and Mass Energy-Absorption Coefficients 1 keV to 20 MeV for Elements Z = 1 to 92 and 48 Additional Substances of Dosimetric Interest," National Institute of Standards and Technology, Gaithersburg, MD, USA, Tech. Rep., 1995.

[39] A. J. F. den Boggende, A. C. Brinkman, and W. de Graaff, "Comments on the ageing effect of gas-filled proportional counters," *Journal of Physics E: Scientific Instruments*, vol. 2, no. 8, pp. 701–705, aug 1969.

[40] H. Andersson, T. Andersson, J. Heino, J. Huovelin, K. Kurvinen, R. Lauhakangas, S. Nenonen, A. Numminen, J. Ojala, R. Orava, J. Schultz, H. Sipila, and O. Vilhu, "Aging of proportional counters with gas mixtures containing impurities of aromatic hydrocarbons," *IEEE Symposium Conference Record Nuclear Science 2004.*, vol. 4, pp. 2053–2057, nov 2004.

[41] K. R. Swanson, "Analysis of Thin Surface Layers by Fe-57 Mössbauer Backscattering Spectrometry," *Journal of Applied Physics*, vol. 41, no. 7, pp. 3155–3158, jun 1970.

[42] J. Frydrych, M. Mashlan, J. Pechousek, and D. Jancik, "Conversion Electron Detectors for ^{57}Fe Mössbauer Measurements," *AIP Conference Proceedings*, vol. 1070, no. 1, pp. 170–184, oct 2008.

[43] M. Takafuchi, Y. Isozumi, and R. Katano, "A Proportional Counter for Mössbauer Spectroscopy by Scattered Electrons," *Bull. Inst. Chem. Res., Kyoto Univ*, vol. 51, no. 1, pp. 13–18, mar 1973.

[44] A. S. Kamzin and V. Rusakov, "Proportional counter for Mössbauer studies of surface-layers at temperatures from 100 to 700 K," *Instruments and experimental techniques*, vol. 31, no. 5, pp. 1150–1153, oct 1988.

[45] Y. Isozumi, M. Kurakado, and R. Katano, "A proportional counter for resonance-electron Mössbauer spectroscopy at low temperatures down to 77.3 K," *Nuclear Instruments and Methods in Physics Research*, vol. 204, no. 2-3, pp. 571–575, jan 1983.

[46] K. Fukumura, A. Nakanishi, and T. Kobayashi, "Hydrogen-filled proportional counter operated at low temperatures and its application to CEMS," *Nuclear Instruments and Methods in Physics Research Section B: Beam Interactions with Materials and Atoms*, vol. 86, no. 3-4, pp. 387–389, apr 1994.

[47] K. Fukumura, A. Nakanishi, T. Kobayashi, R. Katano, and Y. Isozumi, "Operation of a gas-filled proportional counter for CEMS at temperatures between 15–77 K," *Nuclear Instruments and Methods in Physics Research Section B: Beam Interactions with Materials and Atoms*, vol. 61, no. 1, pp. 127–131, jul 1991.

[48] T. Fujii, O. Hosoito, R. Katano, and Y. Isozumi, "Operation of a cryogenic conversion electron proportional counter under strong magnetic fields," *Nuclear Instruments and Methods in Physics Research*, vol. 76, no. 1-4, pp. 207–209, apr 1993.

[49] A. S. Kamzin and L. A. Grigorev, "2-chamber proportional counter for Mössbauer-spectroscopy of conversion electrons and X-rays in temperature range of 100-700 K," *Instruments and experimental techniques*, vol. 33, no. 2, pp. 314–317, apr 1990.

[50] A. S. Kamzin, S. M. Irkaev, Y. N. Maltsev, and L. A. Grigorev, "Automatic Mössbauer spectrometer to detect γ-quanta, conversion electrons, and characteristic X-rays," *Instruments and experimental techniques*, vol. 36, no. 1, pp. 51–58, feb 1993.

[51] Y. Q. Zhang, J. J. Zhu, and S. J. Cao, "A new detection system for backscattering Mössbauer spectroscopy," *Hyperfine Interactions*, vol. 29, no. 1-4, pp. 1505–1508, feb 1986.

[52] B. Keisch, "A detector for efficient backscatter Mössbauer effect spectroscopy," *Nuclear Instruments and Methods IO4*, vol. 4, no. 1, pp. 237–240, oct 1972.

[53] L. Blaes, H. G. Wagner, U. Gonser, J. Welsch, and J. Sutor, "Toroidal proportional detector for backscattered Mössbauer γ-and x-rays," *Hyperfine Interactions*, vol. 29, no. 1-4, pp. 1571–1574, feb 1986.

[54] P. Schaaf, L. Blaes, J. Welsch, H. Jacoby, F. Aubertin, and U. Gonser, "Experience with a toroidal proportional detector for backscattered Mössbauer γ-rays and X-rays," *Hyperfine Interactions*, vol. 58, no. 1-4, pp. 2541–2545, jul 1990.

[55] I. Bibicu and M. Rogalski, "Proportional counter for simultaneous conversion X-ray and transmission Mössbauer spectroscopy Proportional counter for simultaneous conversion X-ray and transmis- sion Mössbauer spectroscopy," *Journal de Physique III, EDP Sciences*, vol. 4, no. 12, pp. 2495–2499, dec 1994.

[56] I. Bibicu, M. Rogalski, and G. Nicolescu, "Toroidal proportional detector for conversion X-ray and transmission Mössbauer spectroscopy," *Nuclear Instruments and Methods in Physics Research Section B: Beam Interactions with Materials and Atoms*, vol. 94, no. 3, pp. 330–332, nov 1994.

[57] A. Y. Dudkin and S. M. Cheremisin, "A toroidal gas-filled proportional counter," *Instruments and experimental techniques*, vol. 37, no. 1, pp. 31–35, feb 1994.

[58] L. Kouril, J. Pechousek, P. Novak, J. Navarik, and P. Kohout, "Toroidal proportional gas flow counter for conversion X-ray Mössbauer spectroscopy," *Nuclear Instruments and Methods in Physics Research Section B: Beam Interactions with Materials and Atoms*, vol. 432, pp. 55–59, oct 2018.

[59] R. Vondrášek, "Plynové náplně proporcionálních detektorů ionizujícího záření," bachelor thesis, Palacký University in Olomouc, 2018.

[60] L. Schlattauer, L. Parali, J. Pechousek, I. Sabikoglu, C. Celiktas, G. Tektas, P. Novak, A. Jancar, and V. Prochazka, "Calibration of gamma-ray detectors using Gaussian photopeak fitting in the multichannel spectra with a LabVIEW-based digital system," *European Journal of Physics*, vol. 38, no. 5, pp. 1–12, sep 2017.

[61] T. Watanabe, H. W. Schnopper, and F. N. Cirillo, "K X-Ray Fluorescence Yield of Argon," *Physical Review*, vol. 127, no. 6, pp. 2055–2057, sep 1962.

[62] R. W. Fink, R. C. Jopson, H. Mark, and C. D. Swift, "Atomic Fluorescence Yields," *Reviews of Modern Physics*, vol. 38, no. 3, pp. 513–540, jul 1966.

[63] J. Frydrych, M. Mašláň, R. Zbořil, J. Pechoušek, and M. Heřmánek, "CEMS and CXMS spectrometer: construction and application," *Acta Metallurgica Slovaca*, vol. 13, no. 6, pp. 298–301, 2007.

[64] A. Kholmetskii, M. Mashlan, K. Nomura, O. Misevich, and A. Lopatik, "Fast detectors for Mössbauer spectroscopy," *Czechoslovak Journal of Physics*, vol. 51, no. 7, pp. 763–771, may 2001.

[65] Z. Klencsár, E. Kuzmann, and A. Vértes, "User-friendly software for Mössbauer spectrum analysis," *Journal of Radioanalytical and Nuclear Chemistry*, vol. 210, no. 1, pp. 105–118, apr 1996.

List of publications

- **L. Kouril**, J. Pechousek, P. Novak, J. Navarik, and P. Kohout, "Toroidal proportional gas flow counter for conversion X-ray Mössbauer spectroscopy," *Nucl. Instruments Methods Phys. Res. Sect. B Beam Interact. with Mater. Atoms*, vol. 432, pp. 55-59, Oct. 2018, (5 years impact factor = 1.297).

- **L. Kouřil**, P. Kohout, P. Novák, J. Navařík, and J. Pechoušek, "Setup of the Mössbauer spectrometer based on stand-alone instruments - A case study," *in AIP Conference Proceedings*, 2014, vol. 1622, no. 1, pp. 58–66, (without impact factor, only reviewed).

- P. Kohout, **L. Kouřil**, J. Navařík, P. Novák, and J. Pechoušek, "Optimized linear motor and digital PID controller setup used in Mössbauer spectrometer," *in AIP Conference Proceedings*, 2014, vol. 1622, no. 1, pp. 50–57, (without impact factor, only reviewed).

- J. Pechousek, D. Konecny, P. Novak, **L. Kouril**, P. Kohout, C. Celiktas, and M. Vujtek , "Software emulator of nuclear pulse generation with different pulse shapes and pile-up," *Nucl. Instruments Methods Phys. Res. Sect. A Accel. Spectrometers, Detect. Assoc. Equip.*, vol. 828, pp. 81–85, Aug. 2016, (5 years impact factor = 1.208).

- P. Novak, J. Pechousek, V. Prochazka, J. Navarik, **L. Kouril**, P. Kohout, V. Vrba, and L. Machala "Time differential ^{57}Fe Mössbauer spectrometer with unique 4π YAP:Ce 122.06 keV gamma-photon detector," *Nucl. Instruments Methods Phys. Res. Sect. A Accel. Spectrometers, Detect. Assoc. Equip.*, vol. 832, pp. 292–296, Oct. 2016, (5 years impact factor = 1.208).

- P. Kohout, T. Frank, J. Pechousek, and **L. Kouril**, "Mössbauer spectra linearity improvement by sine velocity waveform followed by linearization process," *Meas. Sci. Technol.*, vol. 29, no. 5, 057001, May 2018 (5 years impact factor = 1.735).

- J. Pechousek, **L. Kouril**, P. Novak, J. Kaslik, and J. Navarik, "Austenitemeter - Mössbauer spectrometer for rapid determination of residual austenite in steels," under review.

- **L. Kouřil**, J. Pechoušek, P. Novák, J. Navařík, and P. Kohout, "Kruhový detektor ionizujícího záření především pro Mössbauerovu spektroskopii," application for Czech patent, under review of Czech Industrial Property Office from February 2018.

Appendix 1.   Front side of the detector (technical drawing)

Note: As the original size of the technical drawing has to be modified, the scale is not valid.

Appendix 2.   Back side of the detector (technical drawing)

Note: As the original size of the technical drawing has to be modified, the scale is not valid.

Appendix 3.   Detector body (3D model)

Department
of Experimental **Physics**

Summary of dissertation thesis

Design and optimization of proportional gas flow counters for Mössbauer spectroscopy

Author	Lukáš Kouřil
Supervisor	Assoc. Prof. Dr. Jiří Pechoušek
Discipline	Applied physics
Study form	full-time
Year	2018

Declaration of the Author

I declare that I have written this thesis by myself using the cited references. Neither the thesis nor any of its part was previously used for obtaining any other academic degree.

In Olomouc . . . .

signature

Student	Lukáš Kouřil
	Department of Experimental Physics
	Palacký University in Olomouc
	Czech republic
Supervisor	Assoc. Prof. Dr. Jiří Pechoušek
	Department of Experimental Physics
	Palacký University in Olomouc
	Czech republic
Opponent	Prof. Dr. Václav Přenosil
	Faculty of Informatics
	Masaryk University, Brno
	Czech republic
Opponent	D.Sc. Oldřich Schneeweiss
	Institute of Physics of Materials
	Czech Academy of Sciences, Brno
	Czech republic

Date and place of dissertation defense:
. . . .

The dissertation thesis is available at the study department of Faculty of Science of Palacký University in Olomouc, residing at the same address.

Abstract

This thesis presents a new prototype of a toroidal proportional gas flow counter. This detector has been developed to be used in the Mössbauer spectroscopy for characterizing the surfaces of the iron bearing samples. The presented proportional counter allows to register both conversion X-rays (6.4 keV) and the backscattered gamma rays (14.4 keV) in the almost 2π geometry with the sufficient efficiency. This thesis demonstrates the structure description of the detector, its basic features for different counting gases (pure argon, its mixtures with different methane concentrations, and pure krypton) and also the optimization process of its use in the backscattering Mössbauer spectroscopy. Despite that the detector could be used in the transmission Mössbauer spectroscopy as well, this thesis also describes more optimized choice for the transmission geometry - cylindrical proportional gas flow counter.

Abstrakt

Tato práce představuje nový prototyp průtokového toroidního proporcionálního plynového detektoru. Tento detektor byl vyvinut pro účely charakterizace povrchů železo obsahujících vzorků pomocí Mössbauerovy spektroskopie. Představovaný proporcionální detektor umožňuje registraci jak konverzního RTG záření (6,4 keV) tak i zpětně odraženého gama záření (14,4 keV) v téměř 2π geometrii s dostatečnou účinností. Tato práce demonstruje popis konstrukce detektoru, jeho základní parametry pro různé čítací plyny (čistý argon, směsi argonu s metanem v různých koncentracích a čistý krypton) a proces optimalizace pro použití v Mössbauerově spektroskopii zpětného rozptylu. Přestože tento detektor by mohl být stejně tak použit v transmisní Mössbauerově spektroskopii, tato práce také popisuje průtokový válcový proporcionální plynový detektor, který je výhodnější volbou pro tento typ transmisní geometrie.

Contents

Introduction

Gas filled ionization detectors belong to the oldest types of instruments used in the area of nuclear physics. Their low price, adjustment to different experimental conditions (including low and high temperatures, non-sensitivity to external magnetic field, dimension versatility, etc.), ability to register almost all types of charged particles (even X and γ-rays) makes them very common in nuclear physics community.

Proportional gas counters appeared in late 1940s and became very popular in wide area of nuclear techniques requiring spectrometric detector regime (distinguishing particle energy). About twenty years later (after discovery of Mössbauer effect in 1958) proportional gas counters found their utilization in Mössbauer spectroscopy covering large group of Mössbauer effect observations. Nowadays they are commonly used especially in the backscattering ^{57}Fe Mössbauer spectroscopy techniques.

The main aim of this dissertation thesis is to introduce a new toroidal proportional gas flow counter prototype enabling the 6.4 keV X-rays and the 14.4 keV gamma rays registration in almost 2π geometry. It took three years to develop structure and design of the toroidal proportional gas flow counter for meeting all specified conditions. All the prototype versions were printed by 3D printers (the first one even from plastic material and painted by carbon conductive glue). Despite that many versions (including different materials, anode configuration, safety high voltage connector housing, window shapes, etc.) have been tested, the best one is presented in this dissertation thesis. The toroidal proportional gas counter was tested with different counting gases (pure argon, pure krypton and argon-methane mixtures with different concentration) for optimization counter parameters (such as energy resolution and detection efficiency). Consequently, this counter was tested for the conversion X-rays, backscattering gamma and transmission ^{57}Fe Mössbauer spectroscopy.

For the purpose of the transmission ^{57}Fe Mössbauer spectroscopy, the toroidal proportional gas counter was replaced by the cylindrical one. This counter was filled by pure krypton, whose escape peak is usually described as its disadvantage. However, this thesis demonstrates that this ''disadvantage'' could be also beneficial.

1. Proportional gas counters for Mössbauer spectroscopy

Because the proportional gas counters provide a good energy resolution, they are commonly used in the area of Mössbauer spectroscopy. They are widely used for detection of the conversion electrons emitted from different shells of the atoms (K, L and M) on the surface of the sample. As the electrons have a short mean free path in the air, the location of the samples is usually inside the detector [1–3]. The presented proportional detector [4] allows to measure the Mössbauer spectra by collecting the conversion electrons or the conversion X-rays (6.4 keV) in a temperature range from 100 to 700 K. Other studies describe the operation of proportional gas counters recording CEMS spectra at low temperatures down to 15 K using different filling gases (pure helium, He - CH_4, He - H_2, He - N_2, He - CO, pure neon or hydrogen) [5–7]. The next solution demonstrates CEMS analysis at 4.2 K under magnetic field 3 T [8], which is possible only when a pure helium is used as a filling medium. In addition, a combination of two proportional gas counters allows the detection of the conversion electrons and the conversion X-rays at the same time [9].

It is also possible to use three-chambers system for recording three different Mössbauer spectra simultaneously. The three-chambers system consists of the chamber detecting conversion X-rays, the chamber detecting conversion electrons and the chamber detecting transmitted gamma rays (14.4 keV) [10]. Whole system is based on a multiwire gas flow detector using 2π geometry. Furthermore, the sample should be always located directly in the detector. So it is not possible to measure bulk samples, as this method could be destructible for these types of samples. To keep the non-destructive feature of Mössbauer spectroscopy for bulk materials, conversion X-rays or backscattered gamma rays can be detected by a commercial cylindrical proportional gas counter. The detector is located in front of the sample at the proper angle. The beam from the radiation source has to be well-collimated and should not incident on the window of the proportional counter. The same type of the detector could be also used to detect the transmitted gamma rays. This method is suitable for analysis of thin films or powder materials. If one wants enshrine the high efficiency by keeping the 2π geometry, the toroidal proportional counters can be used.

2. Toroidal proportional gas counter

The first construction of "toroidal" proportional gas counter for ionization rays detection was published in 1972 by Keisch [11]. This detector was developed for the purpose of examining works of art containing iron-bearing pigments. In fact, the detector shape was not a true toroid. While the ideal toroid is a ring in the cross section, the presented detector [11] is a hexagon. The body of the detector (cathode) was made from aluminum and the anode (a wire with 25 µm in diameter) was centered via quartz support rods in the middle of the hexagon. The detector windows were made from nylon and sealed by two O-rings. The window interior was aluminized by using the vacuum deposition. The shielding of the detector was provided only by lead. As the detector was primarily designed for the purpose of backscattered gamma rays Mössbauer spectroscopy, the gaseous fill was a mixture of 90 % krypton and 10 % methane. However, the author recommended using flow of a mixture of 90 % argon and 10 % methane to register 6.4 keV conversion X-rays while using an aluminum filter (approximately 250 µm thick) located between the radiation source and the sample for absorbing the non-resonant X-rays.

Next study [12] introduced the first so called toroidal proportional gas counter, which has a ring shape (inside a block of aluminum). The anode (20 µm diameter gold plated tungsten wire or 80 µm Megapyr wire) was located in the middle of the detector. The detector windows were fabricated from the organic material – the acetal resin Delrin (Delrin is a registered trademark of Du Pont) [12]. This material (approximately 500 µm thick) allows to transmit over 92 % of 14.4 keV gamma rays. The shielding part of the detector was made by using the tungsten and lead discs. The authors achieved an energy resolution of 25 % (using Megapyr wire) and 20 % (using gold plated tungsten wire) for 14.4 keV gamma rays, while the Kr-CH_4 mixture (0.1 MPa) was used. The extension of this study [13] provided values of absorption for energy in the ^{57}Fe Mössbauer spectroscopy for three different counting gases (see Table 1).

With respect to reduction of the 1.8 keV escape of krypton, the mixture of argon, krypton and methane is more preferable to register 14.4 keV gamma rays.

Other studies [14, 15] presented a "toroidal" proportional gas flow

Table 1 | *Absorption of 6.4 keV conversion X-rays and 14.4 keV gamma rays in the toroidal detector with different counting gases (0.1 MPa).*

Counting gas	Absorption for 6.4 keV conversion X-rays (%)	Absorption for 14.4 keV gamma rays (%)
90 % Ar, 10 % CH$_4$	80	16
90 % Kr, 10 % CH$_4$	85	91
45 % Ar, 45 % Kr, 10 % CH$_4$	83	73

counter filled with 90 % argon and 10 % methane mixture (0.1 MPa). This detector is a true toroid only from 75 % of its shape. The anode (supported by eight teflon rods) is shifted by 10 % from the center of the diameter of the toroidal cross section towards the symmetry axis of the counter to be closer to the sample. The detector window was made from a metalized plastic foil (mylar) and had flat shape, whereas the windows presented in [12, 13] had a curved shape. In fact, the absorber (sample) is a part of the detector and has a limited size [14, 15]. The energy resolution of this detector for 14.4 keV gamma rays was determined to be 19 %. The line width for the conversion X-rays Mössbauer spectroscopy was 0.37 mm/s and for the transmission Mössbauer spectroscopy 0.47 mm/s. All of the previous studies [11–15] presented the detectors, whose anode wires are not usually circular but polygonal and stand on insulated support rods, which could have negative impact on the energy resolution of the detector. This effect was in details described by Dudkin et al. in [16].

2.1. Design of the counter

The developed prototype of a toroidal proportional gas flow counter (see Figure 1 (a)) [17] has an ideal toroidal shape (a ring shape in cross section). The outer diameter of the detector is 80 mm. The detector body forms the cathode (ground state) and it was manufactured from the stainless steel EN 1.4404 (AISI 316L) using 3D printing technology. This technology (LaserCUSING, layer thickness of 30-45 μm) allows to create a true toroidal shape with a constant thickness of the cathode wall (in this case, 2.5 mm). The inner diameter of the cathode is 25 mm. In

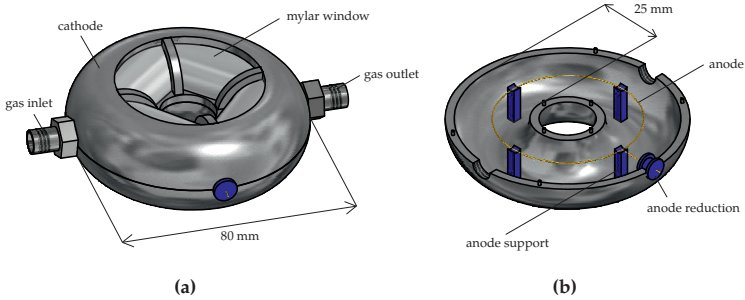fact, the cathode consists of two parts, which originate from the horizontal cross section of the toroid.

Figure 1 *(a) Layout of the developed toroidal proportional gas flow counter and (b) anode configuration inside the counter.*

The first part of the cathode includes four gaps for the windows. The selection of window material is crucial as it has a tremendous impact on the detection efficiency of the detector. It has to transmit as much the 6.4 keV X-rays and the 14.4 keV gamma rays as possible. Thus, the absorption coefficient of this material for these two energies has to be as low as possible. Because curved windows are required (see Figure 2), the use of beryllium was rejected by its brittleness, cost and toxicity. The thin aluminum foils can be contaminated by the trace amounts of iron caused by their fabrication; hence, all the Mössbauer spectra observed with these windows will contain a subspectrum of it. Regarding to this, a plastic foil (mylar) with one side aluminized was chosen as an ideal material for windows. The conductive side of the plastic foil is located inside the working volume of the detector. The electrical conductivity between the shell of the detector and the mylar windows is provided via the carbon conductive glue.

The anode support is mounted in the second part of the cathode. The anode (gold plated tungsten wire with 50 μm diameter) has a circular shape (not polygonal), and it stands on four plastic columns located in the centre of the detector (see Figure 1 (b)). The anode is carried out of the detector through a plastic reduction and soldered to the coaxial cable RG-62A/U (93 ohm, 42.5 pF/m) with crimped SHV connector.

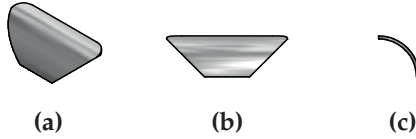Both cathode parts are assembled together and sealed with a two-

9

Figure 2 | *Specific shape of mylar window: (a) layout, (b) front view and (c) side view.*

components putty (Thorlabs' Vacuum epoxy resin) designed for high vacuum chambers down to 10^{-9} Torr. As shown in Figure 1 (a), the detector is equipped with a gas inlet and gas outlet to fill the detector and for continuous exchange of the counting gas or a mixture.

2.2. Experimental setup

The proposed experimental setup (see Figure 3) was designed to determinate the parameters of the detector (such as energy resolution via multichannel analysis and detection efficiency), where gas management with the precise signal processing and data acquisition were provided.

As the detector was tested with different types of counting gases, the pure ones (argon and krypton) were supplied from commercial flashes. However, the gas mixtures (different concentration of argon and methane) were prepared by the gas mixer KM 20-200-3ME (WITT). The whole system of gas tubing (3 mm outer diameter) was fabricated from stainless steel, which does not interact with the methane. For better comparison of different counting gases, the constant gas pressure (approximately 0.1 MPa) and almost the same flow rates of the gases were used.

The toroidal proportional gas flow counter was supplied by the programmable high voltage supply HP2.5PAA025 (Applied Kilovolts), which was controlled by the NI USB-6221 card (National Instruments). The analog output of this USB multifunction card provided signal (0-10 V), which set the relevant voltage on the high voltage supply output (0-2500 V). The signal of 1 V (on the analog output of the multifunction card) corresponds to 250 V (voltage provided by the high voltage supply). For keeping better stability of the high voltage supply (crucial parameter), the burn-in process for 24 hours was followed (e.g. long term measurements like obtaining Mössbauer spectra). Considering the time
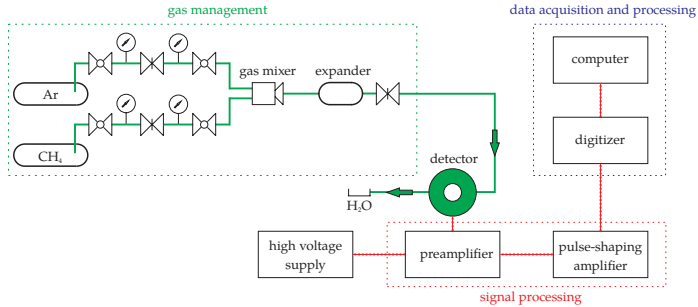
Figure 3 | *Experimental setup used to determinate the parameters of the detector.*

and economy (flowing gas), it was not possible to burn-in the high voltage supply during measuring of the multichannel analysis spectra.

The current pulses with low amplitudes from the detector were converted into the voltage signal with a high signal-to-noise ratio by the 142PC preamplifier (ORTEC). Then the voltage signal was amplified by the 572A amplifier (ORTEC) with the shaping time of the pulses, equal to 1 µs. The fast digitizer NI PCI-5124 (National Instruments) with 8-bits resolution was used to record the data and the LabVIEW^TM-based user application [18] to process the data. With regard to the shaping time of the pulses, the sampling rate of the detector signal was set to 2 MSa/s. The optimal vertical range of the input channel was set in accordance with the observed pulse amplitudes (shapes of the obtained pulses are shown in Figure 4).

2.3. Multichannel analysis

Multichannel analysis spectra were measured in the transmission geometry (^{57}Co radiation source was directed straight into the detector window and no sample was used during the measurements). The lead plate (with a thickness of 8 mm) was used as a collimator with a hole (10 mm in diameter) in the center. The multichannel analysis spectra were measured for pure argon, several mixtures of argon and methane with different concentration and pure krypton. Because the first legible peaks occurred above 1100 V, the high voltage range for every gas or gas mixture was from 1100 V to 1600 V (above this value, the pulse ampli-
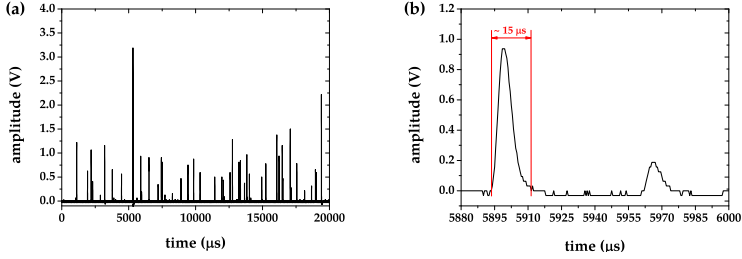
Figure 4 *(a) Amplified signal from the toroidal proportional gas flow counter using 90.0 % argon and 10.0 % methane mixture (1400 V) as a counting gas, and (b) detailed view of pulse shapes.*

tudes were out of vertical range of the used digitizer) with a step of 50 V. Every single voltage step of the multichannel analysis was measured:

a) **without filters** - all the ionization radiation was detected,

b) **with aluminum filter** (approximate thickness of 40 μm) - this filter shields soft X-rays,

c) **with cooper filter** (approximate thickness of 40 μm) – the cooper filter shields soft X-rays as well as low-energy gamma rays.

The location of these two types of filters between the radiation source and the detector allows to distinguish the type of ionization radiation. Considering that every vertical range corresponds to 257 channels in the used application [18], the channels were recalculated to voltage values to observe the changes of pulse amplitudes. Because the purity of the gas could also affect the results, the high purity gases were used as counting gases in the detector (see Table 2). Before the measurements started, the detector was washed by the given gas for 15 minutes to keep the purity of every single gas (or a gas mixture).

As all measurements were not realized during one day, the activities $A(t)$ of ^{57}Co radiation source (1.85 GBq on 15th of November, 2010) were calculated using the equation 1 for every date of the realized measurement.

12

Table 2

Type of gas	Gas label	Purity (%)
Argon	6.0	$\geq$ 99.9999
Methane	6.0	$\geq$ 99.9999
Krypton	5.0	$\geq$ 99.999

Purity of gases used as counting gases in the detector.

$$A(t) = A_0 \left(\frac{1}{2} \right)^{\frac{t}{\tau}},$$ (1)

where A_0 is the initial activity, t is the age of the source and τ is the half-life of the radionuclide. The calculated values of the activities in current day of measurement are shown in Table 3. The uncertainty of $\pm$ 10 % is given by manufacturer of the radioactive isotope (RITVERC) [19].

Table 3 | *Activities of ^{57}Co used to compare different counting gases in the toroidal proportional gas flow counter.*

Date of measurement	Counting gas	Current activity (Bq)
16.3.2018	pure argon	2 005 769 $\pm$ 10 %
4.4.2018	97.5 % Ar, 2.5 % CH$_4$	1 910 898 $\pm$ 10 %
4.4.2018	95.0 % Ar, 5.0 % CH$_4$	1 910 898 $\pm$ 10 %
5.4.2018	92.5 % Ar, 7.5 % CH$_4$	1 906 031 $\pm$ 10 %
31.1.2018	90.0 % Ar, 10.0 % CH$_4$	2 243 948 $\pm$ 10 %
5.4.2018	87.5 % Ar, 12.5 % CH$_4$	1 906 031 $\pm$ 10 %
16.3.2018	85.0 % Ar, 15.0 % CH$_4$	2 005 769 $\pm$ 10 %
6.4.2018	pure krypton	1 901 177 $\pm$ 10 %

As a large amount of data was collected, the multichannel analysis spectra recorded without any filters are presented below. All the multichannel analysis spectra were collected by René Vondrášek, B.Sc. within his bachelor thesis [20] (where L. Kouril was his consultant and laboratory supervisor). The multichannel analysis spectra for the pure argon are shown in Figure 5. The higher voltage applied between the anode and the cathode causes the increase in pulse amplitudes. At 1200 V, only

a small amount of 14.4 keV gamma rays peak is observed. However, at and above 1200 V, both energies (6.4 keV X-rays and 14.4 keV gamma rays) are distinguished, and the energy resolution rises.
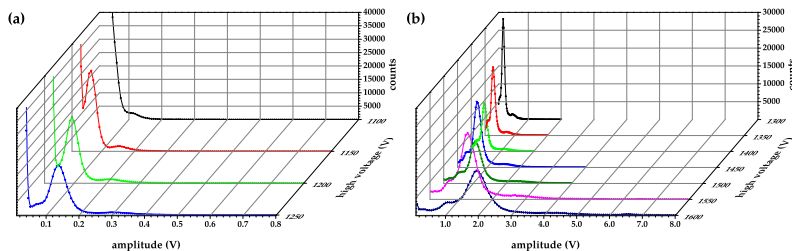

Figure 5 *Multichannel analysis spectra obtained for pure argon, while applying (a) 1100–1250 V and (b) 1300-1600 V supply voltage.*

At high voltage with a value of 1350 V, the characteristic escape peak of argon (3.4 keV) starts to be visible. In argon or its mixtures with other gases (such as methane), about 15 % of photoelectric absorptions are followed by the emission of the photon. This secondary photon has a very long mean free path for absorption. Therefore, it can escape from the detection volume. This process produces the characteristic peak of argon [21]. The multichannel analysis spectra obtained for the 97.5 % Ar and 2.5 % CH_4 in a mixture are shown in Figure 6.
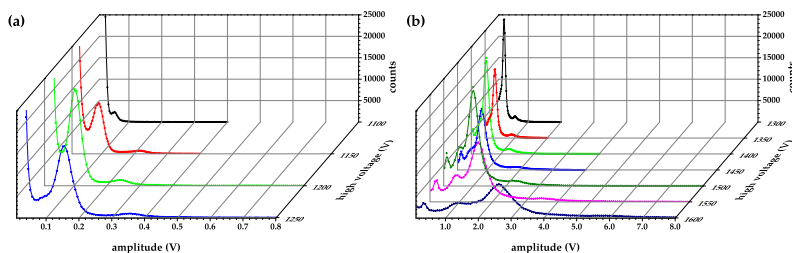

Figure 6 *Multichannel analysis spectra obtained for 97.5 % Ar and 2.5 % CH_4 mixture, while applying (a) 1100–1250 V and (b) 1300-1600 V supply voltage.*

As it is shown in Figure 6, the multichannel analysis are almost similar to the ones obtained for pure argon. However, the decrease in vertical range at lower supply voltage (1100-1150 V) and adding of 2.5 % of methane (quenching gas) caused the better resolution of the 14.4 keV gamma rays peak. Repeatedly, the characteristic escape peak of argon starts to be distinguished from 1350 V.

Figure 7 demonstrates the multichannel analysis spectra, which have been measured while using 95.0 % Ar and 5.0 % CH$_4$ mixture as a counting gas in the detector. This increase in methane concentration leads to earlier particular visibility of the 6.4 keV X-rays peak (it is nearly visible at 1100 V).
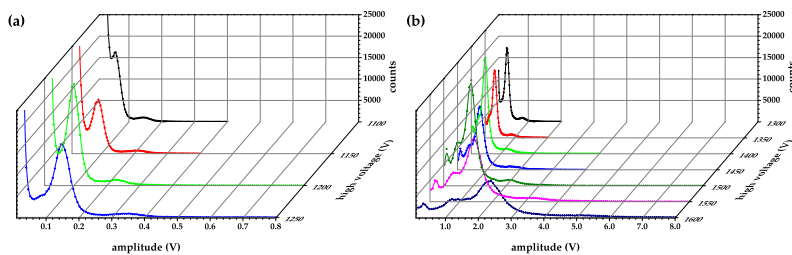

Figure 7 | *Multichannel analysis spectra obtained for 95.0 % Ar and 5.0 % CH$_4$ mixture, while applying (a) 1100–1250 V and (b) 1300-1600 V supply voltage.*

As shown in Figure 8 (multichannel analysis for 92.5 % Ar and 7.5 % CH$_4$ in a mixture), the next increase in the energy resolution is observed at 1100 V. Moreover, the characteristic escape peak of argon is barely visible till 1300 V.

The multichannel analysis spectra for the most common gas mixture (90.0 % of Ar and 10.0 % of CH$_4$) used in the area of proportional gas counters are shown in Figure 9. Unfortunately, the inappropriate option of the vertical range of the input channel (for 1100 V and 1150 V supply voltage) makes the determination of the energy resolution impossible (especially for 6.4 keV X-rays peak).

On the other hand, the detector high voltage working area for this gas mixture is probably higher than 1150 V. Figure 10 presents the multichannel analysis spectra for the 87.5 % Ar and 12.5 % CH$_4$ mixture.
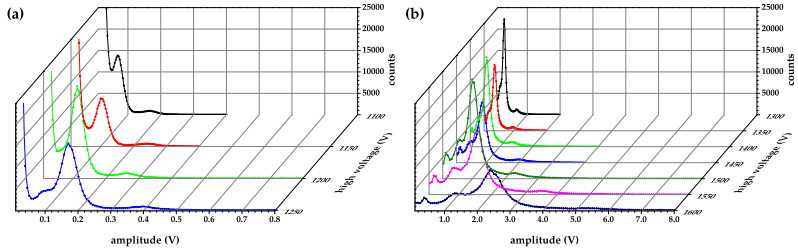
15

Figure 8 *Multichannel analysis spectra obtained for 92.5 % Ar and 7.5 % CH$_4$ mixture, while applying (a) 1100–1250 V and (b) 1300-1600 V supply voltage.*
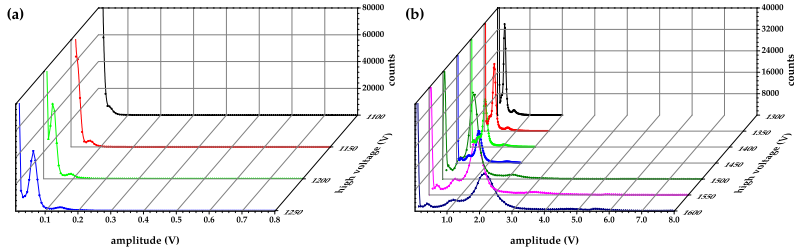

Figure 9 *Multichannel analysis spectra obtained for 90.0 % Ar and 10.0 % CH$_4$ mixture, while applying (a) 1100–1250 V and (b) 1300-1600 V supply voltage.*

While using this gas mixture as a counting gas, the first evidence of the characteristic escape peak argon appears at 1200 V.

The last analyzed gas mixture was 85.0 % of Ar and 15.0 % of CH$_4$. Its multichannel analysis spectra are demonstrated in Figure 11. The results are similar to those, which were observed using the 87.5 % Ar and 2.5 % CH$_4$ mixture. The escape peak is barely visible from 1200 V and the energy resolution increases with the increase in the supplied voltage.

Multichannel analysis spectra obtained with pure krypton as counting gas are shown in Figure 12. While the pure krypton is used, the detector achieves higher energy resolution than with pure argon or its
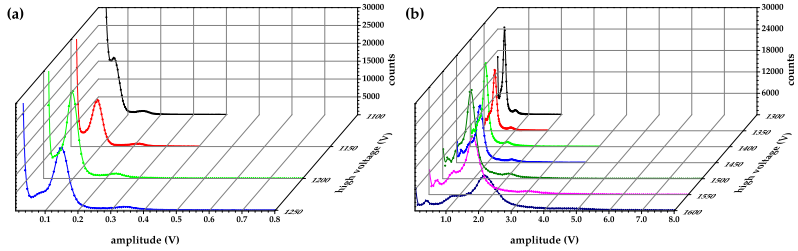
16

Figure 10 | *Multichannel analysis spectra obtained for 87.5 % Ar and 12.5 % CH$_4$ mixture, while applying (a) 1100–1250 V and (b) 1300-1600 V supply voltage.*
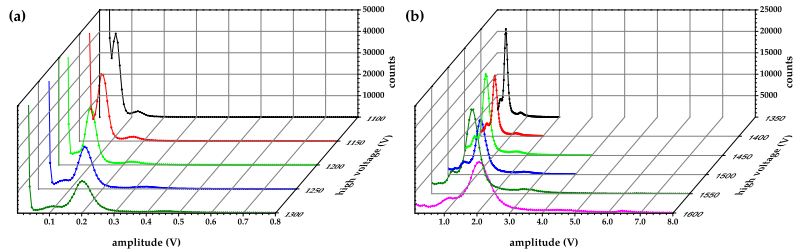

Figure 11 | *Multichannel analysis spectra obtained for 85.0 % Ar and 15.0 % CH$_4$ mixture, while applying (a) 1100–1300 V and (b) 1350-1600 V supply voltage.*

mixtures with methane. The first evidence of the characteristic escape peak of krypton (1.8 keV) is at 1400 V supply voltage. The origin of this escape peak is the same as the one for characteristic escape peak of argon, which was described above. All the measured multichannel analysis spectra prove that with an increase of supply high voltage, the amplitudes of the pulses grow. It leads to a strong dependence of pulse amplitudes on the stability of the used high voltage supply, which is supported by the Diethorn expression [22].
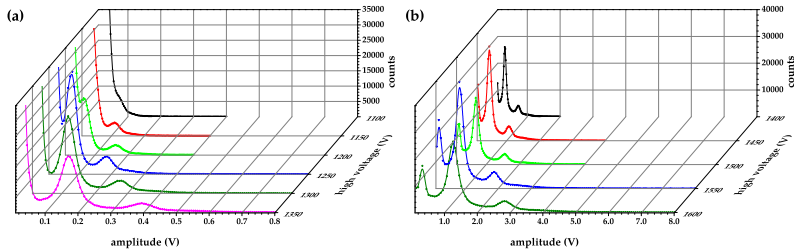
Figure 12 | *Multichannel analysis spectra obtained for pure krypton, while applying (a) 1100–1300 V and (b) 1350-1600 V supply voltage.*

2.4. Energy resolution

Energy resolution R_E for different counting gases was determined from the multichannel analysis spectra shown in Figures 5-12. The energy resolution R_E can be written as

$$R_E(\%) = \frac{FWHM(E)}{E_p}100.$$ (2)

As the energy resolution depends on the *FWHM* (see equation 2) all the observed full energy peaks (6.4 keV and 14.4 keV) were fitted by the classical Gaussian function defined as

$$y = y_0 + Ae^{-\frac{(x-x_c)^2}{2w^2}},$$ (3)

where y_0 is an offset, A is an amplitude, x_c is a center of the peak and w is a width. The *FWHM* was calculated using the equation

$$FWHM = 2w\sqrt{\ln 4}.$$ (4)

The background compensation was provided by the LabVIEW™-based application [23], which is based on the methods used in the commercial spectroscopy systems (ORTEC, CANBERRA). This linear background compensation method is shown in Figure 13 (the 14.4 keV gamma rays peak obtained with pure krypton at 1350 V). The red line (see Figure 13 (a)) represents the background compensation of the experimental data. Afterwards, the background data are subtracted from the recorded

18

spectra and the corrected experimental data are fitted by the Gaussian function (see Figure 13 (b)). The fit quality could be determined by R^2 value (also known as coefficient of determination; ideal fit gives $R^2 = 1$). R^2 value rises with more parameters introduced, but this does not imply a better fit. The adjusted $R^2_{\text{adj.}}$ value accounts for the degrees of freedom and it is a better measure of the fit precision. Hence, this parameter is used for determination of fit qualities below. In this case, the $R^2_{\text{adj.}}$ value is 0.99545, which means that the residual data (residual sum of squares) of the fit are 0.455 %. For all calculations, the Origin$^{\text{TM}}$-software was used.
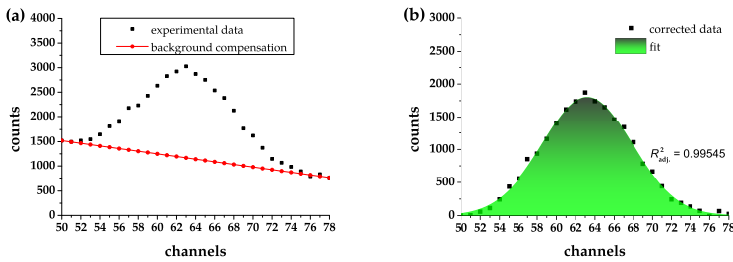

Figure 13 *Full energy peak of the 14.4 keV gamma rays obtained for krypton at 1350 V: (a) linear background compensation and (b) fit of the corrected data.*

Whereas the full energy 14.4 keV gamma peak is simple to fit by one Gaussian function, the ^{57}Fe X-rays full energy peak theoretically consists of three Gaussian functions in the obtained multichannel analysis spectra. The probability of different X-rays emissions and their energies are determined by the decay scheme of ^{57}Fe (see Table 4) [19].

Table 4 *Probabilities of X-rays emissions from ^{57}Fe.*

Type of X-rays	Energy (keV)	Probability of emission
Fe X$_{\text{K}\alpha 1}$	6.40384	16.8 ± 0.3 %
Fe X$_{\text{K}\alpha 2}$	6.39084	33.2 ± 0.5 %
Fe X$_{\text{K}\beta}$	$7.058 - 7.108$	7.1 ± 0.2 %

Basically, it is impossible to achieve enough high energy resolution for distinguishing these low energy differences by using the propor-

tional gas counters. However, their presence affects the fit quality $R^2_{\text{adj.}}$ value. Thus, it is necessary to fit the X-rays full energy peak area at least by using two Gaussian functions. The Fe $X_{K\alpha1}$ and Fe $X_{K\alpha2}$ energies are very close (the difference between them is only 0.013 keV) and their centers correspond to almost same channels in multichannel analysis spectra. On the other hand, the energy difference between Fe $X_{K\beta}$ and Fe $X_{K\alpha2}$ is in the range from 0.66716 keV to 0.71716 keV, so the Fe $X_{K\beta}$ can affect the right side of the total fit. Moreover, at 1200 V and above (for argon and its mixtures), a next peak has to be added to the fitted data, because the escape peak of argon (3.4 keV, created by Fe $X_{K\alpha}$) starts to occur. The argon gamma rays absorption probability (see Table 1) and K fluorescence yield of argon (ω_K is in the range from 0.08 to 0.14 [24]) are low, so escape peak created by gamma rays was not observed in the multichannel analysis spectra. In fact, K fluorescence yield ω_K determinates the probability of escape peak creation. The krypton escape peak (ω_K is in the range from 0.62 to 0.67 [25]) has lower energy (1.8 keV, created by the 14.4 keV gamma rays) and is not included in the fitting data. The condition for the escape peak production is that ionization rays energy has to be higher than the absorption edge of the given gas. The K absorption edge of krypton is 14.32 keV (3.20 keV for argon), so no escape peak is created by Fe $X_{K\alpha}$. Figure 14 (a) demonstrates theoretical fit distribution (including argon escape peak) of different X-rays types in the recorded multichannel analysis spectrum for 95.0 % Ar and 5.0 % CH_4 mixture at 1450 V.
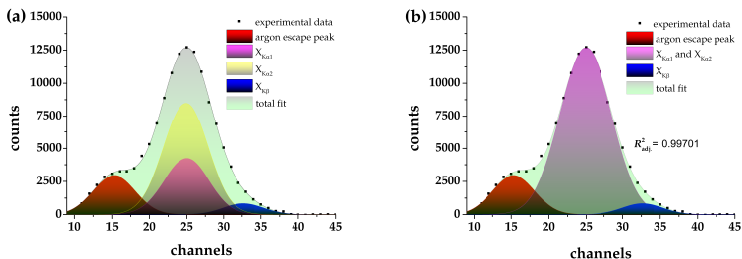

Figure 14 (a) Theoretical fit distribution of the multichannel analysis spectrum obtained for 95.0 % Ar and 5.0 % CH_4 mixture at 1450 V and (b) real fit by using three Gaussian functions.

Subsequently, Figure 14 (b) shows real fit of this spectrum using three Gaussian functions, which were used to determine energy resolution of the toroidal proportional gas counter for X-rays detection.

Energy resolution of the detector was determined separately for the X-rays (Fe $X_{K\alpha 1}$ and Fe $X_{K\alpha 2}$, counted at 6.4 keV) and for the full peak of 14.4 keV gamma rays. In details, the energy resolution R_E values together with the $R^2_{adj.}$ values calculated for all tested gases are available in full text of the thesis [26].

Basically, there is a decreasing trend of all energy resolution values with increasing high voltage value. Generally, the quality of the fit $R^2_{adj.} > 0.99$ for the 6.4 X-rays fit was reached in almost all the cases. This means that the amount of the residual data excluding the fit were lower than 1 %. The same fit quality was achieved for 14.4 keV gamma rays peak (only when krypton was used as a counting gas). Table 5 summarizes minimum reached energy resolution values R_X (for 6.4 keV X-rays) and R_γ (for 14.4 keV gamma rays) with appropriate $R^2_{adj.}$ values for all the tested counting gases.

Table 5 | *Minimum reached energy resolution values R_X and R_γ with appropriate $R^2_{adj.}$ values for all tested counting gases.*

Counting gas	R_X	$R^2_{adj.}$ (for R_X)	R_γ	$R^2_{adj.}$ (for R_γ)
pure argon	37 %	0.99350	16 %	0.72751
97.5 % Ar, 2.5 % CH$_4$	33 %	0.99530	15 %	0.96948
95.0 % Ar, 5.0 % CH$_4$	34 %	0.99545	17 %	0.98508
92.5 % Ar, 7.5 % CH$_4$	32 %	0.99536	12 %	0.94471
90.0 % Ar, 10.0 % CH$_4$	31 %	0.99561	12 %	0.92100
87.5 % Ar, 12.5 % CH$_4$	31 %	0.99292	13 %	0.96031
85.0 % Ar, 15.0 % CH$_4$	32 %	0.99501	15 %	0.97527
pure krypton	28 %	0.99227	15 %	0.99538

While the minimum achieved energy resolution value for 6.4 keV X-rays ($R_X = 28$ %) was reached when the pure krypton was used as a counting gas, the maximum value ($R_X = 37$ %) was determined for pure argon. Adding quenching gas (methane) to argon decreases this value and the lowest energy resolution value ($R_X = 31$ %) was obtained when the gas mixture was 90.0 % of Ar and 10.0 % of CH$_4$. This gas mixture

ratio was found as the best one as in [15, 17, 27]. The same energy resolution value for 6.4 keV X-rays was reached when using the 87.5 % Ar and 12.5 % CH_4 mixture as a counting gas. On the other hand, minimum energy resolution value for the 14.4 keV gamma rays ($R_\gamma = 12$ %) was observed when 92.5 % Ar and 7.5 % CH_4 in a mixture (the same value for 90 % Ar, 10 % CH_4 mixture) was used as a counting gas. The lowest energy resolution value for krypton was $R_\gamma = 15$ %. The published toroidal proportional counters [12, 14, 15] have energy resolution for the 14.4 keV gamma rays (energy resolution values for the 6.4 keV X-rays are not mentioned) in the range from 25 % to 19 %. The toroidal proportional gas flow counter developed within this dissertation thesis reached energy resolution values for the same energy peak in the range from 17 % to 12 %, while various types of gases were used as counting gases.

2.5. Energy proportionality

The characteristic escape peak of argon (at 1250-1300 V and above, see Figures 5-11) appears in the multichannel analysis spectra, and its energy of 3.4 keV is commonly known [21]. For krypton, the escape peak has lower energy i.e., 1.8 keV [13], and it starts to appear at 1450 V and above (see Figure 12). With respect to this fact, energy proportionality of the detector could be beneficially determined by using one radiation source (in this case, [57]Co). The peak maximum channel positions were obtained from the previous Gaussian fits (chapter 2.4). These values correspond to the energies given by the [57]Co decay scheme (i.e., the 6.4 keV X-rays, the 14.4 keV gamma rays and relevant escape peaks of used counting gas). Because energy distribution should be proportional, pulse amplitudes (represented by the channel number) the dependence of on energy values has to be linear. Therefore, the data were fitted by using the simple equation 5

$$y = a + bx, \tag{5}$$

where the a is y-intercept and b is line slope. In fact, energy proportionality is determined by the $R^2_{\text{adj.}}$ value, which represents the linear regression quality (perfect one with $R^2_{\text{adj.}} = 1$). All the linear regressions with energy proportionality deviations for all tested gases are presented in [26].

The developed toroidal proportional gas flow counter achieved high proportionality in the energy region from 1.8 keV to 14.4 keV, where the energy proportionality deviation was in almost all cases lower than 1 % for pure argon and its mixtures with methane (0.1 % for pure krypton). Due to this, the detector is able to work properly in the spectroscopic mode, which requires high energy proportionality.

2.6. Detection efficiency

Detection efficiency ϵ_d of every radiation detector is defined as a ratio of the registered photon events number (sum of counts in the given discrimination window N_c) and the theoretical number of emitted photons N_e incidental on the detector window (see equation 6).

$$\epsilon_d(\%) = \frac{N_c}{N_e}100, \tag{6}$$

The detection efficiency values were calculated via processing the data collected in the chapter 2.3. Firstly, the theoretical numbers of emitted photons N_{eX} and $N_{e\gamma}$ were calculated for every analyzed counting gas. The number of emitted photons was calculated by using the source activities presented in Table 4 and probabilities of different photon emissions (a sum of emission probabilities is shown in Table 4 for the 6.4 keV X-rays including the 7.0 keV X-rays, and probability of the 14.4 keV gamma photon emission is 9.15 ± 0.17 % [19]). Because of the used geometry for recording the multichannel analysis spectra (see Figure 15), the simple point source approximation was calculated to correct the emitted photon number incidental on the counter.
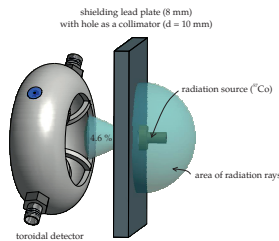

Figure 15 | *Layout of the geometry used for recording the multichannel analysis spectra.*

The number of registered photon events was calculated as the sum of the counts in the relevant discrimination window. For argon and its mixtures, the 6.4 keV X-rays discrimination windows also cover the escape peak (if observed), as it should be a valid detection of X-ray photon. The krypton 1.8 keV escape peak was added to valid detection of the 14.4 keV gamma rays. Detection efficiencies were calculated for manually determined discrimination windows (total sum of counts in the relevant window, see Figure 16 (a)) and also for the same window with the linear background compensation (sum of the background counts were subtracted from the total sum of counts, see Figure 16 (b)).
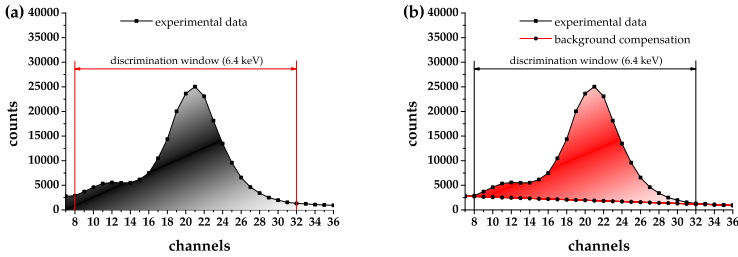

Figure 16 | *The 6.4 keV X-rays discrimination window (90.0 % Ar, 10.0 % CH_4, including argon escape peak) for calculating detection efficiency using (a) all counts in the window and (b) linear background compensation to correct the counts number.*

Detection efficiencies were determined for the whole range of supplying high voltage (usually in the interval of 1150-1600 V, if both peaks were observed). Repeatedly, the detection efficiencies for all tested gases are shown in [26].

As it can be deduced from Table 1, pure krypton has the highest detection efficiency for both ionization rays from all the tested counting gases. The 1.8 keV krypton escape peak was completely hidden in the noise till 1400 V. However, its appearance at 1450 V causes a rapid increase of the 14.4 keV gamma rays detection efficiency. Table 6 provides a summary of the highest calculated detection efficiencies ϵ_d and detection efficiencies with background compensation $\epsilon_{d'}$.

The determined accuracy for all the detection efficiency values was ± 10 % from the calculated value. In fact, this accuracy value eliminates

Table 6 | *Summary of the highest detection efficiencies ϵ_d, and detection efficiencies with background compensation $\epsilon_{d'}$.*

Counting gas	ϵ_{dX} (%)	$\epsilon_{d\gamma}$ (%)	$\epsilon_{d'X}$ (%)	$\epsilon_{d'\gamma}$ (%)
pure argon	8.9	**5.6**	**6.8**	1.2
97.5 % Ar, 2.5 % CH$_4$	9.2	4.8	5.5	1.6
95.0 % Ar, 5.0 % CH$_4$	9.3	4.8	5.7	1.7
92.5 % Ar, 7.5 % CH$_4$	**9.4**	4.7	5.9	**2.1**
90.0 % Ar, 10.0 % CH$_4$	8.5	5.1	6.1	1.4
87.5 % Ar, 12.5 % CH$_4$	9.0	4.8	5.8	1.9
85.0 % Ar, 15.0 % CH$_4$	8.4	5.3	**6.5**	1.8
pure krypton	**10.9**	**36.8**	5.9	**10.6**

any possibility to determine the best counting gas for X-rays regarding the detection efficiency. However, optimal counting gas for the 14.4 keV gamma rays detection is definitely pure krypton reaching up to seven times higher detection efficiency value than pure argon or any of its mixtures with methane.

2.7. Utilization in Mössbauer spectroscopy

The toroidal proportional gas flow counter has been primarily designed for the purpose of the conversion X-rays ^{57}Fe Mössbauer spectroscopy (especially for analysis of the bulk material surfaces). On the other hand, it is also possible to use it for the transmission Mössbauer spectroscopy, when the 14.4 keV gamma rays are registered. In both cases, the experimental setup was modified by adding the velocity driver and the analog feedback [28]. The rest of the experimental setup remains the same as shown in Figure 3. The detection parts of the assembled Mössbauer spectrometers in both geometries are demonstrated in Figure 17.

As the counting gas, the 90.0 % argon and 10.0 % methane gas mixture was used as it is less expensive compared to the krypton usage. This selected mixture of gases provides the best energy resolution (31 % for the 6.4 keV X-rays and 12 % for the 14.4 keV gamma rays, see chapter 2.4). The gas pressure was approximately 0.1 MPa (identical as in all the multichannel analysis measured in chapter 2.3).
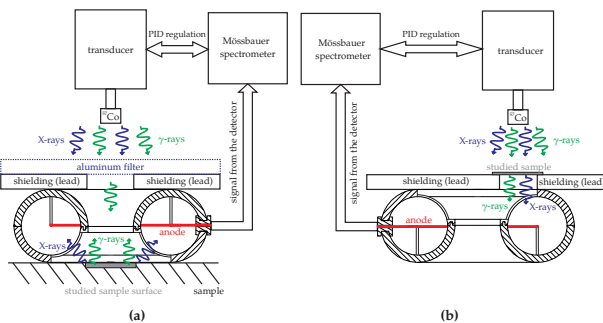
Figure 17 | *Detection part of the Mössbauer spectrometer in the (a) backscattering geometry and (b) transmission geometry.*

It was verified that the optimal high voltage value is 1400 V (compromise between energy resolution and detection efficiency). Before first ^{57}Fe Mössbauer spectrum recording, multichannel analysis spectra (see Figure 18) were measured in both geometries using aluminum and copper foil filters. Multichannel analysis spectrum in the backscattering geometry (see Figure 18 (b)) was recorded when a block of the austenitic stainless steel EN 1.4541 (AISI 321) was used as a sample. In this case, the filters were placed on all four detector windows.
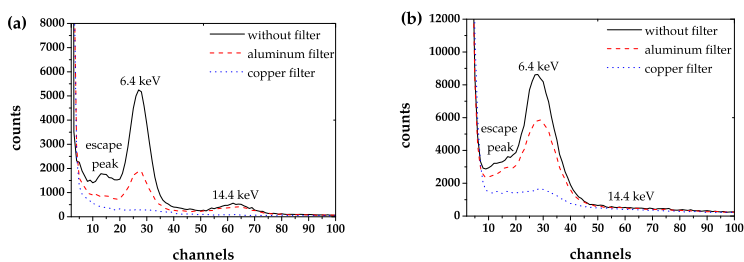

Figure 18 | *Multichannel analysis spectra in the (a) transmission geometry and (b) backscattering geometry.*

Aluminum filters are commonly used in the area of CXMS to reduce the number of lower e- nergy X-rays emitted from the source. These low-energy X-rays are non-resonant and decrease the resonance effect ϵ

26

and the statistical quality Q of the recorded Mössbauer spectrum.

The statistical quality Q is given by the equation

$$Q = \frac{\epsilon^2}{\epsilon + 2} N(\infty), \tag{7}$$

where $N(\infty)$ is the number of counts far from the resonance [29]. A series of aluminum filters with different thicknesses d were placed behind the radiation source (see Figure 17) to evaluate the influence of resonant and non-resonant X-rays. The backscattering ^{57}Fe Mössbauer spectra were obtained for the same period of time (1 hour) for the same sample (a block of the austenitic stainless steel EN 1.4541 (AISI 321)). Then, the data were processed via the MossWinn fitting software [30]. Figure 19 shows the dependence of the calculated effect, statistical quality and the count rate on the thickness of the aluminum filter.
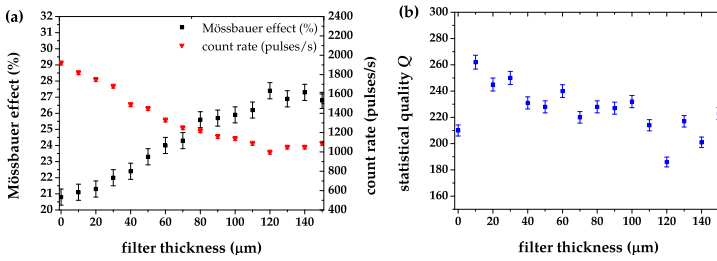

Figure 19 | *The dependence of the (a) Mössbauer effect and count rate and (b) statistical quality on the aluminum filter thickness.*

To keep the high count rate and the filtration of some non-resonant X-rays, a 10 μm thick aluminum filter was used for the following measurements in the backscattering geometry.

Figure 20 (a) represents the ^{57}Fe Mössbauer spectrum of the calibration sample α-Fe, whereas the conversion X-rays (6.4 keV) were registered. The line width was determined as 0.258 mm/s and the resonance effect was 9.3 ± 0.5 %. The obtained spectrum of the austenitic stainless steel block EN 1.4541 (AISI 321) is shown in Figure 20 (b) with the resonance effect of 22.8 ± 0.5 %. Both spectra were recorded for 24 hours.

Figures 21 (a) and (b) demonstrate that the developed detector also allows to register low energy gamma rays. However, the resonance ef-
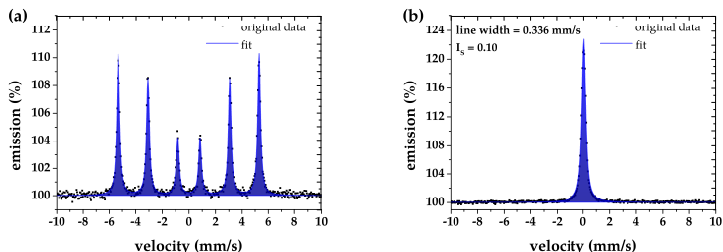
Figure 20 ^{57}*Fe Mössbauer spectra obtained by registration of the 6.4 keV conversion X-rays using the toroidal detector of the (a) α-Fe and (b) austenitic stainless steel EN 1.4541 (AISI 321).*

fect was very low, i.e., 3.2 ± 0.5 % in the backscattering geometry (72 hours spectrum) and 17.3 ± 0.5 % in the transmission geometry (1 hour spectrum). Both spectra were obtained for the calibration sample α-Fe.
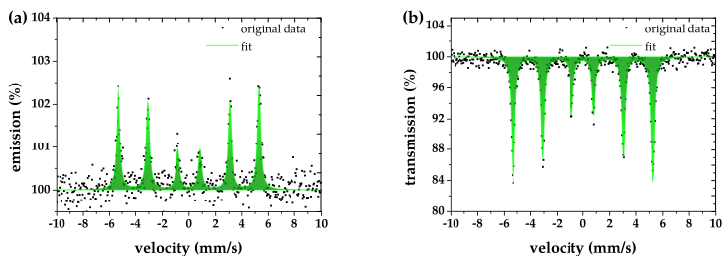

Figure 21 ^{57}*Fe Mössbauer spectra of the α-Fe obtained by registration of the low energy gamma rays (14.4 keV) using the toroidal detector in the (a) backscattering geometry and (b) transmission geometry.*

28

3.   Cylindrical proportional gas counter

As the toroidal shaped proportional gas flow counter (described in the previous chapter 2) is not a very appropriate choice for the purpose of the transmission Mössbauer spectroscopy (only one of four counter windows is used), a cylindrical counter geometry can substitute unnecessarily complicated toroidal shape.

3.1.   Design of the cylindrical counter

The cylindrical proportional gas counter (see Figure 22) was formed by 120 mm long aluminum cylindrical cathode (with an outer diameter of 40 mm, inner diameter of 24 mm). It enclosed central anode (gold plated tungsten wire with a diameter of 50 μm).
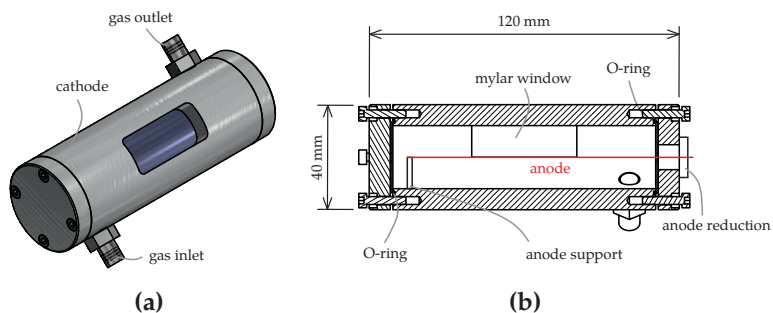

Figure 22 | *Designed cylindrical proportional gas counter: (a) basic layout and (b) cross section.*

The anode was supported only by one ABS plastic column (its distance from counter window was approximately 12 mm), as the anode central position was fixed by the ABS plastic reduction located in the rear counter cover. The anode wire was soldered to the coaxial cable RG-62A/U (93 ohm, 42.5 pF/m) with crimped SHV female connector. Front and rear cylindrical cathode sides included grooves for O-rings (26x1, where the inner diameter was 26 mm and the ring thickness was

1 mm) for better counter sealing. The detector window had lateral location and was made from aluminized mylar foil. This window was curved for keeping the cylindrical counter shape (90° sector) and was 40 mm long. In fact, the mylar foil copied the inner wall shape of the cylindrical cathode. The conductive mylar window layer was located in the counter working volume. Electrical conductivity between the aluminum cylinder and the mylar window was provided by the carbon conductive glue. The counter window was sealed with a two-components putty (Thorlabs' Vacuum epoxy resin) to prevent gas leakages. Both (rear and front) covers were fixed by using four M3 screws for properly O-rings work. Due to the possibility of some gas leakages, this proportional gas counter was designed to work in the continuous flow mode using the gas inlet and outlet.

3.2. Experimental setup and basic parameters

With respect to the observation and experiences obtained with toroidal proportional gas flow counter in chapter 2, the experimental setup was modified for testing the cylindrical proportional gas flow counter (see Figure 23).
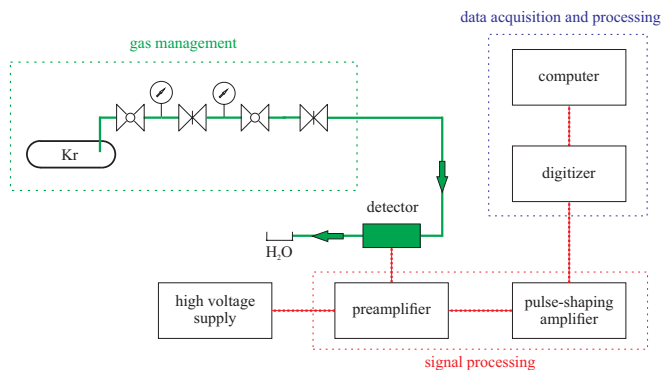
Figure 23 | *Experimental setup for testing cylindrical proportional gas flow counter.*

As most possible utilization of this counter is in the area of the transmission Mössbauer spectroscopy, pure krypton (approximate pressure of 0.1 MPa) was chosen as a counting gas (best detection efficiency for

low gamma rays from the tested gases – see chapter 2.6). The detector was supplied by the very stable high voltage supply 556 (ORTEC). The current pulses were converted into the voltage signal with a high signal-to-noise ratio by the 142PC preamplifier (ORTEC). Consequently, the low voltage signal was amplified (the gain was set to ×5 and the shaping time 0.5 μs) by the 575A amplifier (ORTEC). The amplified signal was recorded by the fast digitizer NI PCI-5124 (National Instruments) and processed by the LabVIEW^{TM}-based user application [18].

As no quenching was added to pure krypton, registered pulses from the detector were slightly longer (see Figure 24) than the ones obtained using the toroidal proportional gas counter filled with a mixture of argon and methane (see Figure 4 in chapter 2.2).
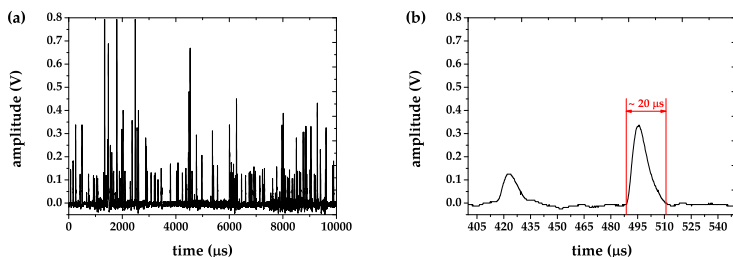

Figure 24 | *(a) Amplified signal from the cylindrical proportional gas flow counter using pure krypton (1550 V) as a counting gas, and (b) detailed view of pulse shapes.*

Multichannel analysis spectra were recorded in the transmission geometry, while ^{57}Co radiation source (1.85 GBq on 18th October, 2013 with a current activity of approximately 22 MBq) was directed straight to the detector window. No samples were used during these measurements. The real time period of the sampled signal was 25 s. Brass disc (with a thickness of 10 mm) was used as collimator with 10 mm diameter hole. Aluminum and copper filters were used to determine the energy arrangement. High voltage supply range was from 1200 V to 1750 V with a step of 50 V. As shown in Figure 25 (a), the low energy gamma rays full energy peak started to appear exactly at 1200 V with a very dominant Compton edge. With further high voltage supply increase, the 6.4 keV X-rays started to be visible (vaguely at 1250 V, clearly at 1300 V

and above). The first evidence of the 1.8 keV krypton escape peak was at 1450 V. Next increase of the supplying high voltage caused better krypton escape peak resolution. The digitizer vertical range was constantly set to ±0.8 V for multichannel analysis spectra recording shown in Figure 25 (a). In the high voltage supply range of 1600-1650 V (1700-1750 V respectively), the digitizer vertical range was ±2 V (±4 V respectively). The multichannel analysis spectra obtained in these ranges are shown in Figure 25 (b). Because of the large amount of data collected, only the multichannel analysis spectra recorded without filters are presented below.
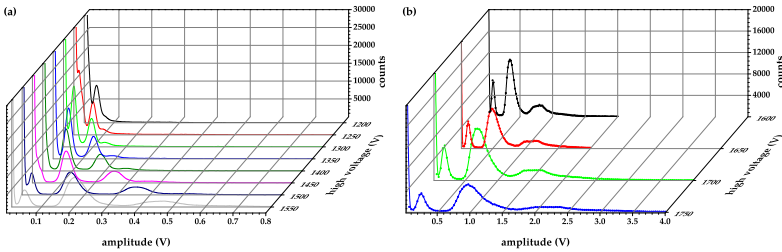

Figure 25 | *Multichannel analysis spectra recorded using the cylindrical proportional gas flow counter with krypton as a counting gas, while applying (a) 1200-1550 V and (b) 1600-1750 V supply voltage.*

Figure 26 shows multichannel analysis spectra at 1500 V using aluminum and copper filter (located between radiation source and cylindrical proportional gas flow counter), where the spectrum recorded with aluminum filter confirms the energy arrangement and the 1.8 keV krypton escape peak gamma registration validity.

Energy resolution R_E values were determined for both types of ionization rays (the 6.4 keV X-rays and the 14.4 keV gamma rays). All the experimental data were corrected by the linear background compensation presented in chapter 2.6. Consequently, the full energy peaks were fitted by the Gaussian function and the *FWHM* parameters were calculated. The energy resolution values for X-rays with appropriate $R^2_{adj.}$ values are shown in Figure 27 (a) (in Figure 27 (b) for gamma rays respectively).
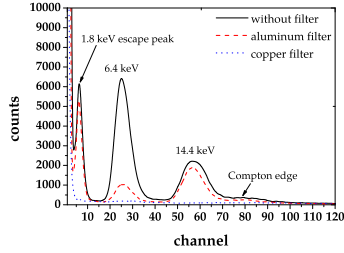
Figure 26 | *Multichannel analysis spectra at 1500 V recorded with aluminum and copper filter.*
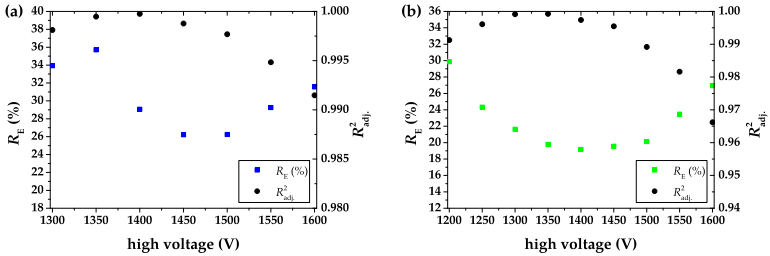

Figure 27 | *Energy resolution R_E and quality of the fit $R^2_{adj.}$ while using pure krypton as a counting gas in the cylindrical proportional gas flow counter for (a) the 6.4 keV X-rays and (b) the 14.4 keV gamma rays.*

The minimum achieved energy resolution value for the 6.4 keV X-rays was 26 % ($R^2_{adj.} = 0.99877$). This value is 2 % lower in comparison with the minimum value obtained for toroidal proportional gas flow counter in chapter 2.4 ($R_X = 28$ %, $R^2_{adj.} = 0.99227$). On the other hand, the minimum energy resolution value for the 14.4 keV ($R_\gamma = 19$ %, $R^2_{adj.} = 0.99741$) was 4 % higher than the one obtained for the toroidal detector ($R_\gamma = 15$ %, $R^2_{adj.} = 0.99538$). As another high voltage supply was used in this experimental setup, this energy resolution value increase could be caused by longer high voltage supply stabilization. Pulse amplitudes strongly depend on the high voltage and even small

high voltage shift can change the amplitude and widen the full energy peak in the multichannel analysis spectrum.

For choosing optimal high voltage supply, detection efficiency was presented via count rates in the discrimination windows corresponding to different energies in Figure 28. Because the 1.8 keV krypton escape peak should be a valid detection of the 14.4 keV gamma photon, it is recommended to use high voltage supply ≥ 1500 V (≥ 1550 V in case of the 6.4 keV X-rays registration, for which an enormous count rate increase is observed).
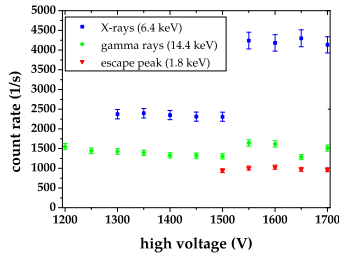

Figure 28 | *Count rates for the 6.4 keV X-rays, the 14.4 keV gamma rays, and the 1.8 keV krypton escape peak.*

As it is shown in Figure 28, the 1.8 keV krypton escape peak forms a significant gamma photon registration part (approximately 40 % of the total gamma rays registration). Table 7 demonstrates percentage representation of the 14.4 keV full energy gamma photon peak and the 1.8 keV krypton escape peak in total gamma registration.

Table 7 | *Distribution of the 14.4 keV full energy gamma photon peak and the 1.8 keV krypton escape peak in total gamma registration.*

high voltage (V)	1.8 keV	14.4 keV
1500	42 %	58 %
1550	38 %	62 %
1600	39 %	61 %
1650	43 %	57 %
1700	39 %	61 %

3.3.   Escape peak influence on the Mössbauer spectrum

For completing the transmission Mössbauer spectrometer (see Figure 29), the experimental setup (see Figure 23) was modified by adding velocity driver, PID controller [28], and the function generator 33521A (Agilent Technologies).
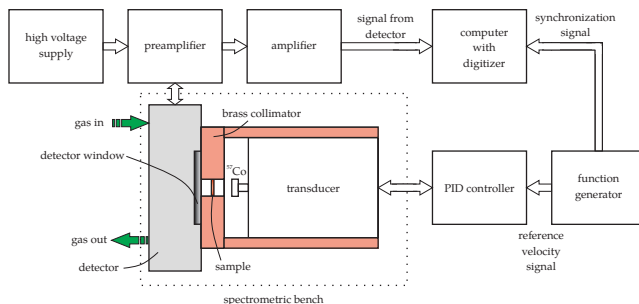
Three ^{57}Fe Mössbauer spectra of the α-iron (with different discrimination windows shown in Figure 30) were recorded simultaneously for the same period of time (116 hours).

Figure 30 | *The 1.8 keV krypton escape peak discrimination window (1) and the 14.4 keV full energy gamma peak discrimination window (2).*

Figure 31 (a) demonstrates the ^{57}Fe Mössbauer spectrum of the calibration sample α-Fe, while the discrimination window (1) covers counts

corresponding to the 1.8 keV krypton escape peak. The line width was determined to be 0.306 mm/s and the resonance effect was 30.4 ± 0.5 %. Simultaneously recorded ^{57}Fe Mössbauer 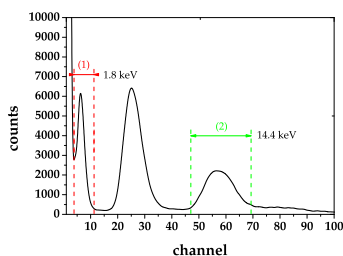spectrum using the 14.4 keV gamma full energy peak discrimination window (2) is shown in Figure 31 (b). In this case, the line width was 0.289 mm/s and the resonance effect was 31.7 ± 0.5 %.
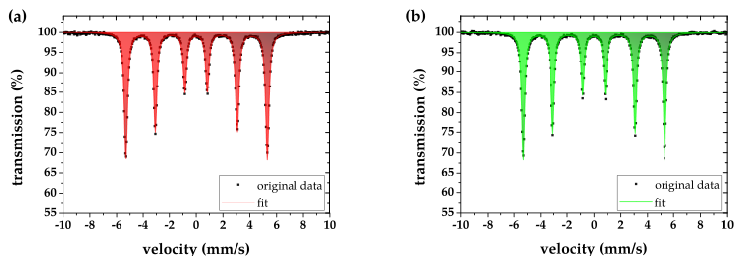
Figure 31 | ^{57}Fe Mössbauer spectra of the α-Fe obtained with cylindrical proportional gas flow counter while using (a) the 1.8 keV krypton escape peak discrimination window and (b) the 14.4 keV gamma full energy peak discrimination window.

The last ^{57}Fe Mössbauer spectrum (see Figure 32) was recorded when both discrimination windows were used for registering the gamma rays. The line width was 0.306 mm/s and the resonance effect was 30.9 ± 0.5 %.
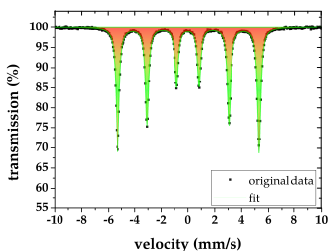
Figure 32 | ^{57}Fe Mössbauer spectrum of the α-Fe obtained with cylindrical proportional gas flow counter while both discrimination windows were used.

Table 8 summarizes the line widths (LW), resonance effects ϵ, statistical qualities Q (see equation 7), and count rates of the presented ^{57}Fe Mössbauer spectra in Figures 31 and 32. To conclude, if the studied sample contains low amount of iron, it is recommended to use both discrimination windows (higher count rate). However, if more precise resolution is required, it is better to use only the 14.4 keV gamma full energy peak discrimination window. This long term measurement also proves that about 48 % of the 14.4 keV gamma photon registration is followed by creation of the 1.8 keV krypton escape peak.

Table 8 | *Parameters of the α-Fe Mössbauer spectra recorded while using different discrimination windows.*

window	LW (mm/s)	ϵ (%)	Q	count rate (1/s)
1.8 keV	0.306	30.4	17838	328
14.4 keV	0.289	31.7	17026	348
1.8 keV and 14.4 keV	0.306	30.9	34828	676

Conclusion

The presented toroidal proportional gas flow counter has been primarily designed for the purpose of the conversion X-rays Mössbauer spectroscopy for analyzing the surfaces of the bulk materials. With respect to the toroidal shape of the detector, it is able to register soft energy X-rays and low-gamma rays in almost 2π geometry with sufficient efficiency.

Several proportional gas counter parameters were determined for different counting gases. The 90.0 % argon and 10.0 % methane mixture provides the lowest energy resolution value ($R_X = 31\%$ and $R_\gamma = 12\%$) from the whole tested argon-methane mixture spectrum. Regarding the error levels of detection efficiency values calculation, it is impossible to determine the optimal gas mixture for the 6.4 keV X-rays registration. On the other hand, pure krypton offers the lowest energy resolution value for X-rays ($R_X = 28$ %) from all tested counting gases. It was also proved that pure krypton is the most efficient counting gas (from the tested group of gases) for both ionization rays, especially for the 14.4 keV gamma rays, where detection efficiency is approximately seven times higher than in the case of argon or any of its mixtures with methane. Generally, pure noble gases are not very appropriate choices as counting gases, because detector pulses are quite long. It is more advantageous to add some more complex gases (like methane) to ensure that every pulse discharge was successfully terminated. This leads to detector pulse shortening, which can be considered as an advantage when high active radiation sources are used. On the other hand, it could also lead to detection efficiency value decrease (it can reduce the number of created pulse discharges).

The energy arrangement was confirmed by recording some ^{57}Fe Mössbauer spectra in chapter 2.7. It was also verified that usage of an aluminum filter (at least 10 μm) can improve the statistical quality of the backscattering Mössbauer spectra. The utilization of the lead shielding (see Figure 17 (a)) was observed as a crucial task as it reduces the saturation of the detector and increases the energy resolution of the detector. However, more optimized solution of stacked plate shielding arrangement [13] would probably improve its performance.

The presented detector is easy to handle and its main advantage is that it does not require any sample preparations to measure backscat-

tering Mössbauer spectra. The detector could be also used to register low-energy gamma rays. In this case it could find an application in the transmission Mössbauer spectroscopy or the backscattering gamma Mössbauer spectroscopy.

This detector is also an essential part of the ''Austenitemeter'' device, which enables fast and non-destructive determination of residual austenite amount in steels. Because of this, the detector is still upgraded to achieve the highest performance. The actual version is made from dural using the CNC technology. As it contains two O-rings between both cathode parts, it prevents more gas leakages. Nowadays, this version already successfully operates in the laboratories of the Department of Experimental Physics (Palacký University in Olomouc). Next step of the development will be focused on the detector and the whole Austenitemeter shielding to enhance its implementation by private companies.

For the purpose of the transmission Mössbauer spectroscopy, it is more optimal using the cylindrical proportional gas flow counter. The calibration sample α-Fe Mössbauer spectra recorded when using this detector proved 1.8 keV krypton escape peak being a valid detection of 14.4 keV gamma photon. In this case, it could be successfully used to improve the statistical spectra quality and count rate. On the other hand, it slightly decreases the resonance effect and increases the line width. This is probably caused by a higher noise influence, as pulse amplitudes corresponding to 1.8 keV krypton escape peak are lower than the pulses belonging to 14.4 keV gamma full energy peak. This advantage of escape peak could be also exploited by using argon or its mixtures in the conversion X-rays Mössbauer spectroscopy (e.g. when using the toroidal proportional gas flow counter).

Stručné shrnutí v českém jazyce

Prezentovaný průtokový toroidní proporcionální plynový detektor byl primárně navržen pro účely Mössbauerovy spektroskopie konverzního RTG záření, která slouží k analýze povrchu objemných vzorků. Díky svému toroidnímu tvaru je detektor schopen registrovat měkké RTG záření a nízkoenergetické gama záření téměř v 2π geometrii s dostatečnou účinností.

Detektor byl testován s různými plynovými náplněmi, pro které bylo následně určeno několik provozních parametrů detektoru. Minimální hodnota energetického rozlišení pro RTG záření 6,4 keV $R_X = 31\,\%$ a pro gama záření 14,4 keV $R_\gamma = 12\,\%$ byla určena pro směs 90.0 % argonu a 10.0 % metanu (ze skupiny směsí argonu s metanem, případně čistého argonu). Z pohledu detekční účinnosti nebylo možné určit nejoptimálnější směs plynů pro registraci konverzního RTG záření (6,4 keV) především díky velké chybě při určování hodnot detekční účinnosti. S čistým kryptonem bylo dosaženo nejnižší hodnoty energetického rozlišení RTG záření ($R_X = 28\,\%$) ze všech testovaných plynů (směsí). Bylo také prokázáno, že právě použitím kryptonu lze dosáhnout nejvyšší detekční účinnosti (ze skupiny všech testovaných plynů) pro oba druhy ionizujícího záření, především však pro nízkoenergetické gama záření, kde byla dosažena přibližně sedmkrát vyšší hodnota detekční účinnosti než u argonu případně jakékoliv jeho směsi s metanem. Obecně však vzácné čisté plyny nejsou příliš vhodnou volbou pro plnění detektorů, jelikož délky impulzů z detektoru jsou relativně dlouhé. Je mnohem výhodnější přidat k jednoduchým molekulám vzácného plynu složitější molekuly zhášecího plynu (např. metanu). Tento zhášecí plyn při správné koncentraci dokáže zajistit, aby každý pulzní výboj byl řádně ukončen. Tento efekt vede ke zkrácení událostí (impulzů) v detektoru, které je žádoucí především při použití aktivnějších zdrojů ionizujícího záření. Na druhou stranu, tento efekt může také zabránit vzniku některých sekundárních ionizací a tím tak snížit účinnost detektoru.

Naměřená mössbauerovská spektra jednoznačně potvrzují správné určení jednotlivých energií v mnohokanálových spektrech. Bylo také ověřeno, že použití hliníkového filtru (tloušťky alespoň 10 μm) pozitivně ovlivní statistickou kvalitu mössbauerovského spektra v geometrii zpětného rozptylu. Velmi významnou roli hraje také olovněné stínění, jelikož zabraňuje přesycení detektoru a také zvyšuje energetické rozlišení

detektoru. Nicméně skládané destičkové stínění podle Schaafa [13] by mohlo ještě více vylepšit vlastnosti detektoru.

Hlavní výhodou prezentovaného detektoru je, že pro měření mössbauerovských spekter ve zpětném rozptylu není potřeba měřené vzorky nijak připravovat. Kromě toho je možné detektor použít i v transmisní Mössbauerově spektroskopii k registraci nízkoenergetického gama záření.

Tento detektor tvoří velmi významnou část zařízení "Astenitometr", které umožňuje rychlé a nedestruktivní určení zbytkového austenitu v ocelích. Z tohoto důvodu je tento detektor stále vylepšován za účelem dosáhnutí nejlepších parametrů. Aktuální verze je vyrobena z duralu pomocí CNC obráběcích strojů. Mezi oběma částmi katody jsou umístěny navíc dva O-kroužky, které zabraňují větším únikům detekčního plynu. V této době je tato verze již plně využívána v laboratořích Katedry experimentální fyziky (Univerzita Palackého v Olomouci). Další krok vývoje bude zaměřen na stínění detektoru a samotného Austenitometru pro jeho širší využití v komerční sféře.

Výhodnější volbou pro účely transmisní Mössbauerovy spektroskopie je použití průtokového válcového proporcionálního plynového detektoru. Měření kalibračních mössbauerovských spekter α-Fe prokázala, že uníkový pík kryptonu (1,8 keV) je platnou detekcí gama fotonu o energii 14,4 keV. V tomto případě jej lze výhodně použít a zvýšit tak statistickou kvalitu spektra a čítací rychlost. Na druhou stranu využití úníkového píku mírně snižuje rezonanční efekt a také zvyšuje šířku čáry (snižuje rozlišení spektrometru). To je pravděpodobně způsobeno větším vlivem šumu na signál, jelikož amplitudy impulzů odpovídající úníkovému píku kryptonu (1.8 keV) jsou nižší než ty, které odpovídají píku úplné absorpce gama záření o energii 14,4 keV. Výhody úníkového píku mohou být využity i při použití argonu (případně jeho směsí) v Mössbauerově spektroskopii zpětného rozptylu (např. při použití průtokového toroidního proporcionálního plynového detektoru).

References

[1] K. R. Swanson, "Analysis of Thin Surface Layers by Fe-57 Möss-bauer Backscattering Spectrometry," *Journal of Applied Physics*, vol. 41, no. 7, pp. 3155–3158, jun 1970.

[2] J. Frydrych, M. Mashlan, J. Pechousek, and D. Jancik, "Conversion Electron Detectors for ^{57}Fe Mössbauer Measurements," *AIP Conference Proceedings*, vol. 1070, no. 1, pp. 170–184, oct 2008.

[3] M. Takafuchi, Y. Isozumi, and R. Katano, "A Proportional Counter for Mössbauer Spectroscopy by Scattered Electrons," *Bull. Inst. Chem. Res., Kyoto Univ*, vol. 51, no. 1, pp. 13–18, mar 1973.

[4] A. S. Kamzin and V. Rusakov, "Proportional counter for Mössbauer studies of surface-layers at temperatures from 100 to 700 K," *Instruments and experimental techniques*, vol. 31, no. 5, pp. 1150–1153, oct 1988.

[5] Y. Isozumi, M. Kurakado, and R. Katano, "A proportional counter for resonance-electron Mössbauer spectroscopy at low temperatures down to 77.3 K," *Nuclear Instruments and Methods in Physics Research*, vol. 204, no. 2-3, pp. 571–575, jan 1983.

[6] K. Fukumura, A. Nakanishi, and T. Kobayashi, "Hydrogen-filled proportional counter operated at low temperatures and its application to CEMS," *Nuclear Instruments and Methods in Physics Research Section B: Beam Interactions with Materials and Atoms*, vol. 86, no. 3-4, pp. 387–389, apr 1994.

[7] K. Fukumura, A. Nakanishi, T. Kobayashi, R. Katano, and Y. Isozumi, "Operation of a gas-filled proportional counter for CEMS at temperatures between 15–77 K," *Nuclear Instruments and Methods in Physics Research Section B: Beam Interactions with Materials and Atoms*, vol. 61, no. 1, pp. 127–131, jul 1991.

[8] T. Fujii, O. Hosoito, R. Katano, and Y. Isozumi, "Operation of a cryogenic conversion electron proportional counter under strong magnetic fields," *Nuclear Instruments and Methods in Physics Research*, vol. 76, no. 1-4, pp. 207–209, apr 1993.

[9] A. S. Kamzin and L. A. Grigorev, "2-chamber proportional counter for Mössbauer-spectroscopy of conversion electrons and X-rays in temperature range of 100-700 K," *Instruments and experimental techniques*, vol. 33, no. 2, pp. 314–317, apr 1990.

[10] A. S. Kamzin, S. M. Irkaev, Y. N. Maltsev, and L. A. Grigorev, "Automatic Mössbauer spectrometer to detect γ-quanta, conversion electrons, and characteristic X-rays," *Instruments and experimental techniques*, vol. 36, no. 1, pp. 51–58, feb 1993.

[11] B. Keisch, "A detector for efficient backscatter Mössbauer effect spectroscopy," *Nuclear Instruments and Methods IO4*, vol. 4, no. 1, pp. 237–240, oct 1972.

[12] L. Blaes, H. G. Wagner, U. Gonser, J. Welsch, and J. Sutor, "Toroidal proportional detector for backscattered Mössbauer γ-and x-rays," *Hyperfine Interactions*, vol. 29, no. 1-4, pp. 1571–1574, feb 1986.

[13] P. Schaaf, L. Blaes, J. Welsch, H. Jacoby, F. Aubertin, and U. Gonser, "Experience with a toroidal proportional detector for backscattered Mössbauer γ-rays and X-rays," *Hyperfine Interactions*, vol. 58, no. 1-4, pp. 2541–2545, jul 1990.

[14] I. Bibicu and M. Rogalski, "Proportional counter for simultaneous conversion X-ray and transmission Mössbauer spectroscopy Proportional counter for simultaneous conversion X-ray and transmission Mössbauer spectroscopy," *Journal de Physique III, EDP Sciences*, vol. 4, no. 12, pp. 2495–2499, dec 1994.

[15] I. Bibicu, M. Rogalski, and G. Nicolescu, "Toroidal proportional detector for conversion X-ray and transmission Mössbauer spectroscopy," *Nuclear Instruments and Methods in Physics Research Section B: Beam Interactions with Materials and Atoms*, vol. 94, no. 3, pp. 330–332, nov 1994.

[16] A. Y. Dudkin and S. M. Cheremisin, "A toroidal gas-filled proportional counter," *Instruments and experimental techniques*, vol. 37, no. 1, pp. 31–35, feb 1994.

[17] L. Kouril, J. Pechousek, P. Novak, J. Navarik, and P. Kohout, "Toroidal proportional gas flow counter for conversion X-ray Möss-

bauer spectroscopy," *Nuclear Instruments and Methods in Physics Research Section B: Beam Interactions with Materials and Atoms*, vol. 432, pp. 55–59, oct 2018.

[18] J. Pechousek, R. Prochazka, D. Jancik, J. Frydrych, and M. Mashlan, "Universal LabVIEW-powered Mössbauer spectrometer based on USB, PCI or PXI devices," *Journal of Physics: Conference Series*, vol. 217, no. 1, mar 2010.

[19] RITVERC, "Mössbauer sources: Cobalt-57 / Co-57." [Online]. Available: http://www.ritverc.com/products/detail.php?ID=1691

[20] R. Vondrášek, "Plynové náplně proporcionálních detektorů ionizujícího záření," bachelor thesis, Palacký University in Olomouc, 2018.

[21] F. Sauli, "Principles of operation of multiwire proportional and drift chambers," CERN/77-09, CERN/77-09, Geneva, Tech. Rep., 1977.

[22] W. Diethorn, "A methane proportional counter system for natural radiocarbon measurements (thesis)," Carnegie Inst. of Tech., Carnegie Inst. of Tech., Pittsburgh, USA, Tech. Rep. NYO-6628, Ph.D. dissertation, mar 1956.

[23] L. Schlattauer, L. Parali, J. Pechousek, I. Sabikoglu, C. Celiktas, G. Tektas, P. Novak, A. Jancar, and V. Prochazka, "Calibration of gamma-ray detectors using Gaussian photopeak fitting in the multichannel spectra with a LabVIEW-based digital system," *European Journal of Physics*, vol. 38, no. 5, pp. 1–12, sep 2017.

[24] T. Watanabe, H. W. Schnopper, and F. N. Cirillo, "K X-Ray Fluorescence Yield of Argon," *Physical Review*, vol. 127, no. 6, pp. 2055–2057, sep 1962.

[25] R. W. Fink, R. C. Jopson, H. Mark, and C. D. Swift, "Atomic Fluorescence Yields," *Reviews of Modern Physics*, vol. 38, no. 3, pp. 513–540, jul 1966.

[26] L. Kouřil, "Design and optimization of proportional gas flow counters for Mössbauer spectroscopy," dissertation thesis, Palacký University in Olomouc, 2018.

[27] J. Frydrych, M. Mašláň, R. Zbořil, J. Pechoušek, and M. Heřmánek, "CEMS and CXMS spectrometer: construction and application," *Acta Metallurgica Slovaca*, vol. 13, no. 6, pp. 298–301, 2007.

[28] V. Evdokimov, M. Mashlan, D. Zak, A. Fyodorov, A. Kholmetskii, and O. Misevich, "Mini and micro transducers for Mössbauer spectroscopy," *Nuclear Instruments and Methods in Physics Research Section B: Beam Interactions with Materials and Atoms*, vol. 95, no. 2, pp. 278–280, feb 1995.

[29] A. Kholmetskii, M. Mashlan, K. Nomura, O. Misevich, and A. Lopatik, "Fast detectors for Mössbauer spectroscopy," *Czechoslovak Journal of Physics*, vol. 51, no. 7, pp. 763–771, may 2001.

[30] Z. Klencsár, E. Kuzmann, and A. Vértes, "User-friendly software for Mössbauer spectrum analysis," *Journal of Radioanalytical and Nuclear Chemistry*, vol. 210, no. 1, pp. 105–118, apr 1996.

List of publications

- **L. Kouril**, J. Pechousek, P. Novak, J. Navarik, and P. Kohout, "Toroidal proportional gas flow counter for conversion X-ray Mössbauer spectroscopy," *Nucl. Instruments Methods Phys. Res. Sect. B Beam Interact. with Mater. Atoms*, vol. 432, pp. 55-59, Oct. 2018, (5 years impact factor = 1.297).

- **L. Kouřil**, P. Kohout, P. Novák, J. Navařík, and J. Pechoušek, "Setup of the Mössbauer spectrometer based on stand-alone instruments - A case study," *in AIP Conference Proceedings*, 2014, vol. 1622, no. 1, pp. 58–66, (without impact factor, only reviewed).

- P. Kohout, **L. Kouřil**, J. Navařík, P. Novák, and J. Pechoušek, "Optimized linear motor and digital PID controller setup used in Mössbauer spectrometer," *in AIP Conference Proceedings*, 2014, vol. 1622, no. 1, pp. 50–57, (without impact factor, only reviewed).

- J. Pechousek, D. Konecny, P. Novak, **L. Kouril**, P. Kohout, C. Celiktas, and M. Vujtek , "Software emulator of nuclear pulse generation with different pulse shapes and pile-up," *Nucl. Instruments Methods Phys. Res. Sect. A Accel. Spectrometers, Detect. Assoc. Equip.*, vol. 828, pp. 81–85, Aug. 2016, (5 years impact factor = 1.208).

- P. Novak, J. Pechousek, V. Prochazka, J. Navarik, **L. Kouril**, P. Kohout, V. Vrba, and L. Machala "Time differential ^{57}Fe Mössbauer spectrometer with unique 4π YAP:Ce 122.06 keV gamma-photon detector," *Nucl. Instruments Methods Phys. Res. Sect. A Accel. Spectrometers, Detect. Assoc. Equip.*, vol. 832, pp. 292–296, Oct. 2016, (5 years impact factor = 1.208).

- P. Kohout, T. Frank, J. Pechousek, and **L. Kouril**, "Mössbauer spectra linearity improvement by sine velocity waveform followed by linearization process," *Meas. Sci. Technol.*, vol. 29, no. 5, 057001, May 2018 (5 years impact factor = 1.735).

- J. Pechousek, **L. Kouril**, P. Novak, J. Kaslik, and J. Navarik, "Austenitemeter - Mössbauer spectrometer for rapid determination of residual austenite in steels," under review.